Atomic-Scale Analysis of the SiC/Oxide Interface to Improve High-Power MOSFET Devices

Inauguraldissertation

zur

Erlangung der Würde eines Doktors der Philosophie

vorgelegt der

Philosophisch–Naturwissenschaftlichen Fakultät

der Universität Basel

von

Dipanwita Dutta

aus Kolkata, India

Genehmigt von der Philosophisch-Naturwissenschaftlichen

Fakultät auf Antrag von:

Prof. Dr. Thomas Jung

Prof. Dr. Ernst Meyer

Basel, 21.05.2019

Prof. Dr. Martin Spiess
Dekan

Dedicated

To

My Beloved Parents,

to their selfless affection and inspiration...

Acknowledgements

During the four year period of my PhD I had the fortune to collaborate with multinational companies as well as world renowned research institutes. My thesis is an outcome of this four years' work and I am grateful to everyone who significantly contributed professionally or personally towards overcoming any challenges arising during this time. I thank you all for imparting the true value of optimism on me and making my research life enjoyable.

Firstly, with my deepest gratitude I would like to acknowledge my mentor and research supervisor Professor T. A. Jung for letting me work in his group. His thinking and selfless dedication nourished me in understanding crucial problems in the early stage of my research. I am also grateful to him, for suggesting such riveting projects to work on. His advices on research and career are invaluable.

I would like to thank the Swiss National Science Foundation for their financial support and the Swiss Nanoscience Institute (SNI) for giving me the opportunity to do my research in a prestigious institute under the guidance of eminent professors (project no. A10.08 Atolys). I acknowledge the support from University of Basel and Paul Scherrer Institute. Especially the valuable discussions with professors during this time of my stay and the knowledge they imparted on me. A special thanks to Prof. Dr. Jens Gobrecht. Apart from being adept, his omnicompetent personality stimulates and motivates people of all ages and fields.

I would like to thank Dr. Hans Sigg and Prof. Ulrike Grossner for the discussions on my project. Also a special thanks to Dr. A. Schoener from Ascatron for providing the MOS capacitors, R. Schelldorfer for solving the difficulties with AFM, Dr. Daniel Fan for Raman measurements and summer student P. Davenport for his contribution in data analysis.

Constant assistance and the friendly nature of the technical staff helped me doing my experiments smoothly. Here I would like to acknowledge the clean room experts Dr. Martin Bednarzik, Dario Marty, also Stefan Stutz and Anja Weber for the in-house SEM. A special thanks to Dr. Elisabeth

Müller for her patience and constant source of help during FIB and TEM measurements in PSI. I would like to show my appreciation to the theory collaborator from Uni Basel in Prof. Stefan Goedecker's group. Apart from Dr. Deb Sankar De and Dr. Shantanu Roy, Prof. Goedecker himself has been available providing his expertise in the field any time necessary.

I am grateful to all the help I obtained from the scientists from ETHZ and Jülich forschungszentrum while performing my experiments there. I am thankful to Dr. Alla Sologubenko from ETHZ who never failed to help me with STEM and for hours of valuable discussions; also Dr. Stephan Gerstl for the LEAP facility at ETHZ. I am indebted to the help I received from Doris Meertens from Jülich for the FIB/Nanomill support and Marc Heggen and Paul Paciock for the TITAN and Chemi STEM support. I am gratified because of the collaboration I had with ABB and thankful for the numerous meetings I had with Prof. Jörg Lehmann and Dr. Giovanni Alfieri who never failed to drive me with ambition and optimism. Also I appreciate Dr. Holger Bartolf for his valuable input towards the success of the project. I shall not forget the guidance and contributions from Corrado Bongiorno from CNR Italy regarding the in-depth understanding of STEM/EELS analysis.

I am also grateful to my fun filled and helpful colleagues Dr. Harald Rossmann, Dr. Jan Nowakowski, Dr. Milos Baljozovic, Dr. Massimo Camarda, Judith Wörle for their valuable inputs on past and present experience in research life. My hearty thanks to all my friends Daniel, Adrienn, Vassia, Matthias, Aisha, Manolis, Yve thanks to you all for the joyous time we spent. I would like to show my gratitude to Prof. Kulkarni and Prof. C.N.R. Rao for always being a source of inspiration for me. I also acknowledge Christian's (Hitch's) contribution towards my thesis. A special thanks to Jan Schaab for being a constant support in difficult times and for always seeing the best in me.

Lastly, I would like to acknowledge the most important people of my life, my parents and mama (my late uncle). Without their love and encouragement all my efforts would have gone to vain. My parents' endearing support has been the backbone for what I am today and what I will be in the future. I am grateful to them for whatever they gave me and I dedicate my thesis to them.

Preface

The world-wide effort to curb the emission of green-house gases has led to an increased push for technologies for the highly efficient generation, transportation and utilization of electrical power. Semiconductor-based inverters for example, are needed to connect photovoltaic arrays to the power grid, enable transport of the electrical energy over large distances and allow the energy-efficient control of electrical motors. To this date, silicon based power devices cover a wide range of such applications. However, SiC if used will enable higher switching speeds at simpler system topologies. This will enable in a reduction of overall system and material cost as well as higher efficiency and reliability. Although SiC has been studied since long it is only recently that the substrate quality, size and manufacturing capabilities are becoming mature enough to enable a reliable large-scale production of power electronic devices with acceptable performance and yield. Wafers with reasonable defect density and sizes up to 6 inches are now available boosting the manufacturing of SiC power devices, mainly unipolar diodes, by large global companies. SiC MOSFETs, in turn, have not unfolded their full potential yet because of the challenges associated with the formation of a high quality gate oxide from SiC.

Within the scope of this dissertation the atomic structure and the electronic properties of the silicon-carbide silicon-dioxide (SiC/SiO_2) interface has been discussed and investigated, motivated by its great importance for high power semiconductor devices. This work gears at the scientific understanding of the structure-property relationship of the gate oxide interface and aims towards identifying a manufacturing procedure to reduce the defect-levels near the interface as they are currently compromising carrier channel mobility in SiC-MOS devices. The content has been organized in chronological order according to the development of the research project. After briefing on the problem and the methods used for my work, the thesis will consist of two main parts. The first one reports about the identification of defects in general and specifically C-defects on the atomic scale and the second one is concerned about how the interface defects can be curtailed using passivation. The project has been a part of the “Nano-Argovia” programme of the Swiss Nanoscience Institute (SNI) and has been investigated in close collaboration of the Laboratory of Micro and Nanotechnology (PSI) with the Department of Physics (University of Basel) as the academic partner and ABB’s Corporate Research Center as the industrial partner.

Abstract

"The history of solid-state physics in general and of semiconductors in particular,
is not so much about great men and women and their glorious deeds,
as about the unsung heroes of thousands of clever ideas and skillful experiments
—reflection of an age of organization rather than of individuality."

— Ernest Braun

This thesis entitled **"Atomic-Scale Analysis of the SiC/Oxide Interface to Improve High-Power MOSFET Devices"** aims at a technology innovation critical for stepping up the energy efficiency in advanced silicon carbide (SiC) based metal oxide semiconductor field effect transistors (MOSFET) for high power semiconductor technology. While the wide band gap, high thermal conductivity, and high saturation velocity are very desirable, SiC has a major disadvantage in comparison with Si or gallium arsenide (GaAs). Compared to state-of-the-art silicon technology, the channel mobility in SiC MOSFETs is very low compared to the bulk mobility and is strongly dependent on its crystallographic orientation and the interface.

In contrast to Si where the passivation of surface states due to the SiO_2 layer was a breakthrough, the more complex nature of the oxidation process is still hampering such developments in SiC. It remains a pestering question, even after decades of intensive R&D, which kind of defects degrade the near-interface mobility of SiC-MOS devices and whether and how the proposed carbon clusters could be involved.

This thesis comprises a new approach in that multiple experimental techniques are combined with minima-hopping density functional theory for atomistic simulations and property prediction. It is by the iterative multi-technique investigation of structures, properties and processes down to the atomic level

that in-depth understanding of complex phenomena and mechanisms occurring at the interface during oxidation can be inferred.

In the present thesis spectro-microscopy and theory investigations have been used to investigate defects in particular C-defect formation during the fabrication of thermal oxides on SiC. The presence of carbon defects at this interface affecting the near interface channel mobility are consistently evidenced i) by a wide range of starting conditions in Density Function Theory and Monte Carlo simulations, and most importantly ii) by in-depth high resolution secondary transmission electron microscopy, EELS and Raman spectra iii) by few of the first Local Electrode Atom Probe (LEAP) experiments performed on SiC/SiO_2 interface samples and iv) by the most recent high resolution STEM data obtained by us allowing for in-depth analysis of the defect structure in addition to modelling, defect spectroscopy and transport measurements.

The thesis has been allocated into six chapters. **Chapter I** introduces SiC as a semiconducting material and its usefulness in power devices. It also briefly establishes the origin and role of various defects at the interface towards reducing the channel mobility. In **Chapter II** we get an overview of how C as a defect has been a controversial topic for decades and unveils the various methods and techniques we have been using in order to detect this C-nucleates. **Chapter III** explains how the sample preparation plays a very important role in order to achieve high-resolution data. Also here, we describe how different samples are prepared for different experiments: AFM measurements required removal of oxide using an etching solution in order to gain morphological information of the interface. FIB has been used to mill thin lamellae and pillars for HRTEM and LEAP experiments respectively. **Chapter IV** pertains to the atomistic analysis in order to find the C-defects at the interface. Using AFM we perceived the architecture of SiC interfaces and consolidated the speculations of C-nucleates being present at the interface. In order to gain knowledge about the various chemical bonds present at the interface we used Raman spectroscopy. HRTEM and LEAP proved that there are also dangling bonds along with stoichiometric dislocations at the interface leading to a broadening of the interface via the imperfect layer by layer oxidation and the penetration of defects into the SiC resulting in deterioration of the channel mobility. EELS and STEM analysis revealed the exact positions at which the C-defects are present and where they are attached to the interface. After reporting the concerting evidence of C-nucleates as defects in chapter IV, the following **Chapter V** deals with passivation and interface treatment methods; and on their potentially beneficial influence on near interface defect densities and electronic properties. Finally, in **Chapter VI** we conclude our thesis with the final results we obtained and provide an outlook towards future investigations and what is to be done next.

Table of Contents

Chapter I: Overview of SiC as a high power semiconductor device material

Chapter II: Carbon defects in SiC/SiO_2 interface and techniques used for their detection

Chapter III: Sample preparation TGO/pTGO

Chapter IV: Atomic analysis of SiC/SiO_2 interface to find C-defects

Chapter V: Relevant parameters for improving thermally grown gate-oxide interface

Chapter VI: Conclusion and Outlook

List of Acronyms

AFM	Atomic Force Microscopy
HR-S/TEM	High Resolution- Transmission Electron Microscopy
LEAP	Local Electrode Atom Probe Tomography
EELS	Electron Energy Loss Spectroscopy
MOSFET	Metal Oxide Semiconductor Field Effect Transistor
DOS	Density of State
DFTB	Density Function Theory Tight Binding
MHM	Minima Hopping Method
APT	Atom Probe Tomography
FIB	Focused Ion Beam
HAADF	High-Angle Annular Dark-Field
EDX	Energy-Dispersive X-ray Spectroscopy
TOF	Time of Flight
NIT	Near Interface Traps
P/TGO	Passivated/Thermally Grown Oxide
I/FFT	Inverse/ Fast Fourier Transform
SEM	Scanning Electron Microscope

Chapter I

Overview of SiC as a high power semiconductor device material

"It was not so very long ago that people thought that semiconductors were part-time orchestra leaders and microchips were very small snack foods."

Geraldine Ferraro

I.1 Introduction

The sustainable supply and efficient conversion of energy is of major concern in today's society and economy and the semiconductor industry plays a pivotal role that commuted the world without a doubt. The birth of semiconductor devices can be traced back to 1874 [1] when C.F. Braun who was that time conducting research on metal sulfide conductivity invented the rectifier as AC-DC converter. The semiconductor industry continued to flourish following the invention of the junction transistor by Shockley in 1948 for which he was awarded the Nobel Prize in Physics in 1956.[2] In 1957

the industry already grew to a scale of 100 million dollars. In parallel, this was the dawn for power electronics.[3] Power electronics is a division of solid state electronics where high-efficiency switches convert and control electrical power for a wide range of applications. This includes the operation of electrical supply grids with decentralized renewable energy sources, i.e. wind, small scale water and solar power plants. Other applications of power electronics includes traction control, recuperation for electric and diesel electric engines and for ships, as well as hybrid and electrical drive trains.[4] Thus, power electronics can save enormous usage of fossil energy in automotive technology. Currently, we can designate the 21st century to be the golden age of power electronics applications because of the evolution of technology leading to major innovations like FET-plus-driver modules, power supplies with best integrated circuit designs and transformers. [5-6]

Solid-state electronics originally started with Ge, but it gradually transformed to using Si as its base. Si quickly became the material of interest since it has larger band gap which prevents leakage currents when the device is in the OFF-state. This is suitable for power applications giving rise to the Si age. Another important reason for Si being popular is because of the high quality oxide/semiconductor interface. This is due to the passivating nature [7] of SiO_2 on the surface states which is important in Metal-Oxide-Semiconductor (MOS) systems. However, Si has its limitations in current high power applications. A high critical electric field is required in a device operating in high frequency and high temperature to withstand large breakdown voltages during the operation of the device in reverse direction. Hence, even wider bandgap materials than Si are desirable and scientists have been looking for materials with favorable properties, despite the success of Si. For these reason compound semiconductors belonging to the III-V compound groups gained more recognition.[8]

I.2 Properties of SiC making it so unique for high power devices

Power applications require high critical electric field (Ec) to withstand large breakdown voltages and materials with a wider bandgap than Si are more suitable. In contrast to silicon (Si) and GaAs, SiC exhibits a wide band gap of 3.2 eV (1.1 eV in Si and 1.43 in GaAs) and a high critical electric breakdown field of above 2.2MV/cm (10 times higher than Si and GaAs). This makes SiC one of the

most promising candidates for manufacturing energy-efficient unipolar devices to operate at voltages exceeding 10 kV, high frequency (20 kHz), and at temperatures above 175 ^{O}C. Furthermore compared to other wide band gap materials (GaAs, GaN), SiC like Si can grow a native oxide (silicon dioxide, SiO_2) that can be produced in an industrially affordable, thermal process. [9] Its attributes make it the most desirable candidate for applications where high power, high temperature, and high speed switching are required and desired, such as aerospace, and renewable energy applications. [10-11]

Property	Si	4H-SiC
Bandgap [eV]	1.1	3.26
Thermal conductivity [W/cmK]	1.5	4.9
Melting point [C]	1420	2830
Breakdown field [x10^5 V/cm] $R_{on} \propto 1/E_c^3$	3	30

Among the 250 known polymorphs of silicon carbide, 4H-silicon carbide (SiC) is the most promising polytype for power electronic devices due to its favorable properties. [10, 12-14] Some of the favorable properties being its mature growth when compared to the other polytypes like 3C and 6H, and also because its electron mobility is up to 10 times higher perpendicular to the c-axis i.e., the [11-20] plane. The growth of a certain polytype is based on impurity doping, especially where the dopant is incorporated in the crystal. Nitrogen dopants for example occupy the C lattice sites and facilitate 4H-SiC growth in C-rich growth atmosphere. Along with this SiC crystals with a certain off-angle are used employing the step flow control technique.[15] Thereby layers of homoepitaxially grown polytypes can be fabricated as the starting material for SiC power devices. 4H-SiC based high-power metal-oxide-semiconductor field-effect transistors (MOSFETs) exhibits superior performance and lower power dissipation. Thus they have very promising perspectives for high power markets that benefit from energy efficiency. Power devices benefitting from SiC MOSFET technology includes electricity grids, traction power-modules, control trains, converters for renewable energy generators etc. For

these reasons, mature SiC power devices have been manufactured in relatively high-batch volumes during the last decade by several corporations (GE, Cree, Mitsubishi, Infineon, Rohm, etc.), with a market volume predicted to grow up to 38% a year up to 436 M$US in 2020.[16]

Predicted impact SiC will make:

- Hybrid vehicles will benefit from a 10% extended driving range.
- Airplanes will benefit from a reduction of weight by at least 1000 lbs with more compact high efficiency power systems
- In medical imaging smaller, more efficient systems will be introduced, saving floor space and energy, towards lower healthcare cost.
- In data centers, the fastest growing segment of electricity consumption, more than 5% energy savings will be possible.
- Renewable sources of energy can be harnessed more efficiently because of a reduction of wasted power in decentralized grids by 50%.

Calculations predict that SiC if used in current devices in high power systems will save one year's worth energy of the canton of Bern and Valais for whole Switzerland.[17]

I.3 Importance of the Gate-Oxide (SiO_2) and SiC/SiO_2 interface for High Power Devices

In MOSFETS, the gate electrode is separated by a thin insulating layer from the semiconductor in which it controls the formation of a conducting channel. Planar, atomically well-defined (~ 10 nm-40 nm) gate insulator layers in nanometer-close proximity (<25 nm) and defect-free semiconducting channels are required to sustain a high carrier mobility and gate-oxide reliability.

If the 'bulk' thermal oxide grown on SiC is compared to that grown on Si there is no evidence of difference in their properties. SiC oxidation also yields stoichiometric SiO_2 whose refractive index, [18] and breakdown field are similar to the Si thermal oxides.[19] However, though SiC can be thermally oxidized to yield SiO_2 over its surface, a fundamental inherent drawback of SiO_2 is its low dielectric

constant, which is about 2.5 times lower than that of the SiC material and also the poor interface properties at the SiO_2/SiC junction. This leads to a proportionally larger electric field enhancement in the SiO_2 dielectric compared to the SiC semiconductor layer underneath. This is the reason why new dielectrics with dielectric constants at least similar to that of the SiC and with lower interface state densities might be required for device applications. Note that these inequalities of dielectric constant often requires device operation at an electric field far below the SiC material breakdown field in order to avoid premature SiO_2 breakdown at the device surface. A variety of oxidation methods has been developed, such as thermal oxides, deposited oxides, hybrid oxides and alternate dielectrics. For each of these oxidation processes various subprocesses exist, each with its advantages and disadvantages.[5] Also, due to the 10 times larger critical field in SiC compared to Si power devices, the oxide is under significant electrical stress in conventional designs.

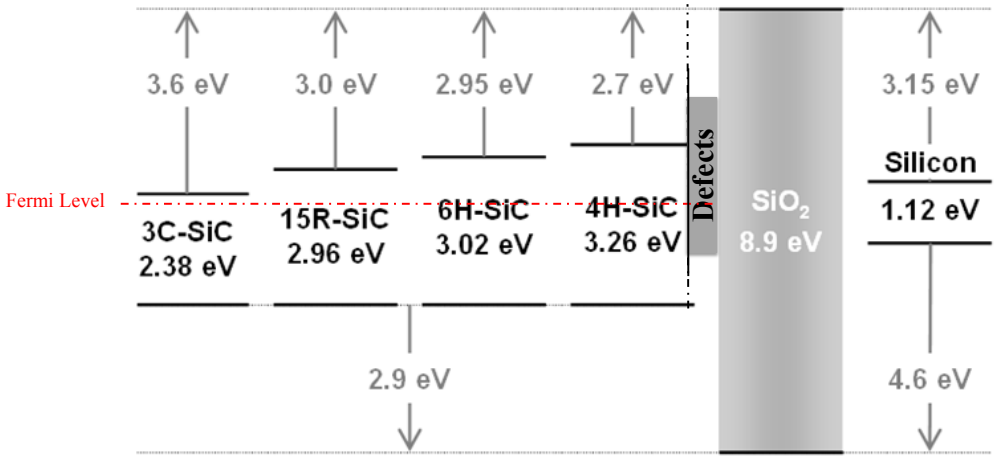

Figure I.1: Energy gaps and band-offsets of Si, SiO_2, and some of the SiC polytypes. Figure compiled from results reported in Afanas'ev *et al.* [20-21] and Rozen el.al.[22]

Also, unlike the properties of the SiO_2 bulk, the ones of the interface SiC/SiO_2 are strongly dependent on the substrate and its orientation. The interface quality affects the channel mobility of MOSFETs directly. Prior to growing the oxide layer, cleaning the surface of the SiC has proven to be a vital step. While many variations of cleaning order and steps exist, J. Plummer et al.[23] established the basic stages of the cleaning procedure. Also surface conditioning or passivation with H_2, N_2, or a combination of both has proven to further decrease D_{IT} but only to a certain limit.[22, 24]

I.4 Defects in SiC-MOSFET

As discussed before, the thermal oxidation of SiC – in contrast to Si – curtails the carrier mobility in the near interface region of the SiC. This effect has been attributed to the presence of defects formed at the interface during the chemically complex oxidation process[20, 25-26] and leads to field-effect channel mobility merely below ~40 cm^2/Vs compared to ~900 cm^2/Vs in the undisturbed 4H-SiC crystal. This decrease in mobility is caused mainly by three different types of defects: dangling bonds, carbon clusters, and near interface traps (NITs).

Each defect contributes in a different order to the interface state density (DIT). Dangling bonds contribute in the magnitude of ~10^{11} eV^{-1} cm^{-2}, carbon clusters around ~10^{12} eV^{-1} cm^{-2}, and NIT's >10^{12} eV^{-1} cm^{-2}. This sums up the interface state density to 10^{12}-10^{13} eV^{-1} cm^{-2} near the conduction band edge (Ec), roughly two orders of magnitude larger than that for Si.[20, 25-26] Several origins for NITs have been suggested. Pippel et al. suggested that NITs in 4H-SiC polypeptide originates from internal defects in the 4H polypeptide.[25] Chang et al. proposed Si-rich areas in 6H-SiC to be the origin of NITs.[27] Carbon clusters, such as carbon dimers, or graphitic microcrystals are sometimes regarded as NITs, too.[25, 28-30] Whatever nature the origin of the traps is, the carriers oblige a certain time to be trapped by defects.[31-32] The shallower the traps are the smaller the necessary entrapment time. Since devices are designed for high switching modes, shallow traps have a particularly large influence on the delay of the carriers.[5]

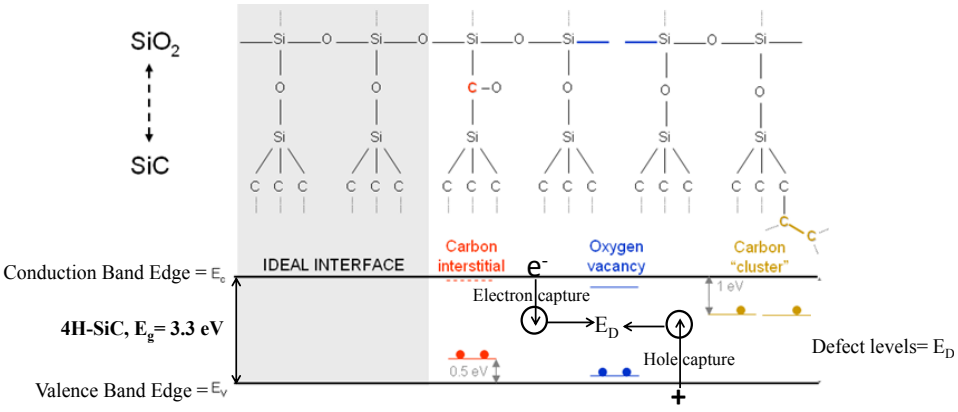

Figure I.2: Schematic of various defects that may occur at the interface along with their energy levels in the 4H-SiC band-gap. Compiled from results published by Wang, Pantelides *et al.* and John Rozen *et al.* [22, 33]

I.5 History on studies of different defects in SiC MOS-devices

Shallow interface traps with energy levels just below the conduction band were held responsible for the low channel mobility of the thermally grown SiC/SiO_2 interface.[5] But based on newer observations, it was concluded that defects responsible for low mobility were physically located near the interface; most recently it has been established by considering quantum confinement effect, that the active NIOTs are energetically located above the bottom of the conduction band and physically located very close to the interface with short response times.[34] Imperfections and defects near the interface were identified utilizing electrically detected magnetic resonance evidencing for significant disorder at the interface[35-36] High-resolution Rutherford backscattering spectroscopy analysis together with cathode luminescence (CL) spectroscopy and TEM suggested that the deviations of stoichiometry and roughness at the interface, defined the effects of the interface of SiO_2/4H-SiC(0001).[37] Investigations in order to solve the confusion and understand the active defects and NIOTs and how to passivate them are still going on. For a decade SiC thermal nitridation followed by oxide deposition provided a route to confine nitrogen at the SiO_2/SiC interfacial region which improved the channel mobility. To investigate the effects of nitrogen it has been incorporated into SiC by annealing in isotopically enriched ammonia. Electrical measurements on such MOS structures revealed poor electrical quality suggesting nitrogen incorporation at the interface has to be done in a very specific manner in order to improve the mobility. [22] Similarly NO and forming gas post oxidation annealing treatments on the interfacial properties were investigated and revealed that forming gas annealing has limited effect on the interface trap density (Dit). It results however, in an improvement of the insulating properties of thermal oxide. On the other hand, NO annealing causes a drastic reduction in Dit across all energy levels, but the reliability of the device is not very effective. Hence a combined treatment leads to a significant reduction in interface trap density and uniform reliability.[22] Recent reports on passivation techniques reveals that $POCl_3$, Ba or N introduce significant changes to the near-interface atomic structure of SiC at SiC/SiO_2 interface but the reason and the mechanism behind the passivation is not clear.[4] In literature constant capacitance deep level transient spectroscopy (CCDLTS) measurements reveals an electron trapping reduction by a factor of 2 at

energy levels within 0.2 eV of the SiC conduction band edge by using Sb at the SiO_2/SiC interface which improves the channel mobility of the MOSFETs.[38-39] Theoretical studies on such systems have been performed for decades by modelling pair of edge dislocations using ab initio methods. Such results disclose that (i) the crystal structure is strongly disturbed in the small vicinity of the dislocation core, (ii) additional energy levels present in the energy gap originate from the atoms with broken bonds in the neighborhood, (iii) spatial tunnels exist, with atoms creating localized states in the band structure and significantly decreasing electrostatic barriers. The later should be considered as one of the primary factors responsible for experimentally observed reduction of the breakdown voltage.[10]

I.6 Inference

The defects at the interface create localized energy levels in the band-gap (which will be discussed in details in chapter IV) leading to enhanced Coulomb scattering thus reducing the carrier lifetime. The channel mobility of SiC MOS devices is therefore lowered to a fraction of its bulk value. The shallow states close to the conduction band edge of 4H-SiC are caused by near-interface defects and C-related defects. Their presence may provide an explanation for the trap levels within the rest of the band-gap. The origin and physical nature of these defects especially C-defects and their effect as carrier traps have been the subject of intense research. This has also been the topic investigated in this thesis with particular focus on C-related defects, their identification and the historic evolution of evidences found to support their presence.

Chapter II

Carbon defects in SiC/SiO_2 and techniques used for their detection

"One of the basic rules of the universe is that nothing is perfect. Perfection simply doesn't exist.....Without imperfection, neither you nor I would exist"

Stephen Hawking

Summary

Defects occur near the gate insulator/semiconductor interface due to the more complex nature of the oxidation process which requires removal of carbon atoms in the form of CO and CO_2 from the SiC crystal. In this chapter we introduce the different forms of carbon defects at and near the interface and the techniques used in my work solely for the purpose of identifying the relevant C-defects compromising the near interface SiC channel mobility.

II.1 Introduction

The excess carbon from the SiC crystal during the complex oxidation process causes various types of specific defects in the near interface region and in the oxide. These not only modify the electronic properties of the inversion channel, but also deteriorate the field-effect channel mobility and introduce scattering centers for the charge carriers, thereby increasing the interface trap density. The physical origin of the Near Interface Traps (NITs) remains unclear, but recent studies suggest the formation of carbon clusters, such as carbon dimers, or graphitic microcrystals at the interface.[25] Experimental evidence of their presence has been concluded from atomic force microscopy (AFM) studies of SiC surfaces after the oxide removal.[20, 40] However, it is also reported that there is no graphite layer exceeding 0.1 monolayer based on in situ XPS studies.[25, 41] So according to the different reported studies carbon clusters were not directly observed at the SiO_2/SiC interfaces but measurements indicate that if present they would be a few atoms in size. In case such small C-nucleates/ clusters exist, the corresponding energy levels would be dependent on the environment of the clusters, which has not been considered in most of the reports before.[22]

Therefore theoretical simulations of the interface are very useful as a complementary tool. Using simulation we can learn about defects in the form of C-clusters (also C-nucleates) and their trap levels. Extensive work has been performed using density-functional theory (DFT) but it is unable to reproduce the real values of the band gaps of the semiconductor.[42] Thus the calculated energy levels may not be 100% accurate. Also, as described before the energy of a defect relies on its surrounding solid matrix where it is embedded. Accordingly the calculated values for each of the cluster-in-matrix configurations will correspond to specific cases. Moreover, the theoretical work done so far considered the kinetics during the oxidation only to a limited extent as it only considers a static interface, where oxide is placed on the interface instead of being grown using unbiased techniques, for the defect identification. Hence, the theoretical results so far provided a broad knowledge of possible C-defects and their impact, without much confirmation.

*Theoretical simulation performed by Prof. Goedecker et al. in Uni Basel.

Our current work goes beyond previous work in that it links extensive experimental results using different techniques to advanced DFTB simulations of the oxidation process to understand the formation of carbon defects and further characterize their atomistic structure.

II.2 Scope of Investigation

Buried interfaces generally impose challenges limiting the investigation of local structure and material properties which compromise the use of e.g. diffraction techniques and require challenging and careful sample preparation procedures even if e.g. well established microscopy techniques like Scanning Electron Microscopy (SEM) and Transmission Electron Microscopy (TEM) are to be applied.

From the theoretical point of view several researchers came up with methods to perform structure predictions as discussed in the introduction above. The Minima Hopping method developed in the group of Goedecker goes beyond previous DFT methods in that the absolute minimum structure can be identified with high reliability. Thus we are able to use some of the latest and most advanced simulation tools that are not yet widely available to study industrially relevant properties in silicon-carbide based electronic devices.

II.3 Methods & techniques to detect C-defects

The wide spectrum of microscopic and structural investigation techniques (Optical Microscopy, Scanning Electron Microscopy, (Scanning) Transmission Electron Microscopy, Atomic Force Microscopy) shall be complemented with chemical and structural investigations with light (Raman spectroscopy) and atom probe tomography. Thereby, macroscopically measured values, like the break-down electric field shall be related to the presence of impurities, defects and also to the crystal and grain structure defect. In parallel to these structural investigations of near interface defects at the atomic scale, numerical simulations on MOSFET architectures shall complement the obtained experimental results.

*Theoretical simulation performed by Prof. Goedecker et al. in Uni Basel.

II.3.1 Atomic force microscopy (AFM):

Atomic force microscopy is a high-resolution imaging technique, specific form of scanning probe microscopy where a small probe with a sharp tip (3-6 um tall; 15-40 nm end radius) is scanned back and forth in a controlled manner across a sample to measure the surface topography at an atomic resolution (lateral resolution ~30nm and vertical resolution 0.1nm). PeakForce Tapping is an AFM technique that enables the highest resolution surface imaging along with highly sensitive nanoscale property mapping.

AFM measurements were conducted in air with a Bruker AFM (Dimension ICON with ScanAsyst). AFM was used in tapping mode to assess the morphology of the specimens at different stages. The NanoScope processing software was used, and samples were typically investigated on different scales ranging from 5 µm down to 100 nm; the noise threshold was set to 0.01 nm and the Z range was fixed to 1 µm.

II.3.2 Raman:

Raman spectroscopy is used for studying low frequency modes like vibrational and rotational modes. Raman is a scattering phenomenon. It depends on inelastic scattering of photons by phonons and thus on polarization changes. So Raman always needs a source for polarizing the molecule. Again this polarisability is a function of interatomic distance making Raman spectrum sensitive to small changes in the local bond lengths, bond angles to provide unique information about molecular morphology.[43]

- D band: It is known as the defective band. The breathing motion of six atom rings gives rise to this band. A defect is required for its activation to be visible in the Raman signal. This involves phonons of the k (k is the wave vector for the electronic transition) zone boundary of the brillouin zone. The phonon mode which satisfies the condition k=q/2 (q is the phonon wave vector) is the origin of the D peak with A1g symmetry. Its position is at 1350 cm^{-1} and changes with excitation energy. The D band reveals the disorders in the electronic structure such as defects, grain boundaries, and functional groups in the sp2 carbon lattice.

*Theoretical simulation performed by Prof. Goedecker et al. in Uni Basel.

• G band : It is named as the graphitic band. The in-plane bond stretching of sp2 carbon atoms gives rise to this band. The G band position is at 1580 cm^{-1}. Here the zone center phonons instead of the zone boundary phonons, with E2g symmetry are required for its origin. Dispersion being proportional to the degree of disorder, the G band disperses more when the degree of the defect or disorder is high.

For experiments in the SiC/SiO_2 specimen a home-built micro Raman spectroscopy setup based on a 532 nm single mode continuous wave laser and an inverted microscope (Leica DM5000 equipped with a 100x NA=0.9 objective, Germany) as the sample stage was used. The laser power on the sample was measured to be 0.75 mW. The scattered light passed through a 532 nm long pass Raman filter (Semrock, Rochester, U.S.A.) with 40 µm slit and onto a 600 lines/mm grid spectrograph (Acton SP500i, Princeton Instruments, U.S.A.). A CCD camera (ProEM 1600^2, Princeton Instruments, U.S.A.) was used as the detector. Raman peaks were fitted using Lorentzian lineshapes (OriginPro, OriginLab, U.S.A.). The spot size for the green laser is ~2.3 µm.

II.3.3 Focused Ion Beam:

Focused ion beam (FIB) is one of the precise maskless fabrication tools which uses both bottom-up and top-down fabrication approaches to fabricate complex 3-D micro-/nano-structures with high precision. FIB instruments can be stand-alone single beam instruments; alternatively, FIB columns can be incorporated into other analytical instruments such as a scanning electron microscope (SEM), transmission electron microscope (TEM), or secondary ion mass spectrometry (SIMS). Small probe (diameter ~ 5 nm) sputtering is facilitated by the liquid metal ion source (LMIS). Gallium is the most commonly used LMIS for FIB and the reasons are: Low melting point of 29.8 °C and can exist in the liquid form near room temperature, low volatility/ vapor pressure, relatively unreactive, good vacuum properties and Ga^+ being a heavy ion makes it good for milling. The Ga^+ beam is used to scan and cut the substrate surface in a vacuum chamber. Ga^+ beam etching was originally developed for sample preparation in electron microscopy. The beam of ions "mill" the specimen surface, via the sputtering process, and this milling can be controlled with nanometer precision. In addition, ion beam assisted

*Theoretical simulation performed by Prof. Goedecker et al. in Uni Basel.

chemical vapor deposition can be used to deposit material at predefined positions. A small quantity of a specific precursor gas is injected into the vicinity of the beam, where it is decomposed by the beam, depositing the nonvolatile decomposition products on the specimen surface while the volatile products are extracted by the vacuum system.[44]

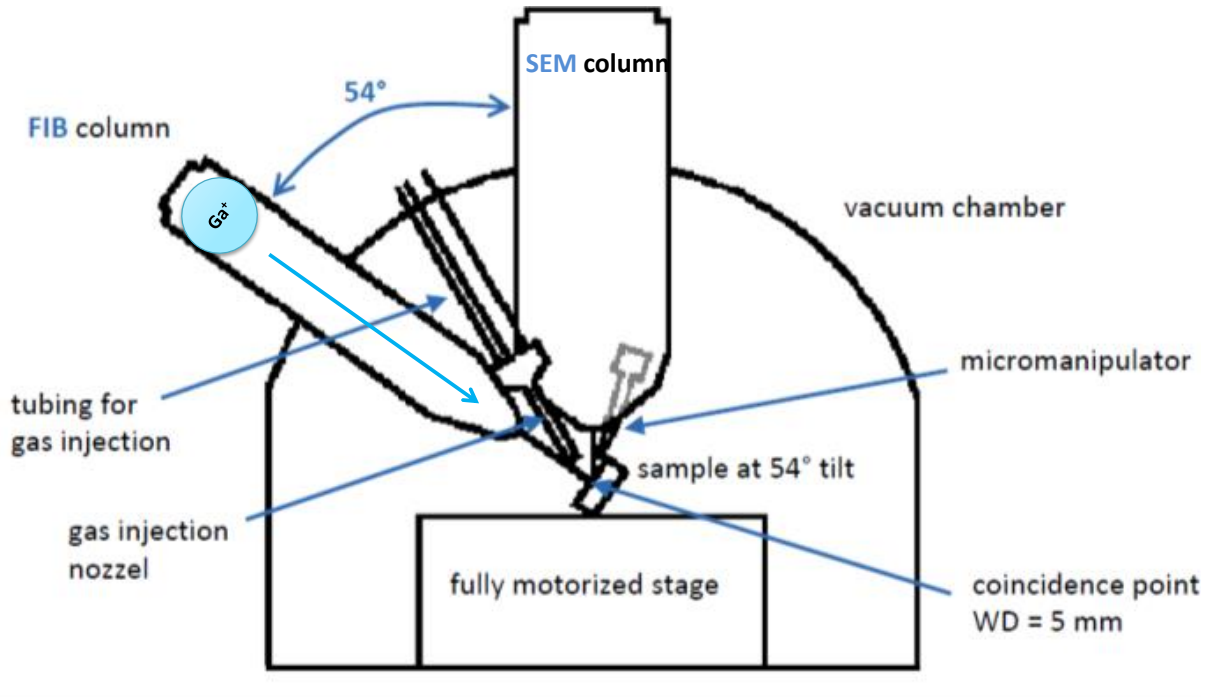

Figure II.1 Schematic showing FIB in a typical beam setup.

A FIB becomes even more powerful if it is combined with a SEM. In the DualBeam system the electron and ion beams intersect at a 54°, depending on the FIB (JEOL or FEI) used, which is the angle of coincidence point near the sample surface, allowing high resolution SEM imaging of the FIB-milled surface. Such systems combine the benefits of the sample modification technique of the FIB with the spatial imaging and characterizing properties of SEM thus providing complementary imaging and beam chemistry capabilities.

The FIB used for our SiC/SiO_2 sample preparation is the FEI Helios NanoLab 400S which is optimized specifically for high resolution scanning transmission electron microscopy (STEM)/TEM sample preparation. The flipStage and the STEM detector can change from sample preparation mode to STEM imaging mode easily without breaking vacuum. Platinum and carbon are the preferred deposited material whether the sample is prepared for LEAP or STEM. Finally the sample is cleaned

*Theoretical simulation performed by Prof. Goedecker et al. in Uni Basel.

and thinned further down using the Nanomill (with Argon Source) from Fischione: Model 1040NanoMill® TEM specimen preparation system.

II.3.4 Scanning/Transmission Electron Microscope:

The scanning transmission electron microscope (STEM) is an invaluable tool for characterizing nanostructures with the ability to provide information on elemental composition and electronic structure with the sensitivity of a single atom. The STEM works like a normal scanning electron microscope (SEM), using a focused electron beam on thin specimens but also has transmission modes of imaging. Typically, when a field emission gun STEM is equipped with a probe spherical aberration corrector along with an electron monochromator and a post column energy filter system the resolution is in the range of sub angstrom.

High-angle annular dark-field (HAADF) imaging is a STEM technique where incoherently scattered electrons, also known as Rutherford scattered electrons, are used making it highly sensitive to variations in the atomic mass of the atoms. The HAADF detector thus senses a higher signal from atoms with a higher atomic number making them brighter in the image. Information about chemical composition on the nanoscale is pivotal for verifying the architecture of nanostructures and devices, and X-ray spectrometry is a well-established, robust and easy to use technique to obtain the comprehensive chemical information. Better yet, in the S/TEM, X-ray analysis pairs microstructural information obtained from high-resolution imaging with accurate chemical composition information. Modern X-ray analysis on the S/TEM employs a well-established technology called ***X-ray energy dispersive spectroscopy (EDX)*** that operates in the following manner: The electron beam ejects atomic core-shell electrons from the sample. The recombination of a higher shell electron into the now empty core state creates X-rays imprinted with this atom's characteristic energy. The X-rays created in the sample are absorbed by a detector and the deposited X-ray energy creates a few hundred to a few thousand electron-hole pairs, which are immediately separated and collected by the detector as a charge pulse. The fast electronics to accurately detect these pulses are robust and reliable, meaning they produce highly-repeatable results that are easily calibrated in energy. As incoming

*Theoretical simulation performed by Prof. Goedecker et al. in Uni Basel.

pulses ("X-ray counts") are binned in energy, a spectrum of atom specific characteristic peaks is accumulated and can be automatically labeled by the computer. [45-46]

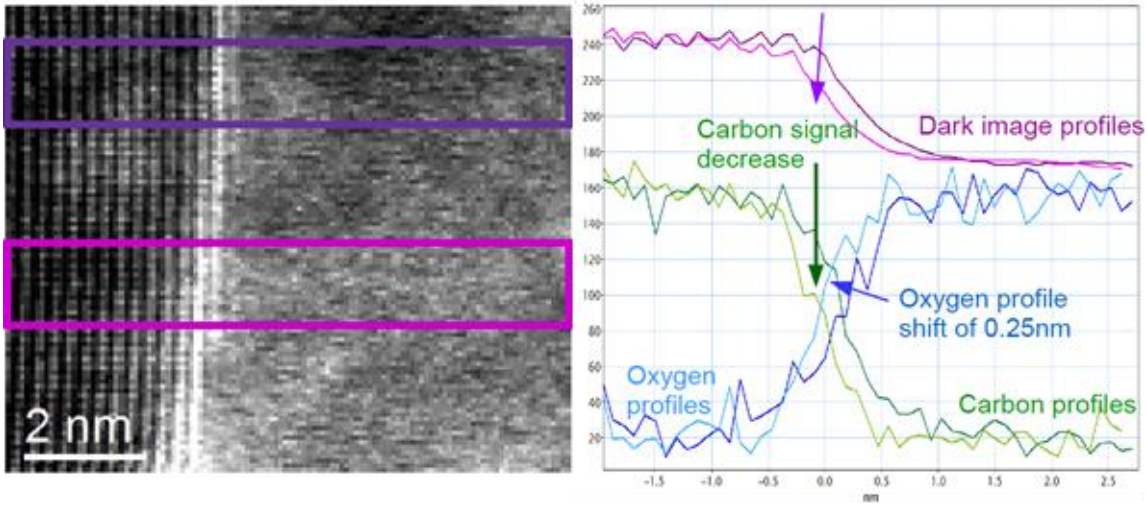

Figure II.2: Sensitivity and resolution: (a) STEM HAADF images with boxes marked as a reference for the image profiles extracted up and down one atomic step.(b) The purple lines shows atomic step resolution as one step goes missing in the lighter purple spectrum compared to the darker purple spectrum which are both marked in (a). Thus detection limit is very high up to $1e^{14}$ atoms/cm^2. A small carbon peak is found at the interface as carbon residual atoms using the atomic step chemical resolution.

The scanning TEM (STEM) was performed with a JEOL ARM200CF with a spot size of 0.13 nm. The accelerating voltage used is 60 keV and spatial resolution was approximately 0.4 nm FWHM. EELS spectra reported in this thesis were collected with a Gatan Quantum Spectrometer. In order to have all the three silicon, carbon and oxygen signals in the same spectrum the energy dispersion was 0.25 eV/pixel.

For high resolution TEM images, a FEI Titan 80-300 setup was used, equipped with a cold field emission electron gun with 80 kV-300 kV accelerating voltage. This high-resolution transmission electron microscope is equipped with a field emission gun and a corrector for the spherical aberration (C_S) of the imaging lens system. Under optimum optical settings of the image C_S-corrector (CEOS CETCOR) the point-resolution is extended up to the information limit of well below 100 pm with 200 keV and 300 keV electrons. Digital images are acquired with a Gatan 2k x 2k slow-scan charged coupled device camera.[47]

*Theoretical simulation performed by Prof. Goedecker et al. in Uni Basel.

II.3.5 Local Electrode Atom Probe:

Atom probe tomography (APT) has been developed to characterize nanoscale features of materials. It is one of the few techniques with single-atom sensitivity and high spatial resolution.

APT utilizes:

- Laser induced field evaporation of surface atoms.
- Reconstruction of the data collected from a time of flight (TOF) mass spectrometer.
- Position-sensitive detector, to reveal the spatial arrangement of atoms with a resolution of better than 0.3 nm in all three coordinate directions.

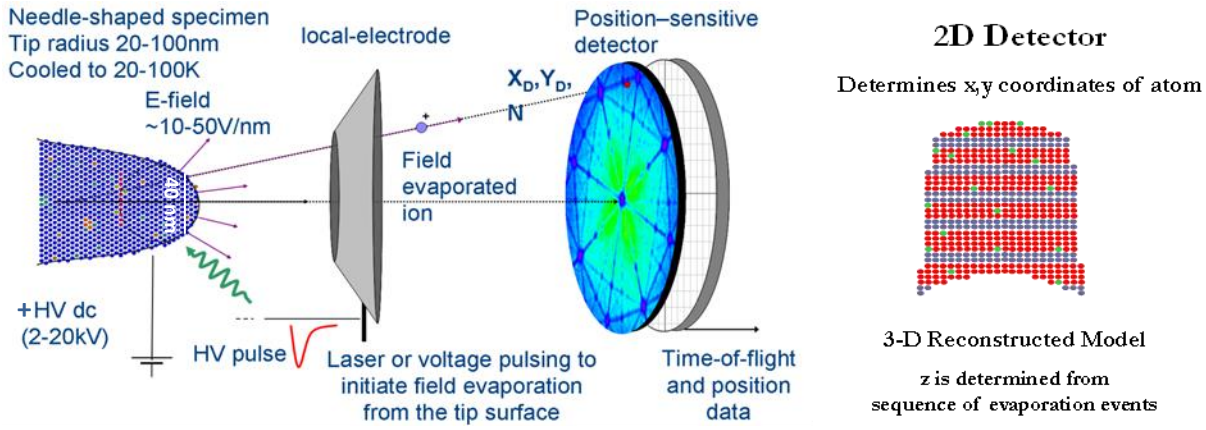

Figure II.3: Schematic showing how LEAP operates

For LEAP the field evaporates (with a voltage and laser pulse) a sharp tip-shaped specimen. The ionized products are collected in a position-sensitive detector; the time-of-flight mass spectrometer determines the atomic species with ppm sensitivity and position from within the original analysis volume with sub-nm accuracy. Currently APT is the only experimental method that can provide both structural and compositional information for subsurface and buried features from a single experiment.[48]

For SiC/SiO_2 Cameca LEAP 4000X-HR was used with multiple alignment CCDs, Chevron MCP and 3-anode Delay-Line position sensitive detectors. The software used for analysis are as follows: LCC (LEAP Certified Consultant) for data collection, Data Analysis Visualization (DAVis) for visualization and Integrated Visualization and Analysis Software (IVAS) for analysis.[49]

*Theoretical simulation performed by Prof. Goedecker et al. in Uni Basel.

II.3.6 Theoretical Simulation:

Theory: Density functional tight binding methods (DFTB+) give a reliable structure prediction but are numerically expensive since they require the diagonalization of a Hamiltonian matrix which scales cubically for large systems.

DFTB explores the potential energy surface in a very efficient way and finds low energy structures. The minima hopping method has been applied to modify the minimization trajectory and to find the energy minima structure with higher reliability. Thus, many systems such as clusters, interfaces, crystalline solids and defects in crystalline solids have been simulated and in many cases entirely new and unexpected structures have been found. On the Density Functional level the Minima Hopping method has been applied to some of the largest systems ever studied by unbiased structure prediction methods with up to 100 atoms. Exploiting the acceleration of the BigDFT electronic structure code possible with GPU, as well as algorithmic improvements it is even able to do density functional based structure predictions for systems of several hundred atoms.

The Density-Functional-Theory (DFT) calculations were performed within the projector augmented wave framework as implemented in the VASP package[50] to refine the geometries and energetic ranking of the most promising candidate structures. We used the generalized gradient approximation with the Perdew-Burke-Erzernhof (PBE) parametrization of the exchange-correlation functional.[51] A plane-wave cutoff energy of 500 eV was used together with a sufficiently dense k-point mesh, resulting in total energies converged to less than 1 meV/atom.

II.4 Inference

After being introduced to the instruments required for the identification of defects at interfaces which can be of few atoms in size, we require very explicit and specific sample preparation as a pre-condition towards employing such highly proficient equipment. For example thin specimens of 30 nm thickness are required in the form of wedges or pillars, called ‘TEM-slices’ – for TEM/STEM and

*Theoretical simulation performed by Prof. Goedecker et al. in Uni Basel.

LEAP analysis. In the next chapter we will learn about preparation of all the different samples with their specific geometry necessary for the various measurements.

The MH-DFT is suited to span the whole range from basic to applied research and we will discuss further in details in the upcoming chapters (theory section).

*Theoretical simulation performed by Prof. Goedecker et al. in Uni Basel.

Chapter III

Sample preparation TGO/pTGO

"By the help of microscopes, there is nothing so small, as to escape our inquiry; hence there is a new visible world discovered to the understanding."

Robert Hooke

Summary

Within this chapter the various sample fabrication techniques for the passivated and non-passivated thermally grown oxides will be explored. Along with the preparation of interface specimen, the preparation of samples for AFM and Raman Spectroscopy will also be discussed. For TEM/STEM and LEAP, samples with very specific geometry, interface architecture and thickness are required as the high resolution images and the analytical results completely depend on these parameters. Hence sample preparation steps are crucial and play a significant aspect in obtaining meaningful results.

III.1 Introduction

Controlling interface architectures and dopant profiles with minimal defect densities on the nanometer scale is of eminent importance to advance the efficiency, reliability and device integration efficiency of semiconductor technologies, in particular to alleviate the current limitations of power semiconductors and SiC-Metal Oxide Semiconductor Field Effect Transistor (MOSFET) devices. The first step would be to have a single crystalline SiC wafer and then develop a fabrication process for defect free gate oxide towards MOSFET.

Growth of single crystalline SiC: It was Lely who obtained single crystalline bulk SiC from sublimation growth technique in 1955 [52]. A graphite crucible with SiC powder was heated to 2500 ^{o}C for its sublimation. Governed by a temperature difference, there is a mass transport between outer and inner part of the crucible of these sublimed species and recrystallization of the single crystalline platelets occurs. These high quality platelets are then used as a seed for other growth techniques. Later Tairov and Tsvetkov developed the seeded sublimation growth[53] and it is till now the most used technique. Also, depending on whether it is a Si or a C face nucleate for the bulk growth it will be either a 6H-SiC or 4H-SiC crystal respectively.[54]

For device manufacturing the crystal faces of SiC used are the (0001) Si-face, the (0001) C-face or the (1120) a-face. For the Si-face: it has 100% Si atoms, for the C-face: it has 100% C atoms whereas the a-face has 50% of each.[55] Because of the largely different surface termination layer, the oxidation rates and interface properties become different for each of the faces.[54] For the Si face, SiO_2 is thermally grown on SiC, this is one of the reason for which it is the best successor for silicon technology as the already developed tools can be directly reassigned and used for its processing. “Dry” oxidation of SiC for oxide growth happens at 1150 ^{O}C, this high temperature is a requirement in order to grow oxides faster. This is because the oxidation is almost 10 times slower for Si-face in SiC than on Si (100). Whereas, the oxidation is 5 times slower for the C-face of SiC.

*Theoretical simulation performed by Prof. Goedecker et al. in Uni Basel.

The kinetics of the thermal oxidation of SiC relates to the complex oxidation at the interface which requires removal of carbon:

$$2\,SiC + 3\,O_2 \rightarrow 2\,SiO_2 + 2\,CO \qquad (1)$$

Development of SiC MOSFET: The fabrication of MOSFET includes contacting the source, drain and gate electrodes. In hindsight there are resemblance between the established Si-based technology and the SiC technology. The biggest challenge for SiC technology however, is its low channel mobilities for MOS-devices.

III.2 Scope of Investigation

Although passivating effects have been achieved by post oxidation annealing treatments the performance of SiC MOSFETs remained limited. To assess the problem a multi-technique approach for the atomic scale investigation has been chosen. The sample preparation is of utmost importance as the conclusiveness of the experimental data obtained by different high resolution microscopes and spectroscopes is completely dependent on the sample preparation including its thickness, height, position and orientation.

III.3 Sample Preparation

To investigate the near-gate oxide interface region, thermal SiO_2/SiC interfaces have been fabricated within a planar Metal Oxide Semiconductor (MOS) capacitor according to a standard manufacturing procedure using oxygen at 1150 ^{O}C, these samples are referred to as TGO for Thermally Grown Oxide. As a reference we also investigated pTGO (for Passivated Thermally Grown Oxide) oxidized in passivating N_2O atmosphere. The 50 nm thick SiC/SiO_2 epilayers were grown on 4H-SiC wafers with 4^{O} off-cut from the same boule by Ascatron, Kista, Sweden. The SiC wafers were exposed to a pure oxygen atmosphere at 1150 ^{O}C for 9 hours for the TGO sample and N_2O at 1250 ^{O}C for 14 hours for the pTGO sample. The samples used for all the experiments in this thesis are TGO and pTGO which are referred in Mikhaylov et al's work as DRY and TGO respectively.[56]

*Theoretical simulation performed by Prof. Goedecker et al. in Uni Basel.

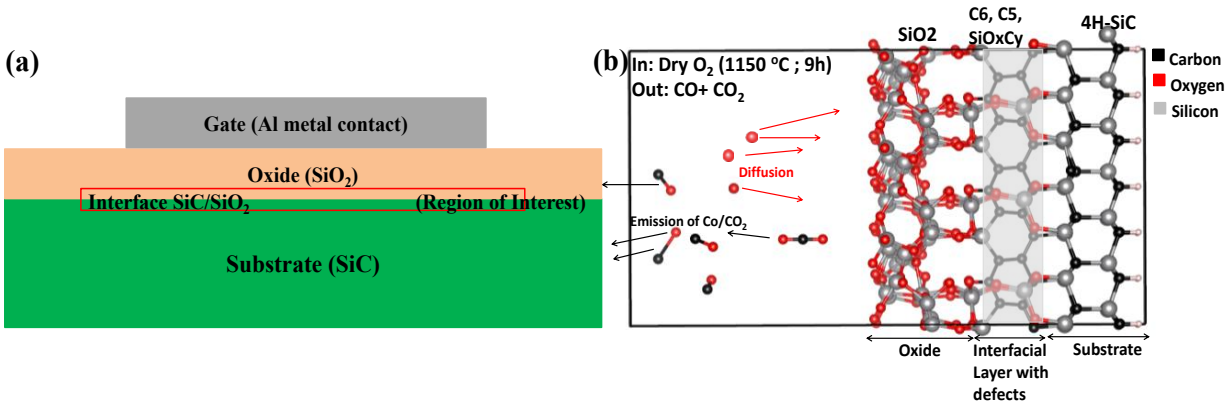

Figure III.1. Role of thermal oxidation to fabricate the gate oxide in SiC power devices (a) Schematic of a basic gate structure with the interface marked as the region of interest. (b) Schematic representation of the thermal oxidation process for SiC at 1150 ^{O}C: In the presence of O_2 diffusive mass transport leads to the progressive oxidation of the carbon in SiC to CO and CO_2. This carbon oxide diffusion via the growing SiO_2 layer becomes difficult as the oxidation continues and a thicker SiO_2 layer is formed leading to defects in the interface or gate oxide near channel region reducing the carrier mobility for the MOSFET device.

III.3.1 Samples for AFM and Raman:

For our experiments the top layer contacts of the fabricated MOS capacitors were stripped off after their optical and electrical characterization for quality control. This was performed by using a standard etching solution followed by a subsequent SiO_2 removal cycle in 2% HF bath. The duration of this HF exposure was systematically modified and controlled in order to analyze the effect of the progressing etch process. The standard etching solution used to remove the oxide contained nitric acid (HNO3), 7% hydrofluoric acid (HF), and acetic acid CH3COOH) (HF : HNO3 : CH3COOH in ratio 5 : 1 : 12). The typically used etching time was 2 mins (and 3 mins extra to further remove nucleates on the TGO sample) for all samples.

We then used room temperature AFM to investigate the MOS capacitor interfaces that have been prepared by stripping the oxide off as just described, thereby exposing the misoriented 4° off (0001) Si face of the SiC below the SiC/SiO_2 interface.[57]

For Raman analysis we used samples with and without removing the top layers for both TGO and pTGO and focused the laser at the concerned region of interest. The absorption of light at 532 nm in SiC is negligible; hence getting a reasonable signal was possible even after focusing the laser inside the sample. Consequently, Raman scattering (scattering of a photon by molecules which are excited to

*Theoretical simulation performed by Prof. Goedecker et al. in Uni Basel.

higher energy levels) for a laser focused at the interface provides interface information; whereas the spectra after setting the laser focus within the bulk SiC will be dominated by the two-phonon bands from the pure SiC substrate with a negligible interface signal. For SiC the depth of focus is >10 µm[58] and our samples were analyzed by moving the focal point from 0 µm to +5 µm.[59]

III.3.2 Samples for S/TEM:

For STEM we need uniformly thin samples with a uniform thickness of 30 nm or less which were prepared using a Focused Ion Beam (FIB). Before preparing lamellae the region of interest had been protected and capped using Pt or C of thickness around 50 nm. This also helps to reduce the curtaining effects which are a very common problem during preparation of thin lamellae with layers of different chemical composition. The curtaining artifact occurs when the FIB-sputtering rates are different at different locations and produces striations across the milling face and thus the specimen will no longer have uniform thickness for detailed quantitative image analysis. Thin lamellae were milled with a focused-ion-beam of Ga at 30 kV with different currents and the final current being 80 pA to 15 pA. The dual mode was used to image the samples using SEM at 5 kV and final milling imaging was performed at 2kV. while milling the sample consecutively. Since the sample had different layers and the etching rates were not constant some bending is inevitable. So with caution and precision samples were thinned down to 40 nm which was later confirmed using EELS.

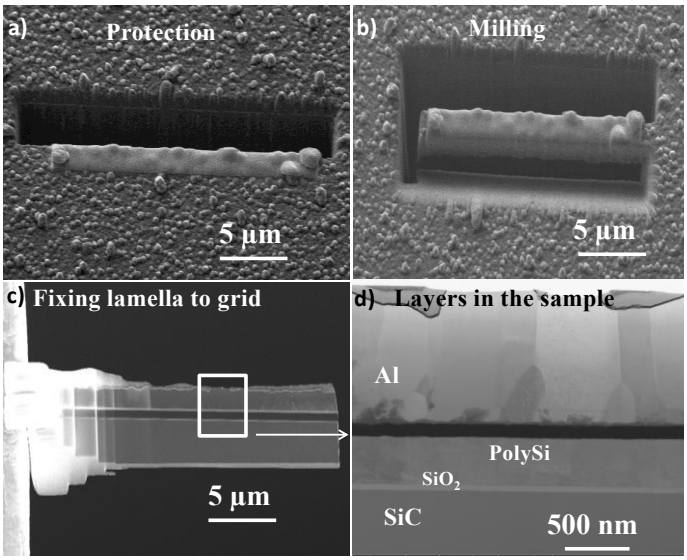

Figure III.2 The steps for preparing lamellae for TEM/STEM. a) The area of interested is protected using C or Pt followed by b) milling using ion beam and finally lifting the sample using a manipulator and c) attaching it to the TEM grid. Final thinning is done using ion beam and then Nanomill where Argon is used as the ion source so it is much gentler than FIB with Ga ion source. d) Shows the different layers of the sample and the region of interest being the SiC/SiO_2 interface.

Subsequently, the samples were further thinned and finally cleaned using the

*Theoretical simulation performed by Prof. Goedecker et al. in Uni Basel.

Nanomill system. The lamellae was nanomilled using 900 eV followed by 500 eV for 10 mins each on both sides of the wedge. The orientation of the lamellae was chosen to be orthogonal to the surface steps.[60]

III.3.3 Samples for LEAP:

LEAP specimen should be needle shaped with diameter of maximum 40 to 50 nm. This is done by taking a cross section through the MOS-capacitor by FIB milling as described above; Needle of 50 nm diameters was fabricated using annular milling where different layers of the MOS capacitor along with their corresponding thickness were visible. The region of interest was chosen to be close to the tip to obtain data faster that is why the final LEAP specimen contains only SiC/SiO_2 with a small cap of Poly Si on top.

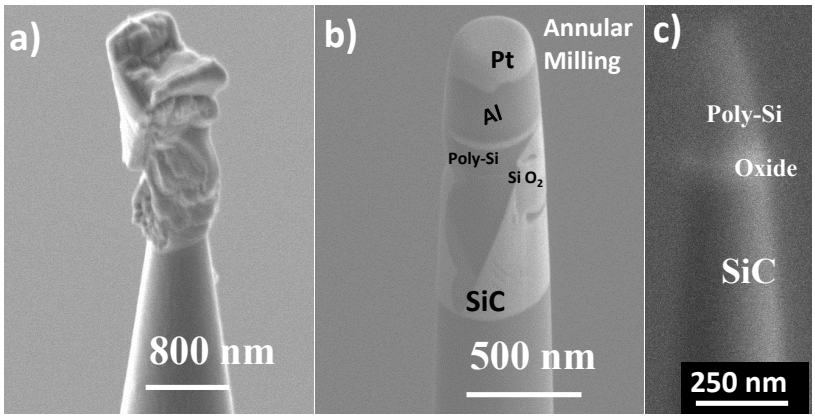

Figure III.3 steps on how LEAP pillars are prepared. a) The wedges are placed on LEAP compatible sample holders and fixed. b) The sample is further thinned into the needle shape using annular milling where all the different layers of the sample are visible. c) Finally the required diameter of 50 nm is reached with the region of interest being very close to the top.

III.3.4 Samples for theoretical simulation:

The investigated structures are in most cases derived from structures constructed by hand or are the result of a short quenching molecular dynamics run. In such approaches, relevant structures which are characteristic for a certain type of interface and its electric properties can easily be overlooked. The situation for defects is similar where most defect structures were found by trial and error and even simple defect structures were overlooked for decades.[61-63] In the present day, the situation has drastically changed.

*Theoretical simulation performed by Prof. Goedecker et al. in Uni Basel.

Minima hopping method (MHM)[61, 64-65] simulations were performed using the MINHOCAO package based on the DFTB[66-68] scheme to evaluate the potential energy landscape. The MHM is a highly efficient algorithm to identify the ground state structure of any condensed matter system by sampling the energy landscape, based solely on the information of the chemical composition. Short molecular dynamics escape steps are performed to overcome energy barriers while exploiting the Bell-Evans-Polanyi principle in order to accelerate the search[69] followed by local geometry optimizations. The structural searches were conducted with surface slabs with supercell sizes of 1x1 and 4x4, scanning several hundred different structures. Initial SiC/SiO_2 structures were randomly allowed to generate in an unbiased way. The surface model was constructed with a 10Å vacuum gap perpendicular to the surface. The atomic structures were relaxed until the forces on the atoms were less than 3 meV/ Å and the stresses were less than 0.1 eV/ Å. The normal modes were calculated using the DFTB scheme.

III.4 Inference

The sample preparation is time consuming and very difficult because of the different layers with different etching rates. Hence maintaining a uniform sample thickness and avoiding bending for the layered specimen is complex. After learning about the various sample preparation techniques we shall now concentrate on how to investigate them near our region of interest.

*Theoretical simulation performed by Prof. Goedecker et al. in Uni Basel.

Chapter IV

Atomistic analysis of SiC/SiO_2 Interface to find C-defects

"A picture is worth a thousand words. An interface is worth a thousand pictures."

Ben Shneiderman

Summary

The key to the mobility enhancements is the identification of the defects along with their origin and discovery of further new or improved passivation methods to conciliate the interfacial defects. In this chapter we present thorough investigations and unique concerting evidence supporting the presence of interface defects in the form of carbon nucleates, due to the complex thermal oxidation of SiC during the gate oxide fabrication.

IV.1 Introduction

In SiC MOSFETs, the inversion channel significantly contributes to the total on-resistance. The quality of the interface is thus crucial for device performance as it highly affects the channel mobility. The density of interface states at the SiO_2/SiC interface is at least two to three orders of magnitude higher (~10^{12} eV−1 cm−2) compared to the relatively matured Si/SiO_2 interface.[21]

As reviewed in chapter I and II the quality of the interface is directly reflected in the channel mobility of MOSFETs. Carriers when injected in the ON and the OFF state it may get trapped at the SiC/oxide interface defect states and cause Coulomb scattering. The trap density is critical as it determines the device stability and also reliability. As discussed in chapter II carbon is found to be one of the stable defects at the interface which can be present in a variety of configurations. For example, if we consider a Si-O-Si bridge: the single carbon atom can interfere and form Si-C-Si bond with another oxygen or can form Si-O-C-Si bond linked to a Si atom on a neighboring ring. These defects can be stable in either the neutral state or the negatively charged states. This yields to a "C-cluster" also called "C-nucleate" of around 6 atoms. Such defect have been debated over for decades and plays an imperative role towards improving future SiC MOSFETs.

In this chapter both theoretical and experimental approaches to investigate the atomistic and electronic structure of the SiC/SiO_2 interface have been discussed in order to draw conclusions in view of SiC device technology.

IV.2 Scope of Investigation

As discussed in the previous chapters excess carbon atoms can aggregate to form graphitic clusters at the SiO_2/SiC interface and they can be of different sizes. Depending on the cluster size and the atomic environment the π orbital of these *sp*2-bonded carbon can give rise to different energy levels. For example small C-clusters should give rise to energy levels near the lower part of the band gap whereas large clusters would have graphite-like energy levels in the gap. There can also be a third C-related

*Theoretical simulation performed by Prof. Goedecker et al. in Uni Basel.

energy level near the upper region of the band gap due to 3C-SiC inclusions at the SiO_2/4H-SiC surface.[70-71]

The current scientific literature on the presence or absence of certain defects is overall inconclusive and partially contradictory. There are reports concluding that carbon clusters may be present while others conclude that near interface carbon clusters are just myths and that it is the interface roughness which plays a vital role in reducing the mobility in SiC device. Hence both theoretical and experimental investigations are of immense priority for finding the carbon defects.

IV.3 Results and Discussion

For both samples TGO and pTGO, we observe terraces and step bunch areas on SiC in the AFM images, which can be attributed to regions (steps/terraces) with different surface/interface energies.[72-73] The quasi-periodic step like structure is interesting as it looks similar to the surface morphology after step-flow[74] like growth processes,[75-76] but occurs here below the surface, at the oxide/SiC interface. Analysis of the AFM data reveals that the step-bunched areas vary in height.[77-78] Single step heights are in the order of ~0.75 nm while the larger step bunched areas exhibit a step height of ~1.5 to 3.5 nm, close to the size of one 4H-SiC unit cell (4 bilayers along the 001 direction).

(The work in section IV.3.1 to IV.3.3 is submitted to APL)

IV.3.1 Visualizing the C-defects at the interface:

The most striking characteristics of the AFM micrograph of the oxide stripped TGO interfaces are the clearly observable nucleates (size ~2 to ~6 nm) arranged like arrays of pearl necklaces. These are small particles, nucleates, which are especially apparent in the AFM images after the first oxide removal and cleaning cycle (2 mins, 2% HF) (Figure IV.1a) and are frequently, but not exclusively, located on the bunched step areas. After a second cycle of HF cleaning for another 2 mins, the number of these nucleates declines drastically (Figure IV.1b). In contrast to the TGO samples, the wafers oxidized in N_2O i.e., pTGO show a clean surface morphology with virtually no etch resistant nucleates present on the interface after oxide stripping (see Figure IV.1c). It is well known that

*Theoretical simulation performed by Prof. Goedecker et al. in Uni Basel.

oxidation in a passivating atmosphere like N_2O produces interfaces with less electronically active defects.[79] It is, thus, plausible to see significantly less nucleates at interfaces prepared by oxidation in the N_2O passivating agent. This may explain the poorer MOS performance of gate oxide interfaces grown in pure oxygen atmosphere (TGO) compared to the significantly improved, but still dissatisfactory, performance of the N_2O passivated samples (pTGO). The poor performance of the SiC MOS in comparison to Si is thus attributed to the presence of Carbon in the oxidation procedure. The oxidized carbon is expected to diffuse to the surface through the growing SiO_2 layer and to be released as CO/CO_2 into the process gas. The continuous diffusion of C and O during the thermal oxidation process will modify the solid matrix and leaves defects behind that broaden the interface and affect the structural integrity of the SiO_2 and the near-interface region of the SiC.[26] The nucleates present at SiC/SiO_2 interfaces resisted HF etching but could be removed by Ozone. We attribute the behavior to the fact that the nucleates are carbon clusters, an observation in our own findings (chapter V) in agreement with an earlier report.[40, 80] The strong dependence of the observed nucleate density on the oxidation process rules out that the nucleates originate from imperfections in the SiC wafer, since the wafers are from the same batch.

In order to provide a better microscopic understanding of the defects occurring during the thermal oxidation of SiC, we have performed atomistic simulations based on advanced structural sampling algorithms. We employ the Minima hopping (MH) structure prediction method [61, 69] together with the Density Functional Tight Binding (DFTB) scheme[66-68] to explore the complex energy landscape during the oxidation process. To this end, we use two different chemical configurations to model two distinct conditions during the oxidation process. In model A, we provide a larger amount of oxygen (more than the oxygen required to convert the topmost layer into a stoichiometric SiO_2 pattern) at the interface than required to oxidize the first surface layer, which corresponds to a one-step oxidation process. In model B, we create an oxygen deficient reaction environment to mimic a two-step oxidation process. Thereby, the surface is first oxidized with half of the oxygen required to convert the topmost layer into a stoichiometric SiO_2 pattern before more oxygen is added.

*Theoretical simulation performed by Prof. Goedecker et al. in Uni Basel.

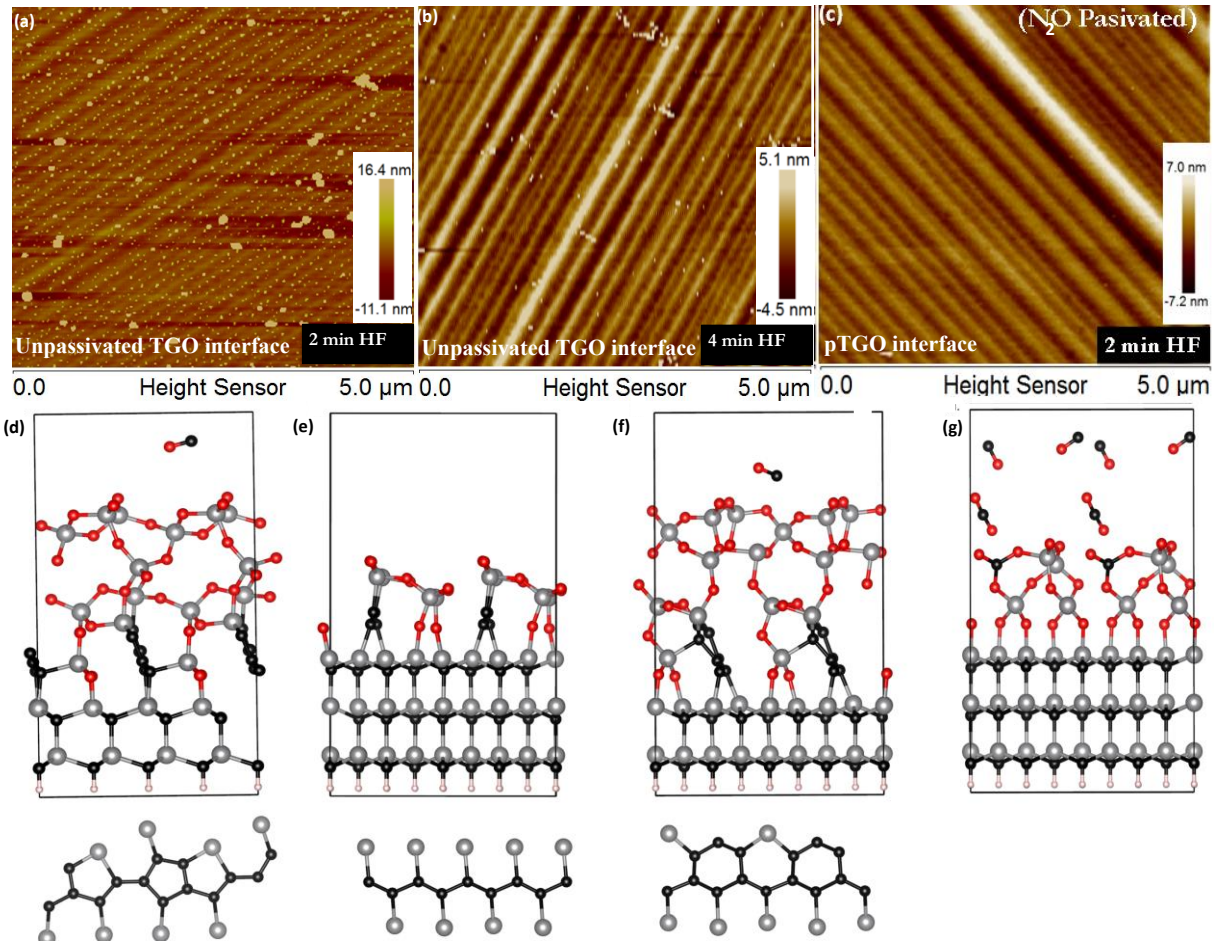

Figure IV.1. Etch dependent Atomic Force micrographs and MHM simulations evidencing nucleates at the SiC/SiO_2 interface after thermal oxidation: (a-c) AFM images of the interface morphology after oxidation in pure oxygen ('TGO' sample) and passivating N_2O ('pTGO' psample) and subsequent oxide removal using HF. (a) 2 min HF etch for TGO sample: 2 to 7 nm sized etch residues line up at steps. (b) 4 min HF etch for TGO sample: significantly fewer residues persist; (c) 2 min HF etch of a pTGO oxide: Virtually no nucleates are detected by AFM when compared with (a). (d-g) Computationally predicted atomic structures of the interface after oxygen deficient oxidation (model B, see main text) and subsequent oxide removal. The carbon nucleates are anchored via Si to the interface (d-f). Thus, the nucleates are not easily removable by HF, consistent with the AFM observation of high HF etch resistance. Characteristic structural features for carbon nucleates observed in our numerical studies: d) carbon five ring chain. e) Si bound carbon chains $[C-(Si-R)_{2n}]$ f) carbon six ring. g) absence of carbon nucleates in the very initial oxidation stage.

The Minima Hopping Model (MHM) simulations of both models show that the low-energy portion of the corresponding energy landscapes comprise structures which exhibit carbon nucleates in the form of clusters with varying size and geometry. While the oxygen excess (model A) promotes C mobility and results in nucleates both at the interface and within the SiO_2 layer, the oxygen deficient model B produces nucleates predominantly at the interface. The latter nucleates persist even if sufficient

*Theoretical simulation performed by Prof. Goedecker et al. in Uni Basel.

oxygen is provided in a second step. The structural features of the carbon nucleates are similar in both models, and consist of characteristic five (C5) and six (C6) membered rings. In presence of sufficient oxygen (model A), these carbon rings form covalent bonds to the surrounding Si atoms in the SiC and/ or SiO_2 matrix (Fig. 2d). On the other hand, the oxygen-deficient model B leads initially to chain-like carbon structures, which subsequently convert in a second step to interlinked chains of carbon rings as the MHM simulation progresses (chains of C5 (Figure IV.1d) or of C6-rings (Figure IV.1f), and zig-zag carbon chains [C-(Si-R)2]n (Figure IV.1e)). These chain structures exhibit an especially high energetic stability at specific interface sites: the periodic silicon carbide matrix anchors/passivates the chains and ribbons from the bottom, while the Si atoms from the SiO_2 layer bond from the top. Occasionally the simulation finds cases where the carbon atoms contained in the unit box do not nucleate (Figure IV.1g), but form merely CO and CO_2 as the oxidation products.

The simulated C5 and C6 clusters readily represent the initial stages of the nucleation and growth process resulting in the HF etch resistant nucleates with a certain carbon content.[81] Figure IV.1d-g shows how the nucleates form in the initial state of the oxygen deficient oxidation (model B). The C nucleates are attached to the SiC matrix in agreement with the AFM results. Figure IV.2c-h shows the C nucleates formed after further oxygen was provided in the second step (model B). In this case the nucleates are not only present at the interface but move into the SiO_2 as well. In our AFM data we observed the etch resistant carbon to preferably nucleate at or near SiC steps, thereby extending the pre-existing nucleates into larger structures while maintaining contact to the growth front of the interface as it moves deeper into the SiC wafer. Thus, the observed 2-5 nm sized nucleates emerge from the thermal oxidation as it progresses into the wafer. The pearl necklace morphology indicates that certain interface features, e.g., step bunched areas may also play a role.

IV.3.2 Chemical analysis for unwanted C-bonds at interface:

A conclusive determination of the structure and composition of these nucleates is not possible based solely on the previous results. Hence, we use second order Raman spectroscopy to analyze the binding of the different carbon species in the near interface region. Depending on the focus setting and on the

*Theoretical simulation performed by Prof. Goedecker et al. in Uni Basel.

focus position with respect to the interface, this technique allows us to distinguish different regions below and above the interface within micrometer scale resolution. The Raman spectra contain the integral signals from the structures present within the interaction volume of the focus spot. Our system's spot volume is at most 2 µm wide and 3 µm deep and we focused at the interface and +5 µm into the bulk. The signal at the +5 µm focus position i.e. with the focus set within the bulk SiC sample contains insignificant, below noise level, contributions from surface/interface scattering. The bulk signal is of high intensity as the penetration depth of the laser light at 532 nm wavelength into SiC is large. Each spectrum was recorded for 2 min and integrated over 15 measurements. The systematic change of the shape of Raman spectra with changing position of the stage and focus position is clearly shown in Figure IV.2a. The samples used were the same TGO and pTGO after the oxide was removed from the top. To facilitate the identification of the carbon bonds at the interface of SiC, we subtract the background/ reference spectra from the TGO spectra. Two background/ reference spectra have been used for more statistical confirmation: as discussed in detail in Figure IV.2a. The resulting Raman spectrum after the background correction with a clean SiC wafer shown in Figure IV.2b, exhibits ten sharp peaks corresponding to vibrational excitation modes of bonds associated with the different carbon species in different bonding states (Table 1).[58] We identified 10 distinct peaks in the background subtracted Raman data and after comparing them to literature values we found each of them to corresponded to a C-peak which is different from the sp3 carbon in SiC and which should not be present at the interface or inside SiC/SiO_2.[58]

We compared our results with the report by Borowicz et al.[58] to find that Finite size carbon crystals and/or benzene-like rings are associated with the Raman peak at 1477 cm^{-1}. The Full Width at Half Maximum (FWHM) we observe here, however, is broader than observed in typical such bands.[82-84] This broadening might be associated to the very small size of the C-defects in our samples. The main Raman signals associated with carbon bonds in graphite are the D (defective) and G (graphitic) bands characterized by the highest intensity at 1350 cm^{-1} and 1580 cm^{-1}, respectively.[85] Importantly, there is the possibility for the G band to shift depending on the C=C vibrations to higher frequencies of about 1620 cm^{-1}.[86] The graphitic carbon is recognized by the graphitic band or G-band @ 1622 cm^{-1},

*Theoretical simulation performed by Prof. Goedecker et al. in Uni Basel.

corresponding to C-C vibrations of sp2 dimers embedded in an sp3 environment; [85-87] If graphitic carbon structures are present in a similar bonding arrangement as they are observed in amorphous carbon (a-C) this can also induce peak shifts in the G band up to 1570 cm^{-1}. Under these circumstances the intensity of the D band (1350 cm^{-1}) becomes very small or disappears completely. The amorphous carbon is recognized by the virtual absence of the defective graphite or D-band characterized by a peak maximum @ 1573 cm^{-1}.[20, 28-30] This agrees well with our Raman data: the peak maximum here is found at 1573 cm^{-1}. Overall this Raman analysis provides clear evidence for the simultaneous presence of both graphitic and a-C in the vicinity of the interface. The D band is very sensitive to edge defects which are more frequently observed for smaller C-nucleates.

Table 1: Comparison of experimentally and theoretically found Raman signals with literature values and the corresponding, most plausible undesired/defective carbon bonds

Experimental Results	Theoretical Results	Literature Review [20, 28-30]	Association of each peak
1477		1470	benzene related vibrations in finite size crystal
1524	1523	1530 1523	3 coordinated amorphous C; polyene
1543	1530	1554	G band for C film with low sp3 content
1573	1554	1594/1582	G band shift of the graphitic band (1582) due to epitaxial strain for graphene on SiC
1605			aromatic C=C stretching
1622	1622	1622	Aromatic C=C and sp2 dimers in sp3 phase
1653		1660	G band for ta-c
1688	1686	1686	C=C or C=O

*Theoretical simulation performed by Prof. Goedecker et al. in Uni Basel.

1713	1717	1712 / 1720	C=O stretch symmetric stretching carbonyl / Benzene related
1740		1735	asymmetric stretching of carbonyl C=O

Chemical bonds that have been identified in the Raman analysis: (1) threefold coordinated amorphous carbon (a-C) film (1524 cm−1 and 1543 cm^{-1} peaks in the G-band identify amorphous carbon film with low sp3 content), (2) distorted graphitic carbon (possibly peak at 1573 cm^{-1}), (3) sp2 hybridized carbon in C=C or C=O double bonds (peak at 1688 cm^{-1}) and (4) benzene like structures (peaks at 1713 cm^{-1} and 1740 cm^{-1} in the higher wave number regime).

The band centered at 1688 cm^{-1} is attributed to sp2 hybridized carbon in C=C or C=O. The strong band found between 1500 cm^{-1} and 1600 cm^{-1} has been attributed to the G (graphitic) band of amorphous carbon film with low sp3 content. In our case those bands are 1524 cm^{-1} and 1543 cm^{-1} corresponding to threefold coordinated a-C (Figure IV.2b).[84] Bands with a maximum around 1580 cm^{-1} have been identified with the G band for distorted carbon, in our case possibly the peak at 1573 cm^{-1}.[58, 85, 87-88] In the higher wave number regime the peaks at 1713 cm^{-1} and 1740 cm^{-1} are corresponding to the range of benzene-like vibrations.[82-83] The presence of such carbon bonds are further confirmed by the reduction in the number of carbon nucleates after cleaning the oxide stripped TGO samples in Ozone;[20, 40, 80] both in AFM and Raman as well as in a numerical simulations (chapter V). The interpretation of the experimental Raman spectra is supported by the computed frequencies of the normal vibrational modes [Table 1] for all the structures we have calculated using model B, i.e. the two step reaction process, where carbon rings are formed (Figure IV.1d-g and IV.2c-h). Notably, a numerical calculation of the full Raman spectrum is not feasible due to the very large number of atoms. Further, laser heating or quantum confinement may lead to certain shifts in the value between theory and measured Raman peak position.

*Theoretical simulation performed by Prof. Goedecker et al. in Uni Basel.

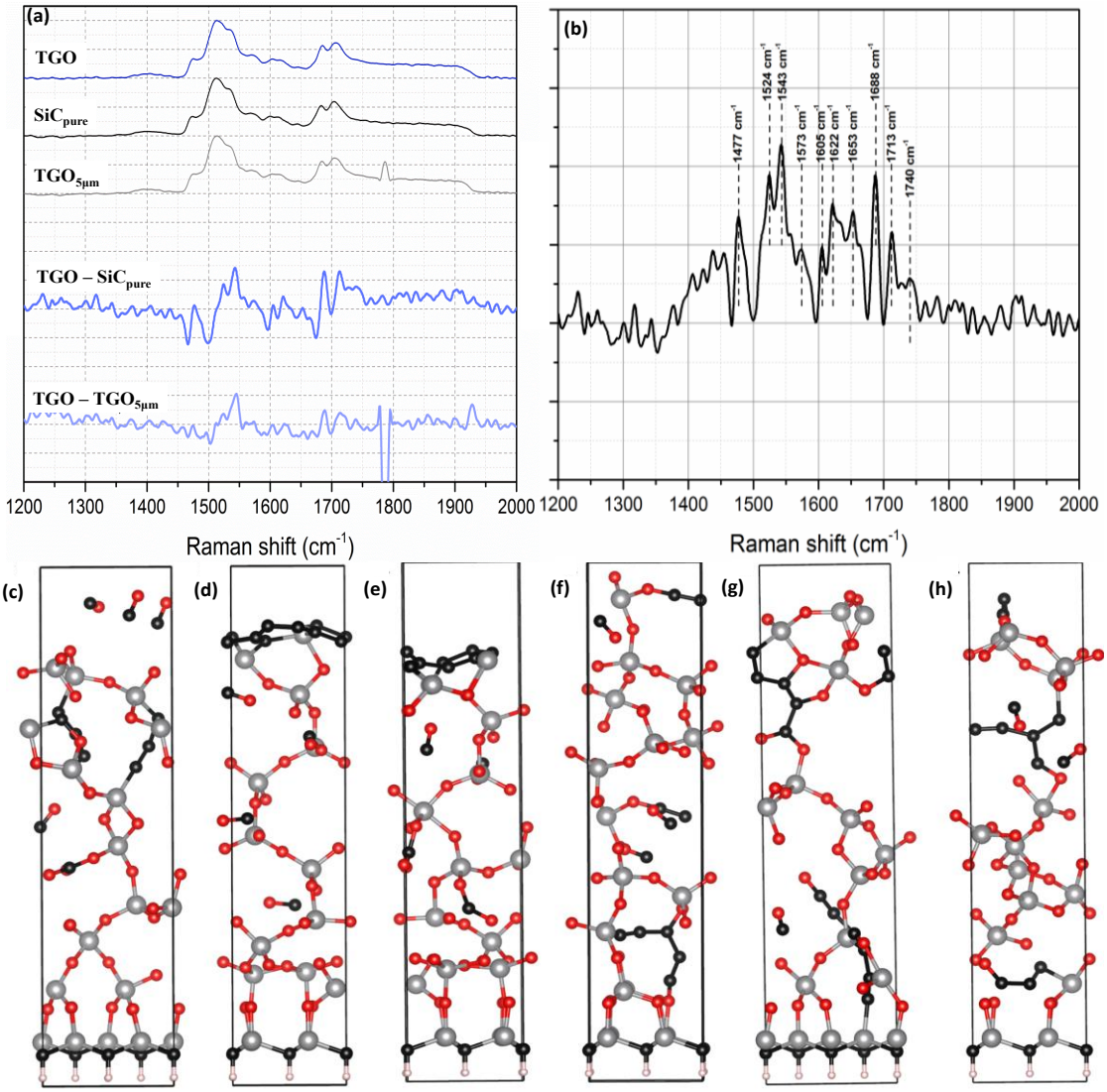

Figure IV.2. Chemical analysis for carbon bond detection at the SiC/SiO_2 interface in comparison to numerically simulated structures. (a) Second order Raman spectrum of oxide stripped SiC/ SiO_2 interfaces for TGO samples fabricated in pure oxygen. Focus is set at the interface position after careful oxide removal using HF etching for 2 mins. The secondary peaks of SiC tend to mask the carbon peaks corresponding to the non-SiC carbon nucleate. Thus the Raman spectrum of unprocessed 'SiC_{pure}' wafer and spectrum taken with a beam focus 5 µm below the interface ('$TGO_{5\mu m}$') have been used as reference for background correction. Raman data after the respective background correction are plotted as (TGO – $TGO_{5\mu m}$) and (TGO – SiC_{pure}) of (a); (b) Baseline corrected TGO – SiC_{pure} with the dominant graphitic peaks labelled between 1440 cm^{-1} and 1800 cm^{-1} (see also table 1); [20, 28-30] (c-h) Computed structures of the characteristic nucleates obtained by an oxygen-rich process. These nucleates and the neucleates from figure IV.1d-g were used to simulate the Raman normal modes of vibration for comparison with the identified experimental data in (b) (Table 1) (c) Carbon nucleate in SiO_2, d) and e) carbon nucleates formed on the surface of. f)-h) carbon nucleate in SiO_2 as well as at the interface of SiO_2 and SiC and also at the surface of SiO_2.

The Raman spectra were calculated with the RAMAN-PY package within the VASP package.

Theoretical values for the Raman Intensities (RIi) of the i-th normal mode have been derived from

*Theoretical simulation performed by Prof. Goedecker et al. in Uni Basel.

Raman active bond vibrations in normal mode using the following relationship obtained from basic Raman scattering theory.

$$R\, I_i = C\,(v_0 - v_i)\, 4 \cdot v_i^{-1} \cdot B_i \cdot S_i \qquad (1)$$

where C is a scaling constant (10^{-13}), v_0 is the argon laser excitation frequency, v_i is the calculated frequency of the I-th normal mode and S_i is the corresponding activity for this mode. The B_i factor accounts for the contribution of excited vibrational states to the intensities:

$$B_i = (1-\exp(-h \cdot v_i/kT)) \qquad (2)$$

in this expression, h, k, c, and T are, respectively: the Planck and Boltzmann constants, the speed of light and the temperature in Kelvin. C=C and benzene related vibrations can be identified from the calculation.

The chemical bonding analysis is done by studying the Crystal Orbital Hamiltonian Population (COHP) as implemented in the Local Orbital Basis Suite towards Electronic-Structure Reconstruction (LOBSTER) code.[89-92] The analysis was based on wavefunctions computed with VASP. For the purpose of identifying the peaks in the experimentally observed Raman spectra, we analyze the vibrational spectrum by diagonalizing the dynamical matrix to investigate the underlying chemical bonds. The selection of the Raman active modes is based on identification of corresponding frequencies in numerical and experimental Raman data in consistency with symmetry considerations. In this way, we can attribute some experimental peaks such as 1523 cm^{-1}, 1622 cm^{-1} and 1686 cm^{-1} to the vibrational modes of 1524 cm^{-1}, 1622 cm^{-1}, and 1688 cm^{-1} respectively [Table 1]. Further, the two distinct modes from our simulations at 1530.18 cm^{-1} and 1554.51 cm^{-1} are close enough to be associated with the experimentally observed 1543 cm^{-1} peak, while the computed mode at 1717.71 cm^{-1} can be identified with the experimental peak at 1713 cm^{-1}.

IV.3.3 Density of State for C- defects near the bandgap:

Density-of-states calculations have been performed for clean interfaces and defect containing interfaces determined from MH runs (Figure IV.3 and Figure IV.4 a). We have considered two types

*Theoretical simulation performed by Prof. Goedecker et al. in Uni Basel.

of defects, a C7-Si ring and a C9-Si ring. The C7-Si ring consists of a pentagonal carbon ring (C5) connected to a 4-ring carbon cluster and one Si atom (C4-Si), whereas the C9-Si ring consists of a 6-carbon-atom ring (C6) connected to a ring made out of a 5 carbon atoms and one Si atom (C5-Si). For C7-Si defect the pentagonal carbon ring consist of both sp2- and sp3-hybridized carbon atoms. In the C4-Si ring, C-C and C-Si bonds are single bonds where these C-C bonds act as a linker between C5 and C4-Si rings and two units of C7-Si rings are connected by a C-C double bond. The carbon atoms are anchored to the Si atoms of the SiC surface (bond length ~ 1.8 Å) and are also bonded to the Si atoms in the oxide. A similar behavior can be observed for the C9-Si ring. In the oxide, a variety of chemical bonds of Si and O is observed. We observe two-fold coordinated oxygen atoms (Si-O-Si) and three-fold coordinated oxygen atoms. Some oxygen atoms change their chemical bonds from three-fold coordination to two-fold. In this transition, however, by changing these chemical bonds around the oxygen atoms, (from three-fold to two-fold coordinated), some silicon atoms inevitably are left with dangling bonds. In order to reduce the number of the aforementioned dangling bonds, these Si atoms bond to carbon clusters.

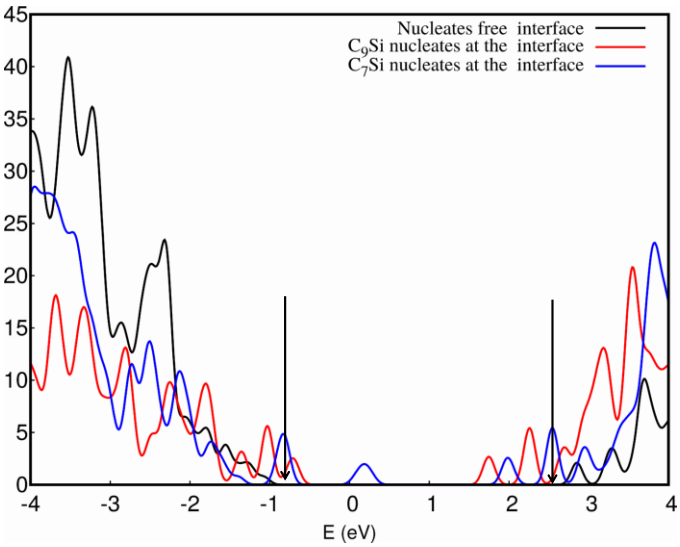

Figure IV.3. DOS of SiC/SiO_2 interface structures with different carbon nucleates: The interface without any carbon nucleates, with 5-atom carbon ring (C7-Si) and 6 carbon ring (C9-Si) nucleates. Initially, in the absence of nucleates the energy gap is around 3.1 eV (the arrow shows the valence band and conduction band edge for the nucleate free interface). New states arise near the valence band edge if carbon nucleates are present at the interface.

*Theoretical simulation performed by Prof. Goedecker et al. in Uni Basel.

Finally, we use Density Functional Theory (DFT) calculations to analyze the electronic band structure of the SiC/SiO_2 interface based on our atomistic model. Most of the previously reported Density of States (DOS) calculations were performed for small carbon cluster doped SiC or linear carbon clusters at the SiC/SiO_2 interface.[50, 93-96] We compute the DOS for the structural models in Figure IV.3 which consist of C-Si rings as defect states and compare them to the DOS of pristine SiC. Figure IV.3 shows that defect states emerge in the band gap of the pristine semiconductor. An atom projected DOS is shown in Figure IV.4, which clearly associates these defect levels to the p-states of the carbon nucleates in the vicinity of the interface. These results support the assumption that the carbon nucleates cause low mobility at the interface due to electronic states in the band gap which are responsible for the deterioration of the interface-near electronic properties.

The band gap calculated for SiC/SiO_2 interfaces depends on the methods used. It is 2.84 eV using the Perdew–Burke-Ernzerhof (PBE) potential; with different hybrid potentials such as PBE0 the band gap is calculated to be 4.1 eV and by using the Heyd-Scuseria-Ernzerhof (HSE) potential it is 3.4 eV. The band gap determined by HSE is significantly closer to the experimental value.[30] Hence all electronic properties were calculated using the HSE06 hybrid functional with the kpoints of 6X6X1. We find that the bandgap of structures which contain carbon nucleates is reduced. There are new states formed near the valence band and some mid-gap states are also observed depending on the nucleate shape.

For 5-ring C nucleates (C7-Si in Figure. IV.3 and Figure. IV.4), the valence band edge is shifted up and the conduction band edge is shifted down significantly reducing the band gap to 2.3 eV. In addition a very stable defect state occupying the mid-gap state appears at -0.5 eV above the shifted valence band edge. The most important contribution for these new states comes from overlapping p_x states between the neighboring carbon atoms in the nucleates. A smaller contribution originates from p_y and p_z states. The occupied levels appear due to the p-p interaction between the nearest neighbor carbon atoms in the carbon nucleate.

For 6-ring carbon nucleates (C9-Si in Figure. IV.3 and IV.4) at the interface, the valence band is shifted upwards by 0.5 eV and the conduction band edge is shifted downward by 1.3 eV. The carbon

*Theoretical simulation performed by Prof. Goedecker et al. in Uni Basel.

nucleates at the interface contributes to the new states, both at conduction and valance band edges. Partially oxidized Si at the interface also contributes to the new states. After analyzing the partial Density of States (pDOS) for all atoms, it has been observed that the major contribution comes from the p_y states of the carbon nucleate at the interface; p_z and p_x also contribute to those states as observed in Figure IV.4. There is no mid-gap state observed in this case.

Different numerical simulations based on different model assumptions for the interface structure show a continuous distribution of states rising towards the band edges.[20-21, 30, 97] The sensitivity of these model calculations is dependent on the energy with respect to the band edges. Therefore, the position of these structures (or even the presence or absence of peaks) should be regarded with some caution. However, most of the experiments confirm a peak at 0.8 eV and at 2.7 eV above the valence band edge. These peaks are consistently observed in our DOS calculations.

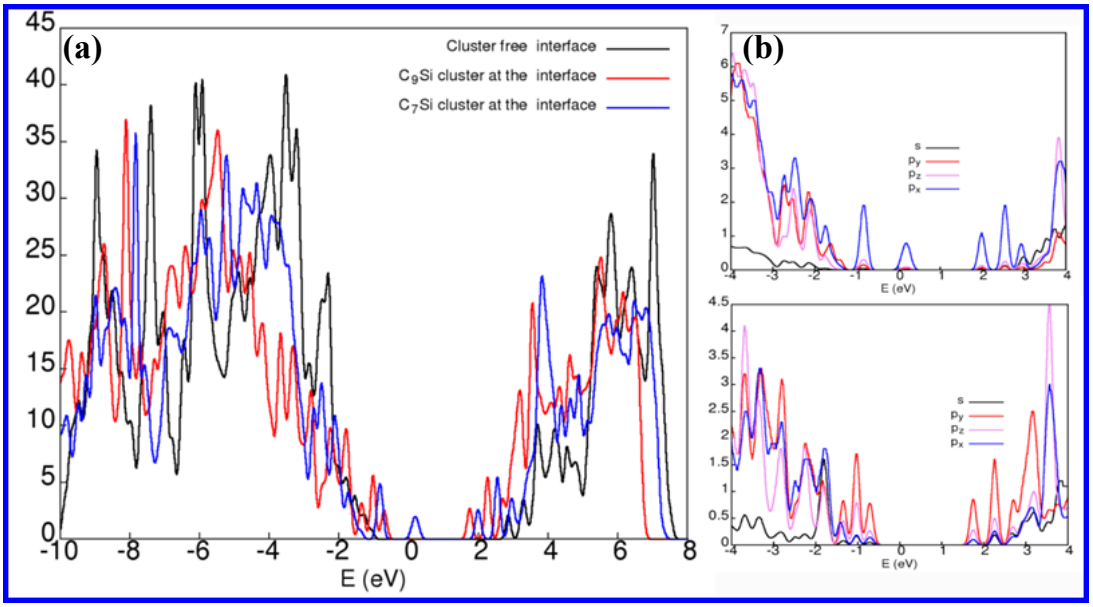

Figure IV.4. a) The density of states (DOS) of SiC/SiO_2 interface structures in the absence of carbon nucleates, with 6-atom carbon and with 5-atom carbon nucleates (denoted as 'clusters' in the legend) located at the interface. In the absence of carbon nucleates the energy gap is around 3.1 eV. New states arise near the valence band edge when carbon nucleates are present at the interface. b) shows the pDOS for the carbon from 5-atom carbon nucleates in the new state. It is emerging from the p_y state of carbon. The s, p_x and p_z orbitals contribute less to the new state. A similar situation is observed for the system comprising a C6 nucleate at the interface (lower panel).

For further analysis of the nature of the bonds, we performed crystal orbital Hamiltonian population calculations implemented in the Local Orbital Basis Suite Towards Electronic-Structure

*Theoretical simulation performed by Prof. Goedecker et al. in Uni Basel.

Reconstruction (LOBSTER) code. Both the crystal orbital Hamiltonian population (COHP) and its integral (ICOHP) were calculated. Negative and positive values of the COHP correspond to bonding and antibonding, respectively. The ICOHP is considered as a measure of bond strength. This analysis showed that the strength of the bonds between carbon atoms in the nucleates and between the carbon atoms and the silicon atoms in the silicon carbide (ICOPH = 6.74) is very similar to the strength of silicon carbon bonds within bulk silicon carbide (ICOHP= 6.63).

IV.3.4 3D chemical imaging of the carbon nucleates:

After having knowledge about the unwanted C-bonds near the interface we were interested in the exact position and size of this C-nucleates. The best procedure in order to have an insight on both of this simultaneously is to have a 3D chemical imaging of the SiC/SiO_2 interface. The atom probe tomography (APT) as discussed before is one of a kind 3D imaging facility where it is expected that the presence of any sub nanometer carbon nucleates can be confirmed.

LEAP disassembles a certain volume of the specimen, in an atom by atom or cluster by cluster mode and analyzes the chemical nature of each piece by Time of Flight Mass (TOF) Spectrometry. Thereby a reconstructed 3D 'tomography' (Figure IV.5) is obtained which reveals the local stoichiometry across the interface, but not the exact atomic structure and bonding. We employed laser induced field evaporation of surface atoms to the tip apex in conjunction with a force field of 10 MV/m. A position-sensitive detector reveals the spatial arrangement of the atoms in all three coordinate directions which in conjugation with the TOF mass spectrometry data leads to the reconstruction of a 3D tomography of the chemical composition of the pillar (Figure IV.5). In LEAP, with the high field of evaporation rate and SiC/SiO_2 phase being insulating there is a high probability of the tip to fracture. Hence to have the highest yield of data from each pillar, the tip was milled in FIB till the region of interest is close to the apex so that data accumulation can be initiated as soon as the sample is placed inside the APT chamber. After the reconstruction of the elemental distribution, obtained from TOF mass spectra, for elements C, O and Si the region of interest is designated.[48, 60, 98]

*Theoretical simulation performed by Prof. Goedecker et al. in Uni Basel.

This is the first time that SiC has been run in LEAP hence it needed many iterations to come to the optimum voltage and the energy of the laser required to start acquisition.

Laser energy = 35 pJ

Rate used = 0.14 %

Pulse rate =146 kHz

Voltage = 6700 V

The field generated at the tip of the needle shaped sample:

$$V/(kR) = 6700/(3.3x0.002) = 1x10^{6}\ V/m$$

Where, K is a geometric parameter

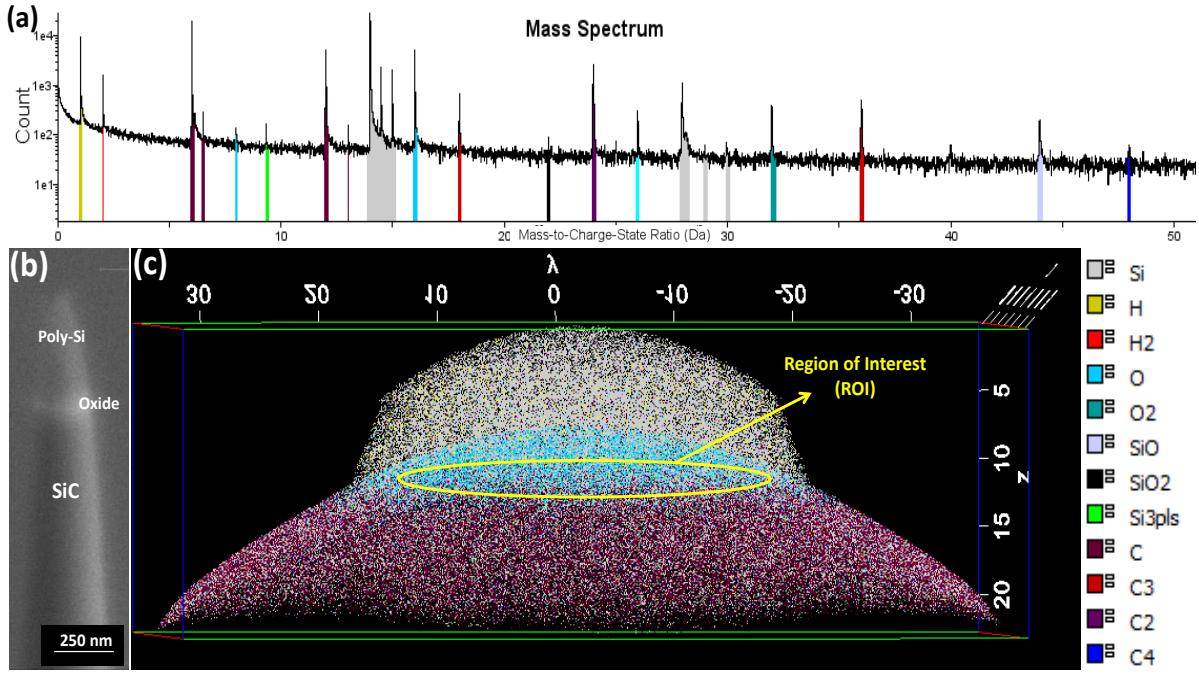

Figure IV.5 Mass spectrum showing the atoms and clusters as they originated from the apex of the pillar during its systematic disintegration in a LEAP experiment. (b) SEM image of the tip showing contrast for the different layers i.e. poly-Si, amorphous oxide and crystalline SiC layers. (c) The reconstructed chemical map of the LEAP pillar which integrates the overall shape from SEM and the chemical information obtained from TOF mass spectrometry. Notably both non-destructive SEM and destructive LEAP need to be combined to obtain such datasets. The Region of Interest (ROI) is the region where few layers of oxide have grown on SiC (*further zoom in Figure IV.6)

The specimen analyzed by LEAP favorably revealed high resolution chemical 3D maps. The transition layer across the interface is wide, ~4 nm thick and the stoichiometry is gradual, not changing abruptly (Figure IV.6). As can be seen in the proxigram of Figure IV.6, O is detected inside the SiC region. This can be an effect of the thermal oxidation at 1150 ^{O}C but could also be the artifact

*Theoretical simulation performed by Prof. Goedecker et al. in Uni Basel.

due to the oxidation of the tip between the FIB preparation and before the tip is introduced in the APT system. The bin box for sampling was chosen to be 0.3 nm^3 which was oriented perpendicular to the interface within the proxigrams and avoiding the surface oxidation region. Using this data, concentration profiles were calculated as shown in Figure IV.6.

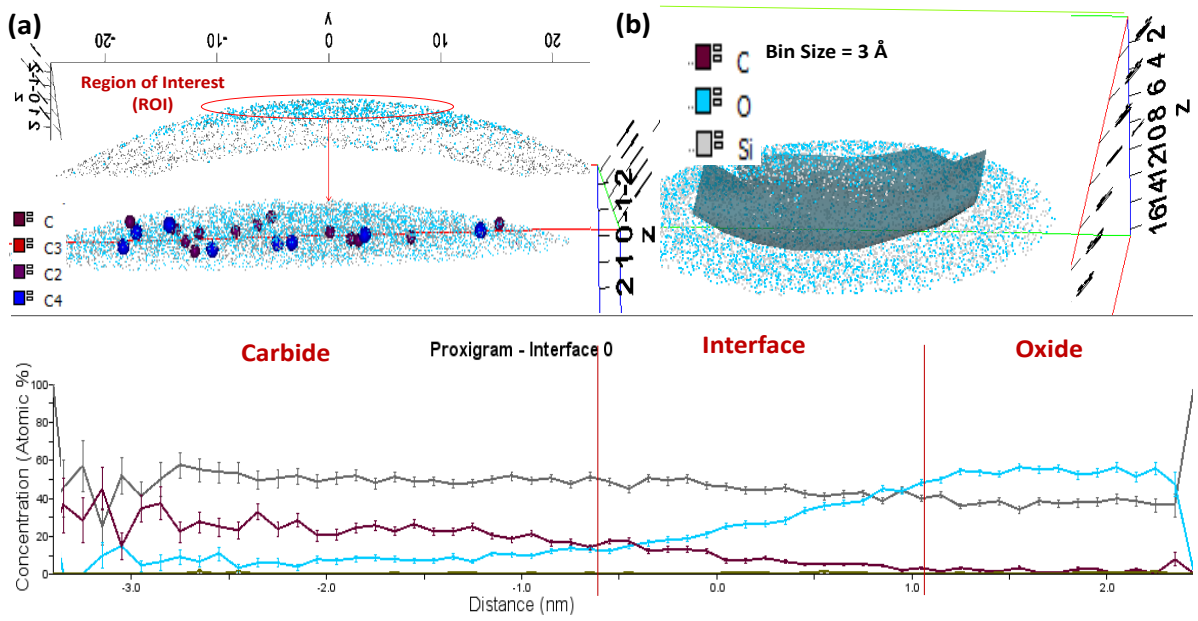

Figure IV.6 Zoomed-in data section of the ROI with the positions of C clusters denoted. The C_4 is quite frequently detected among the other C clusters (b) Isosurface for the oxide layer has been determined at the interface drawn in the ROI. The atomic concentration of C_n, O and Si was analyzed as a function of distance from the isosurface. The interface as identified in this automatic routine extends across 1.5 nm and does not exhibit a sharp boundary. In this region LEAP detects gradually less C_n without showing any sharp peak; hence there is no significant accumulation of average C_n, while there is some evidence that carbon rich areas are occurring at the interface.

Notably the overall C concentration is rather smoothly decaying towards the SiO_2, while C4 clusters are frequently detected in proximity of the interface as recognized by an iso-chemical composition recognition routine (Figure IV.7). After the ROI (Region of Interest) has been designated we create an isosurface which is the surfaces with uniform O concentration marked in Figure IV.6b. By defining the isosurface 1 at the interface and isosurface 2 near the SiO_2/polySi junction (Figure IV.7) the ROI is defined, the atomic % of C were analyzed within this ROI. Various C-nucleates were observed. While C2 and C3 nucleates are very small and can develop due to the migration of C atoms during the fast kinetics occurring in the tip placed in the high field; the detection of C4 clusters close to the

*Theoretical simulation performed by Prof. Goedecker et al. in Uni Basel.

interface however, provide some evidence that C-nucleates near the interface were formed during thermal oxidation of SiC and do not stem from the laser pulse induced field evaporation in the LEAP.

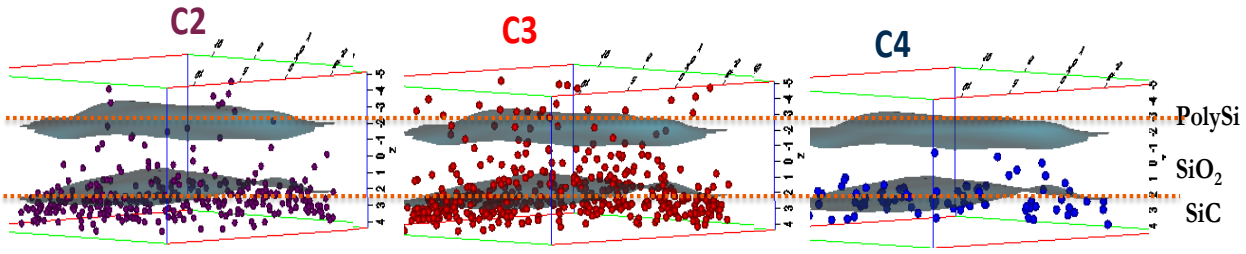

Figure IV.7 The two isosurfaces inside SiO_2 marked. One being at the interface of SiC/SiO_2 and the other one is at the SiO_2/PolySi top interface. The region was analyzed for various C-clusters. Each dot represents a cluster. And as we see along with C2 and C3 clusters, C4 cluster is very prominent and appears only near the SiC/SiO_2 interface.

Further LEAP analysis is currently in progress i) to improve the data acquisition in view of the difficult-to-map SiC/SiO_2 interface and ii) in order to improve the reconstruction parameter sets. Also SiC/SiO_2 being highly insulating sample provides a challenge to be used in LEAP (Chapter III) Insulating material under high fields sparks due to electric discharge. This leads to either bending of the pillar or even breaking of the pillar. To prevent the problems it has been recently considered beneficial to prepare pillars in FIB with different geometry and orientation. Such pillars can be fabricated as follows: Within FIB while placing the sample on the sample holder the tip is rotated 90^{O} using the manipulator and it is placed vertically instead of horizontally as shown in Figure IV.8. Thus LEAP progresses along and not across the interface as the interface now runs along the tip throughout (Figure IV.8). Even if some part of the sample breaks in the high electric field there will always be some interface present along the tip to continue the analysis.

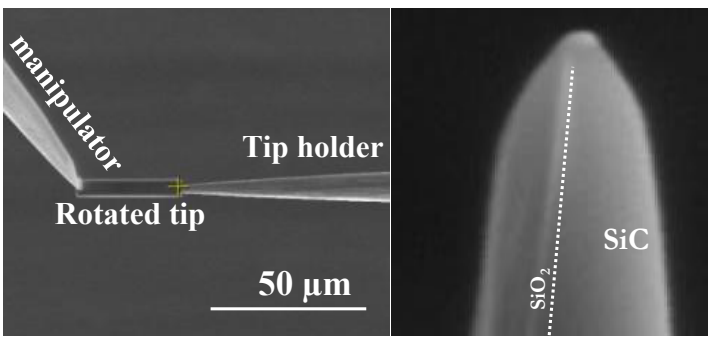

Figure IV.8 The sample is rotated by 90 before placing it on the tip holder. This aligns the interface vertical instead of horizontal (Figure IV.5) The oxide interface runs parallel to the long axis and not perpendicular. This decreases the chances of losing the sample as the charges can distribute now easier than before hence breaking will be less probable.

*Theoretical simulation performed by Prof. Goedecker et al. in Uni Basel.

LEAP is providing the regional composition of a specimen but not atomic coordinates, this stems from the fact that most solids rearrange significantly as the atom-probe process progresses. This obstacle is expected to be less pronounced for 'hard' materials like SiC. The etching rates of SiC and SiO_2 are so different that the sample preparation itself becomes a challenge. Transmission Electron Microscopy (TEM) analysis on the other hand is less destructive than LEAP and thereby can provide insight into the local atomic structure around certain defects as well as about their occurrence. Therefore TEM is considered an important complementary technique to LEAP with regard to understanding the influence of interface defects and specifically C-nucleates.

IV.3.5 Chemical Imaging to understand position and size of the C-defects:

In literature there have been many contradictory conclusions regarding TEM and EELS results. Some claimed observation of a transition layer of 5nm in the [11-20] direction and 2.5 nm in [1-100] direction whereas, in the in-axis the transition layer was claimed to be 2nm (2 pixel).[99] There have also been results evidencing a transition layer of 2nm ± 1, with no sign of C-rich layer at the interface.[98] Although Zheleva et al claimed that in their result O/C profile shows 3 nm C-rich layer in SiC and 4 nm C rich layer in SiO_2 but the data is not very convincing. In all these cases either the resolution of the TEM is poor or the data analysis is not justified in details.[100]

In our measurements, for HRTEM we used FEI Titan 80-300 setup and for EELS the samples were analyzed in Catania (IMM-CNR) with a JEOL ARM200CF (both described in chapter II). Further EELS and HAADF data were verified using FEI Titan G2 80-200 CREWLEY which is a fourth generation TEM equipped with 80 kV-200 kV accelerating voltage, a Cs probe corrector (CEOS DCOR), an in-column dispersive X-ray spectroscopy (EDX) unit (ChemiSTEM technology), an angular dark-field (ADF) scanning TEM (STEM) detector (Fischione Model 3000). The STEM spatial resolution is 0.8 Å and energy resolution is < 136 eV. 300keV accelerating voltage was used for the HRTEM images with beam size of 0.1 nm. Figure IV.9 shows the high step density of SiC. Several regions for each of the samples were imaged for analysis to yield the results in this study. The orientation of the lamellas during FIB preparation was chosen to be orthogonal to the SiC surface

*Theoretical simulation performed by Prof. Goedecker et al. in Uni Basel.

steps. The oxidation happens layer by layer with side step oxidation being faster than vertical oxidation. The high step density also facilitates the side step oxidation. The oxide layer is amorphous and has a uniform thickness.

As can be seen in Figure IV.9, for TGO samples at the interface there are unsatisfied Si atoms. The defects appear most frequently near the step edges and extend to the next atomic layer. Figure IV.10 shows the schematic representing the plausible reaction happening at the step edges leading to defects. In the TGO sample the oxidation occurs at an elevated temperature of 1150 ^{O}C. The step edges are the obvious active reaction sites where the oxidation is initiated and has a strong driving force for the interface controlled transfer of the oxidation of SiC to SiO_2.

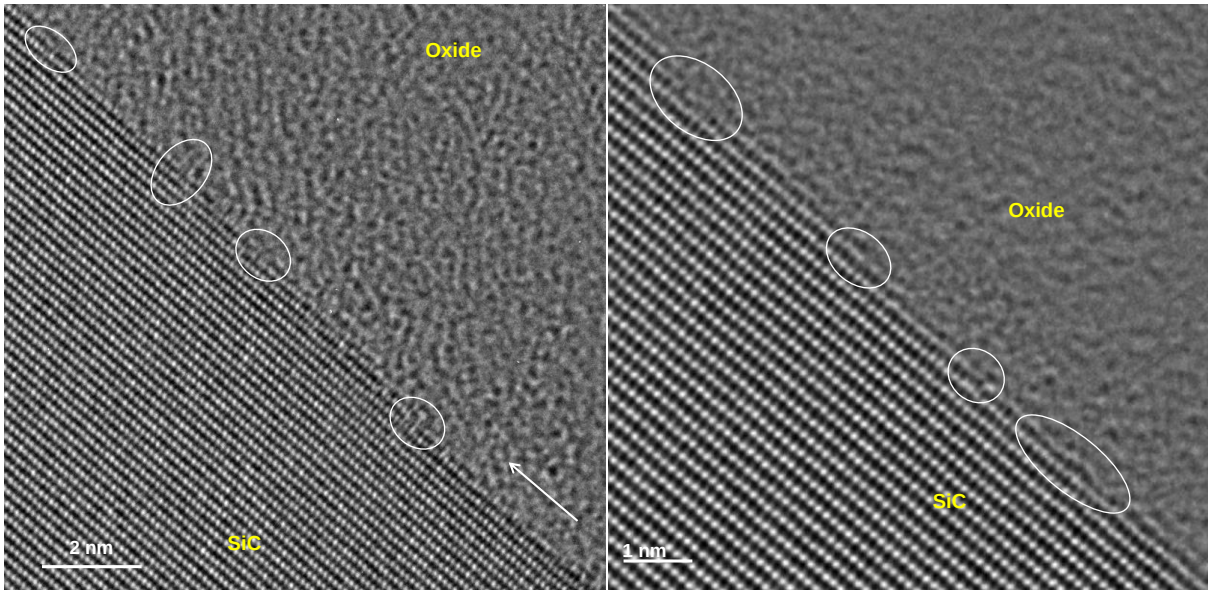

Figure IV.9 HR-TEM image of the interface perpendicular to [0001] face of SiC. Two different regions of the interface are shown with the arrow showing the direction of the oxidation along the steps of SiC at the interface. The marks indicate defective regions at the interface. Terrace edges are most active in the oxidation process as seen from the contrast in SiC atoms (faded atoms) at the interface. The second layer atoms at the step edges also show contrast difference of being faded away as it is affected by the oxidation of the top layer atom. The defects mostly contain Si-Si bond, unsatisfied Si atoms, dangling bonds and partially oxidized atom. As the oxidation of the preceding layer progresses there is mass redistribution mainly at the step edges of the atomic layers causing dislocation of atoms giving rise to strain.

The temperature being high and the oxygen being very reactive it not only oxidizes the first atomic layer at the step edge but the SiC atoms in the second atomic layer gets affected too; thus weakening the atoms of the adjacent layers. This creates a defect in the second atomic layer as can be seen in the

*Theoretical simulation performed by Prof. Goedecker et al. in Uni Basel.

marked regions in Figure IV.9. The Si atoms of the second atomic layer close to the affected region thus have unsatisfied bonds and form defects in the form of dangling bonds or Si- clusters as described in Figure IV.10. This dangling bonds needs to be satisfied for higher mobility which is achieved by passivation.

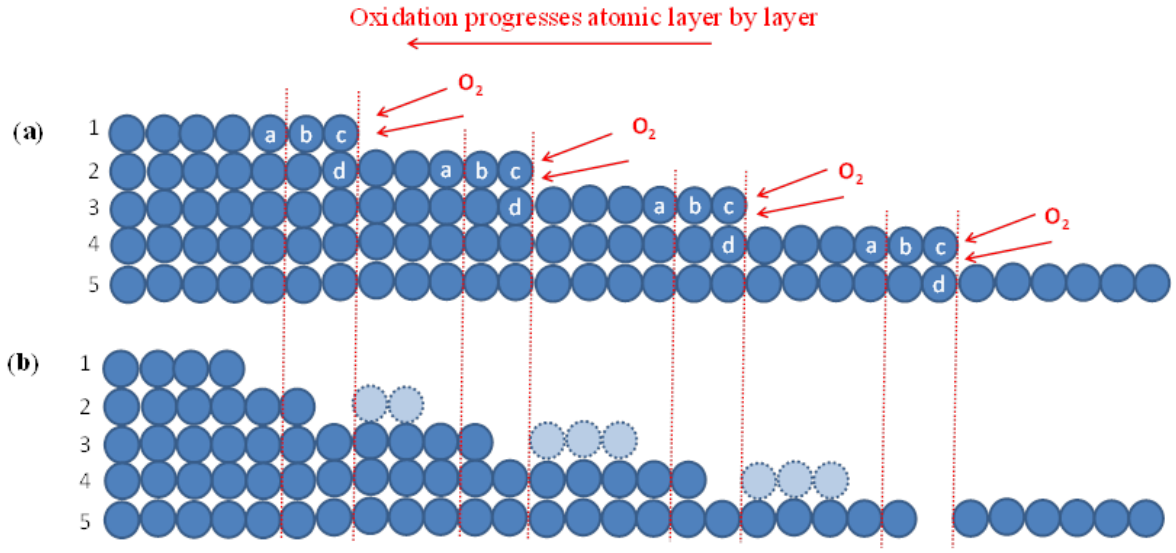

Figure IV.10 The schematic representing the process of oxidation at the step edge. The oxidation progresses atomic layer by layer in the direction as shown. The active oxidizing agents (O_2 for TGO and NO for pTGO) attack the step edges which are the active reaction sites. In a) the atoms a, b, c in atomic layer 1 gets oxidized; the atom d from the atomic layer 2 gets weakened too as it is adjacent to the step edge of the previous atomic layer. The strong reaction thus creates a defect in the atomic layer 2 as can be seen in all the other step edges. Due to this an island of unsatisfied Si atoms is left behind on each of the atomic layer marked as light blue in b). This creates dangling bonds and strain leading to dislocated atoms.

Also for the complete oxidation at the step edges two O atoms and a Si atom redistribution is needed which requires double the volume of a unit cell of SiC (C atom = 4 bonds, O atom = 2 bonds, SiO_2 volume is 2 times the SiC unit cell volume). For this reason the oxidation not only generates many dandling bonds, Si-Si bonds, but also strain. This strain causes dislocations of the Si atoms which are visible and marked in both Figure IV.9 and Figure IV.11. Using Nitrogen during passivation the isolated defects are removed but it surely decreases the number of dangling bond for Si as well thus achieving lower energy intermediate state stabilizing the transition from early oxidation stage until the mass redistribution occurs. Hence in pTGO when N_2O is used instead of pure O such abrupt defects in the atomic layers adjacent to the previous step edge are not prominent. The slower oxidation rate and less aggressive oxidation provides an alternative reason for achieving smoother interfaces than TGO

*Theoretical simulation performed by Prof. Goedecker et al. in Uni Basel.

samples as shown in Figure IV.11. As can be seen the second atomic layer below each of the steps is not affected as much for pTGO and looks different from the TGO samples.

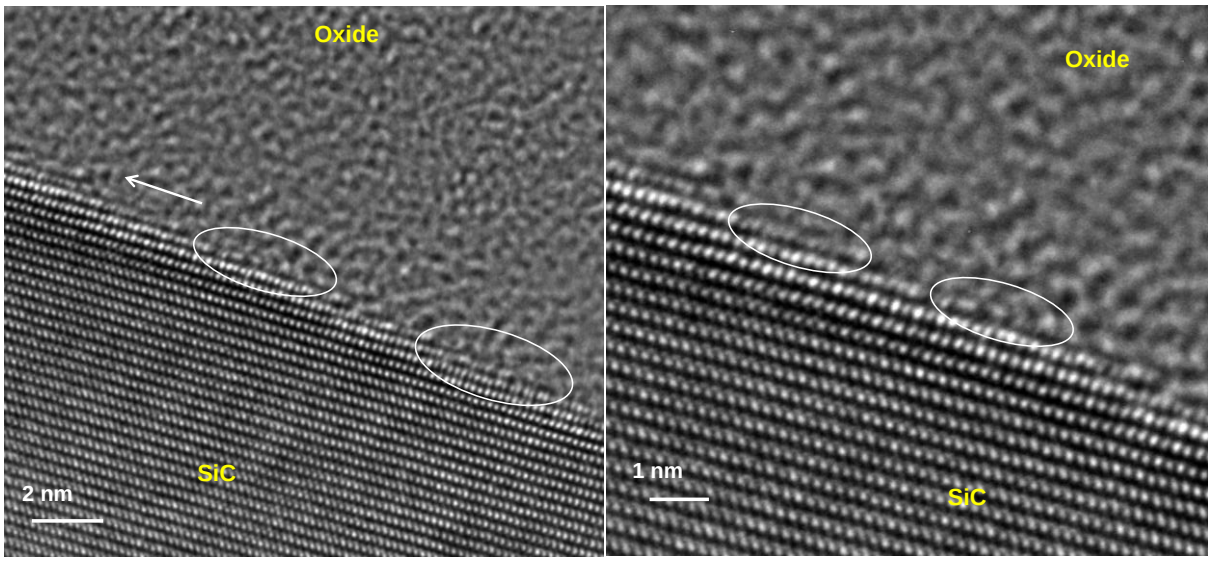

Figure IV.11 The HR-TEM images of the interfaces for pTGO samples. Unlike TGO the sudden defects in the atomic layer below the step edge are lower in number. The marked circles show the partially oxidized Si atoms at the interface in the SiC crystal.

The unsatisfied Si atoms at the interface give rise to dangling bonds as mentioned earlier. This has been proven also with the EELS analysis where Si with different oxidation state (SiC_xO_y) apart from Si^{+4} (SiC/SiO_2) has been identified and marked in Figure IV.12. The spectra has also been compared to Si^0 state and the peak position proves that it is neither pure Si clusters nor Si from SiC or SiO_2. The Si edge shift due to the electron affinity and the intermediate oxidation states appear due to the partially oxidized atoms. The transition layer for the interface was found to be between 3.5 to 4 nm which is in complete agreement with our LEAP data analysis.

Scanning Transmission Electron Microscopy has been used to generate a detailed image of an intact, thin sliced 4H-SiC/SiO_2-interface to prove the presence of the undesired five-carbon clusters as they have been evidenced in our DFTB study. STEM results revealed the presence of C-defects at the interface region where there are no step edges (Figure IV.12). Chemical maps across the interface were obtained in the form of EELS spectrum. An increase in the intensity of the carbon signal was measured at the interface for different samples. The peak position was exactly 0.2 nm away from the interface towards SiO_2 as shown in Figure IV.12. Note that the bond length of Si-C in SiC is 1.87 Å.

*Theoretical simulation performed by Prof. Goedecker et al. in Uni Basel.

Hence the defective carbon atoms present at the interface are covalently bonded to the SiC substrate with a bond length of 2.0 Å (SiC bond length). This also is exactly what we also concluded from our AFM and DFTB simulation results discussed earlier. Thus these defects are not lying freely on the interface but are bonded to Si of the SiC crystal. The signal, though fairly weak, was observed for

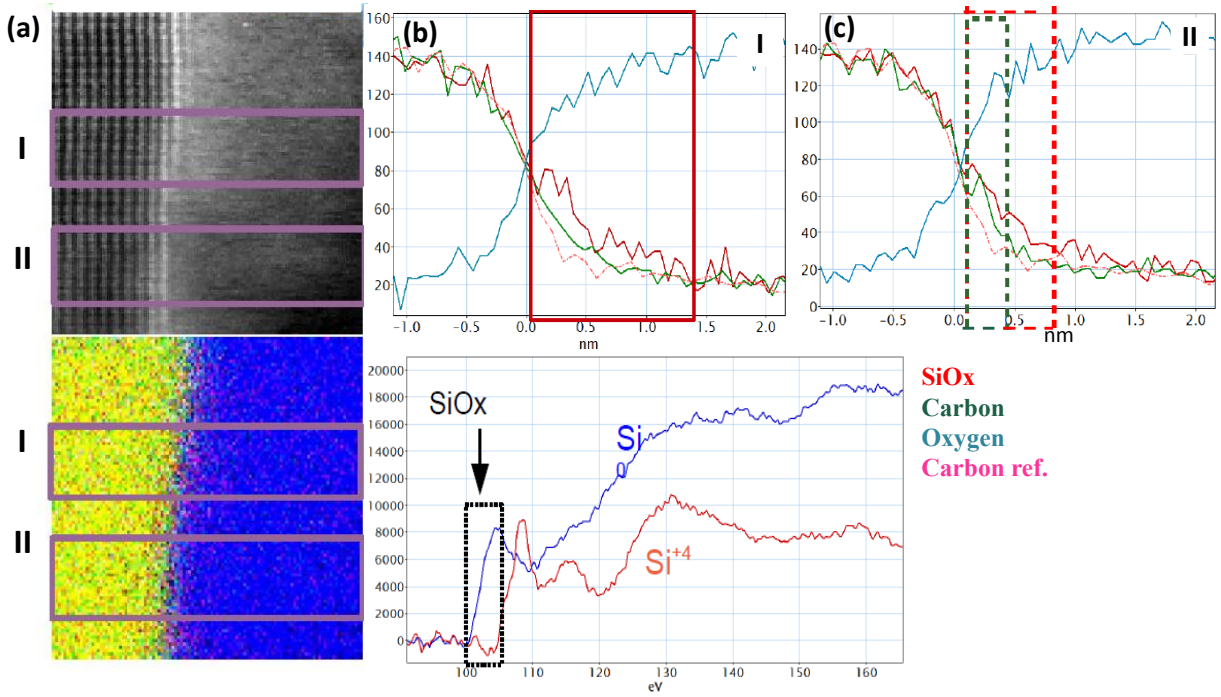

few different samples and always at the same distance from the interface, suggesting a definitive C-defect contribution.

Figure IV.12. (a) The HAADF STEM images of the interface with marked region (I) being the area of the interface containing an atomic step and region (II) containing no steps and step edges. The TEM used has dual EELS option allowing a simultaneous read-out of EDX (shown in the lower panel of a) and EELS signals (b) EELS profile of marked region I shows Si defects at the interface with the increase in signal for SiOx (red line). The lower panel shows silicon edge in SiC and SiO_2 (Si^{+4}). SiO_x signal is related to the unsatisfied Si atoms at the interface giving rise to dangling bonds marked in the black box. Si^0 has been used for a comparison to prove that the peak is an intermediate oxidation state of Si and it neither Si^0 nor Si^{+4}. (c) EELS spectrum of marked region II is enriched in carbon defects and is always 0.2 nm away from the interface.

Resolution in HAADF STEM being high we used it to analyze samples parallel with EDX for compositional analysis and elemental mapping of samples with atomic resolution. The only issue during the experiment was the drifting of the sample. But after drift correction and many iterations of the experiment we found few C-defects near the interface.

*Theoretical simulation performed by Prof. Goedecker et al. in Uni Basel.

The oxide layer as discussed before is uniformly amorphous. But upon thorough monitoring of the amorphous layer near the interface using fast fourier transform FFT, definite but modest changes in diffraction pattern were detected. HRTEM image is built up of the wave function coming out of the sample. So, when we apply the Fourier Transform function to the selected region of interest in the high resolution image we have the diffraction pattern (reciprocal space) showing the symmetry of the "lattice" fringes of the image. The number of frequencies contained in FFT corresponds to the number of pixels in the spatial domain image, *i.e.* the image in the spatial and Fourier domain is of the same size. So FFT would not pick up or show difference in pixel if there is no crystalline structure present. In our result the signal to noise ratio being high, the intensity modulation of the diffraction pattern is thus real in FFT. This can happen only if there is a local ordering or a crystal structure present in the amorphous layer. Although the diffraction signal is weak but it is explicitly distinct hence the ordering present or embedded inside the SiO_2 cannot be few atoms or less than 8 to 10 atoms. This is because FFT cannot be obtained from just one unit cell but it requires repetition of the unit cell to have the diffraction pattern. Also to minimize any redeposition during sample preparation from Ga or SiC and to minimize the effect of Ga damage due to FIB, samples were cleaned in a gentle Ar chamber using Nanomill system for 20 mins. To avoid hydrocarbon which can occur as a contamination before and during TEM analysis, samples were plasma cleaned with an Ar/O_2 plasma at 50 eV for 4 min immediately before inserting in the TEM system. Hence, for these newly prepared samples crystalline structures from either redeposition or other sample preparation effect can be ruled out. The data obtained is essentially due to crystalline structure which are present in the SiO_2 due to the thermal oxidation of the SiC crystal.

Following this, Inverse Fast Fourier Transform (IFFT) analysis was obtained from the diffraction signal. IFFT is the image formation procedure by selecting specific diffraction spots in the FFT. As seen in Figure IV.14 there is a graphitic like structure inside the amorphous oxide in the image plane. IFFT shows the contrast difference in the data due to the atoms but does not show the actual atoms so it is only a filtered image projection. The graphitic flake can be a result of excessive C at the interface which could not leave as CO molecules because it is kinetically limited due to the thick oxide above.

*Theoretical simulation performed by Prof. Goedecker et al. in Uni Basel.

During postoxidation annealing the C trapped at the interface gets enough energy and can diffuse through the oxide. Notably, graphitic structures are the most stable structure known; thus the redundant C gravitates towards forming bonds with each other to forms inter-carbon bonds and eventually graphitic sheets inside the SiO_2.

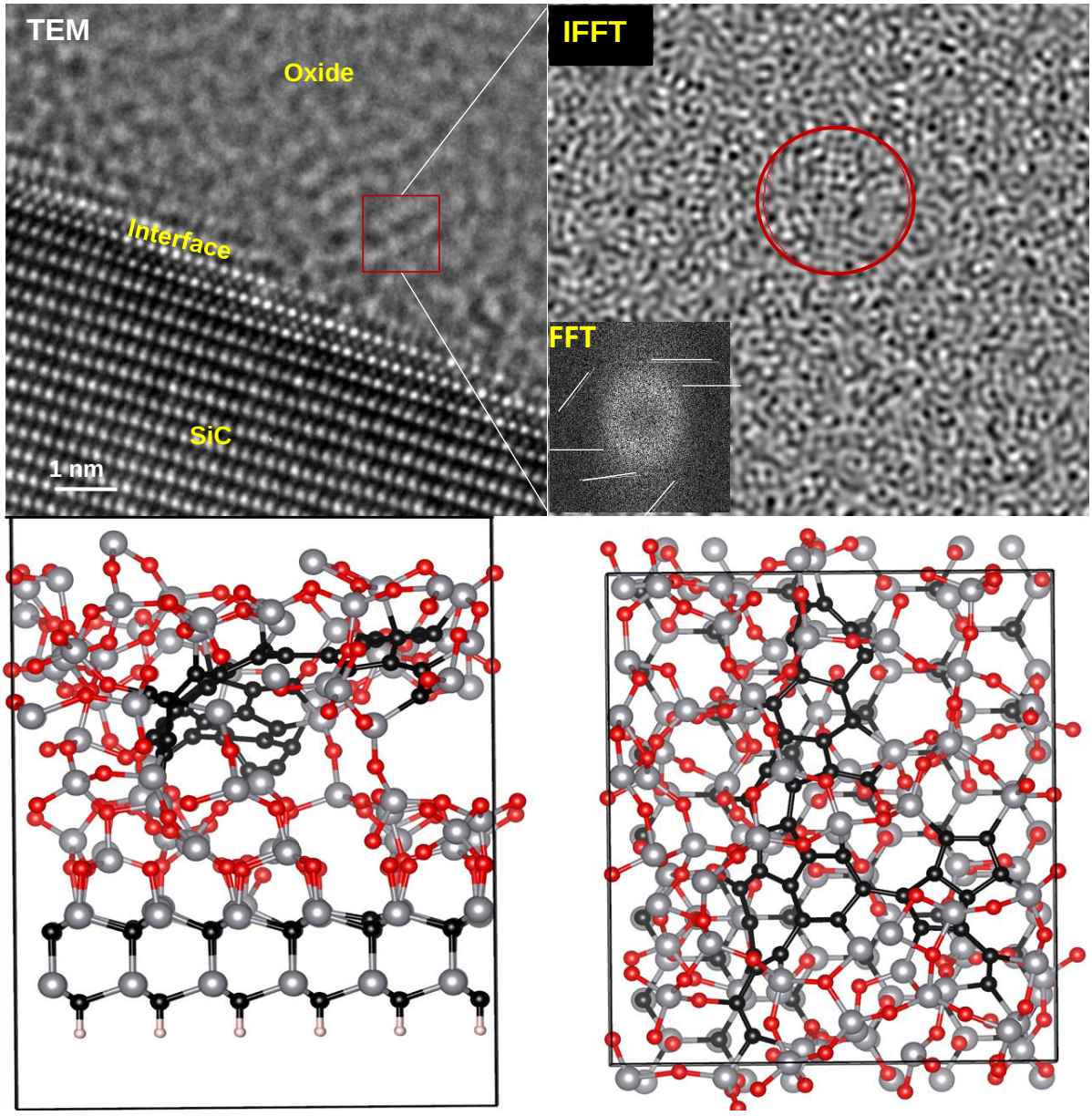

Figure IV.13: The interface as seen in HRTEM is not sharp. After thorough investigation of the oxide near interface using Inverse Fast Fourier transform (IFFT) we found a sheet of C-defects formed by interconnected rings. This observation was confirmed by DFTB modelling. In the simulation the C-defects from the interface break and join as they move into the SiO_2 and form sheet-like structures.

This is exactly the result obtained by the theoretical simulation in Goedecker's group. While trying to understand the bond strength between the C-clusters and the interface the carbon chains were

*Theoretical simulation performed by Prof. Goedecker et al. in Uni Basel.

deliberately pushed away from the interface inside the SiO_2 during minima hopping runs. In DFT, the carbon inside the oxide was found to condensate to form quasi-planar structures as shown in Figure.1V.13. This observation suggested that inside SiO_2 the graphitic like quasi-planar carbon structures are more stable unlike the interface where carbon liked to form nucleate in form of carbon clusters or chains determined by the energy minima of the structures.

IV.4 Inference

In this chapter, the observed changes at the SiC/SiO_2 interface were associated with the complex oxidation at the interface leading to C-defects. C-rich nucleates at distinct locations along the interfaces were identified by AFM, Raman, HRTEM and EELS. The high C levels at the interface are due to the formation of excess carbon during SiC oxidation to SiO_2 because the removal of CO molecules is kinetically limited. Stoichiometric changes were also evident in the SiC layers adjacent to the interface. In order to conciliate these defects improved passivation methods are required which will be discussed in the following chapter.

*Theoretical simulation performed by Prof. Goedecker et al. in Uni Basel.

Chapter V

Relevant parameters for improving the thermally grown gate-oxide interface in SiC

"Quality is free. It's not a gift, but it's free. The 'unquality' things are what cost money."

Phil Crosby

Summary

Extensive efforts have been undertaken to improve the near-interface mobility, e.g., via surface conditioning or passivation of the SiC during interface fabrication. The oxidation of the SiC surface marks the first step towards a passivated surface. Therefore it influences the quality of the SiC/SiO_2 interface greatly and is of enormous importance. In this chapter we discuss on the interface treatment and passivation mechanisms and on how these influence the defects at the interface.

V.1 Introduction

In order to achieve high mobility in thin conduction channels, the number of interface defects has to be as low as possible. In case of Si-based devices this goal has been achieved by passivating interface states, such as, dangling Si bonds by annealing in a hydrogen atmosphere[21, 26, 33] Most of the devices use silicon dioxide (SiO_2) as a passivation layer protecting the device surface and also as gate dielectric. The performance of the SiO_2/SiC interfaces for MOSFETs (and for BJTs as well) has also been improved by various oxidation and nitridation methods.[22, 24]

An inherent property of wide band gap semiconductors is charge build-up in the oxide during device operation leading to oxide breakdown in MOSFETs. As the high power devices operates at higher fields and temperatures there is an increase in tunneling of carriers both from the semiconductor and the metal used as gate. In previous reports, it was disclosed that passivated oxides do not generate interface states when electron injection happens. Similarly, when nitrogen is incorporated at the SiO_2/SiC interface via high temperature annealing it passivates the active defects at the interface, thus improving the inversion channel mobility in the device. As a matter of fact it suppresses the negative charge buildup at the interface states explaining the enhanced negative charge for thermally grown non-passivated oxides.[101-106] This improves the voltage stability of MOS capacitors. Nitrogen incorporation not only improves the mobility but can also improve the reliability. It is however reported that Si/SiO_2 interfaces treated with high N_2 concentration at times contain a higher density of hole traps than thermally grown oxides, which in turn can be detrimental for the reliability of devices. Thus the right amount of N_2O passivation along with the thorough characterization of the oxide and the interface after passivation with nitrogen is crucial in order to bring SiC MOSFETs into commercial applications.[22]

V.2 Scope of Investigation

Silicon carbide received increasing attention because of its potential technological advantage for the fabrication of high-power devices for a wide range of applications. The material properties making it

*Theoretical simulation performed by Prof. Goedecker et al. in Uni Basel.

superior to Si have been reviewed in the previous chapters. Also because of its ability to grow a thermal gate oxide it is a preferred material of choice compared to other wide band-gap semiconductors. The most significant improvement towards SiC MOSFET technology has been the treatment of the interface in terms of cleaning and passivation of the gate dielectric using nitrogen as it resulted in a tenfold reduction of active defects. The atomic-scale mechanisms behind this passivation remain unclear, but reports convey that it removes the excess three coordinated amorphous (polyene) C nucleates.[20, 33, 70, 101, 107-110]

Towards improved near-gate oxide mobilities in SiC devices it is important to investigate the impact of SiC surface treatment either with ozone or HF and most importantly post oxidation nitrogen treatment on the gate oxide. Ideally, the analysis should be conducted on the atomic scale. The role of Ozone cleaning and Nitrogen passivation at the SiC/SiO_2 interface have been investigated using AFM, Raman and also by using simulations performed by Deb Sankar De in the group of the Theory partner, Prof. S. Goedecker.

V.3 Results and Discussion

In chapter IV interface defects have been identified and C-nucleates were detected as a major Near Interface Traps (NITs). Also we compared thermally grown oxide (TGO) with the passivated oxide (pTGO) oxidized in an N_2O environment (Chapter IV). The first remarkable difference is reflected in the AFM morphology presented in Figure IV.1: there is a drastic reduction in the number of nucleates at the pTGO interface compared to the non-passivated TGO interface. To further establish our results and to investigate possible routes to reduce the carbon defect density we also treated our interface with HF and ozone. This behavior of the carbon accumulates or defects under oxidizing atmosphere shall be reported in the present chapter V.

V.3.1 Visualization & characterization of the interface after Ozone treatment:

The observed nucleates at the SiC/SiO_2 interface emerge during the thermal oxidation as it progresses into the wafer, as discussed in chapter IV. When the interface of the TGO (not passivated) sample is

*Theoretical simulation performed by Prof. Goedecker et al. in Uni Basel.

ozone cleaned for 2 mins followed by HF etching a drastic reduction in the number of nucleates is observed in the AFM micrographs. This is in agreement with an earlier report[40, 80] stating that the clusters (in our terminology nucleates) were 'apparently composed of carbon'. This is confirmed by the consideration that ozone, a highly oxidizing agent, will attack the C-nucleates and oxidize them more effectively than the HF that is used to selectively etch the oxide in the preceding step. In Figure V.1a we compare how the density of nucleates is changing for both TGO and pTGO interfaces after HF cleaning. In Figure V.1b a TGO interface is compared before and after ozone cleaning. With only HF cleaning (without ozone) the C-nucleates will also be reduced, but the etch rate is significantly slower and the sample has to be dipped inside the HF etch bath for a longer time. This is because carbon needs an oxidizing agent to get etched and the acidic water being a slower oxidizing agent than ozone it takes a longer time to oxidize the same amount of C-nucleates at the interface.

To understand the effect of ozone on the carbon nucleates at the SiC/SiO_2 interface, DFT simulations have been performed by Goedecker's research group. Using DFT simulations it is found that carbon nucleates only form if no CO_2 can be formed in an initial stage, i.e. in an oxygen deficient process. In this case, CO diffuses away from the interface through the growing SiO_2 layer to the surface. During the diffusion process, the carbon atoms bind to different nearby oxygen atoms, exchanging their partner many times before they are eventually released in form of CO or CO_2 gas. Hence if the interface is treated with ozone the C receives enough oxygen to react with. By performing MH-DFTB simulations[111] for the reaction of ozone with H-passivated carbon chains and ribbons at the SiO_2 stripped interface, we confirm the experimental finding that ozone is reducing the presence of carbon nucleates due to oxidation. The carbon nucleates in the form of clusters and chains as they have been created by the thermal oxidation in pure oxygen 'in-silico' are broken into smaller pieces and CO is released as shown in Figure V.1c and d. We therefore assign our DFT and AFM observations to the reactive splitting of the long C-chains into smaller fragments and to their removal in the form of defect migration via the oxide to the gas phase in the oxidation chamber.[25]

*Theoretical simulation performed by Prof. Goedecker et al. in Uni Basel.

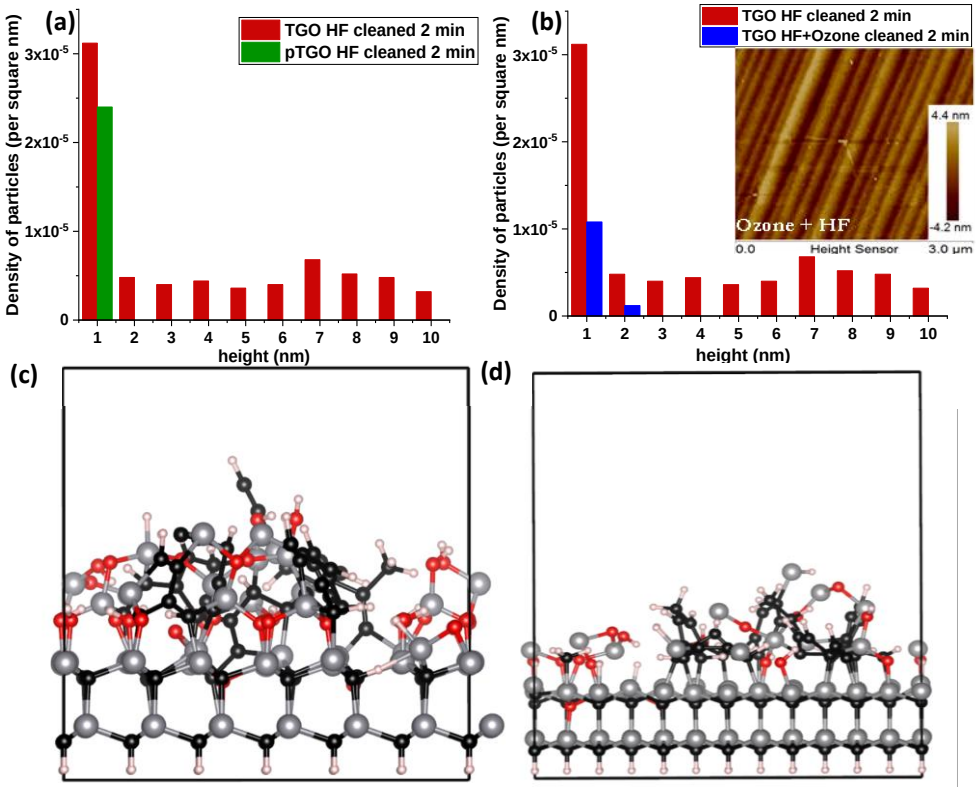

Figure V.1. Etch resistance of the nucleates in experiment and theory: The histogram analysis of the AFM data from Figure IV.1 a) compares the nucleate density at the interface for pTGO sample passivated in N_2O to TGO non-passivated sample b) reveals the reduction of the nucleates at the TGO interface after Ozone cleaning. The inset in b) shows the AFM morphology with reduced nucleates at the interface of the TGO sample after ozone cleaning. c) and d) MH-DFTB simulations of a carbon chain exposed to ozone. In c) a 5 carbon ring chain and in d) a 6 carbon ring chain are broken up by the reaction with ozone and smaller carbon nucleates remain on the surface. Due to the Ozone oxidation of the nucleates at the interface the carbon gets completely oxidized or breaks down to smaller nucleates.

This DFT result is in agreement with our experimental Raman analysis in that no significant change in the bonding state of the remaining C from bulk SiC has been observed. Only the non-SiC (defective) carbon, recognized by the C-C bond, is reduced as these atoms get oxidized in ozone. We have studied the intensity changes in the Raman peaks after the pure oxygen processed sample has been cleaned using Ozone (Figure V.2). There is a decline in the Raman intensity of the carbon peak due to the reduced number of non-SiC carbon bonds at the interface after ozone treatment. This is caused by the removal or reduction of the average size of the C-nucleates. Further, oxygen stripped TGO samples were also dipped in 7% HF etch for 1 min and 2 min respectively where we observed a reduction of ≈ 5% in the Raman intensity of the carbon peaks. This result provides evidence towards

*Theoretical simulation performed by Prof. Goedecker et al. in Uni Basel.

the presence of different forms of carbon at the interface and also that the acidic HF-water solution oxidizes the C-nucleates (Figure V.2 a) but the oxidation rate is much slower than ozone.

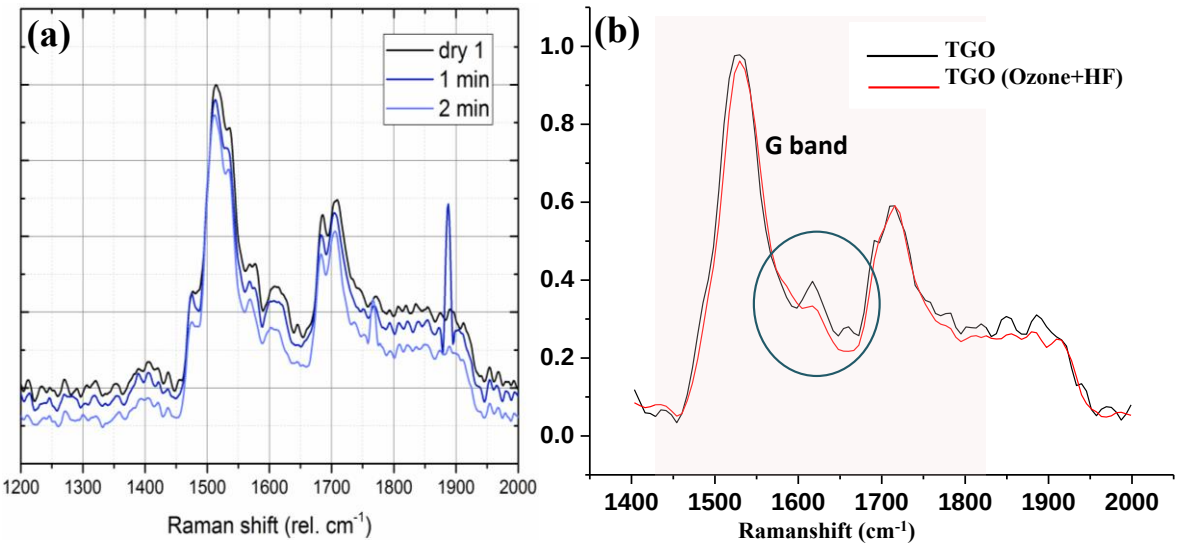

Figure V.2. (a) Evolution of the graphitic carbon (raw, unsubstracted data) of the nucleate-rich interface after initial oxide stripping followed by progressive cleaning and etching for 1 and 2 min, respectively. The intensity drops by ~6% for the shoulder at ~1530 cm^{-1}. (b) Raman spectroscopy reveals how the peak intensity of the G band region (marked by red background in graph) decreases once the pTGO sample has been cleaned using Ozone and HF; Raw data without SiC background subtraction.

V.3.2 Visualizing the interface after N_2O treatment/passivation:

The mechanism of nitridation is not fully understood on scientific grounds yet. Some studies propose nitrogen to compensate for the unpaired electrons at the interface. One possibility is that nitrogen with its different valence electron structure terminates the Si dangling bonds and replaces oxygen in strained Si –O– Si bonds. Also there are reports on nitrogen helping the removal of carbon defects from the interface. Afanasev *et al*. described a reduction in dangling bonds as well as a stronger decrease in the interface trap density near the conduction band of 4H-SiC if SiC oxidation was performed in a more nitrogenated environment.[112] This improves significantly the electron mobility at the oxidized 4H-SiC surfaces.[113]

*Theoretical simulation performed by Prof. Goedecker et al. in Uni Basel.

There is a significant difference between TGO and pTGO samples (vide supra). As observed in AFM micrographs and reported above, the number density of C-nucleates is lower for pTGO samples compared to non-passivated samples. To determine the chemical composition of the nucleates we performed Raman spectroscopy not only for the TGO sample but also for the pTGO sample. In our comparison and as seen from Figure V.3, we found a reduced intensity for the C-defective peaks for passivated samples (pTGO) which can be associated to a decrease in defect density. The Raman line 1524 cm^{-1} which is related to 3 coordinated amorphous carbons (polyene) has decreased its intensity by 12.3 % as was predicted before in some reports.[33, 70, 101, 107-110, 114] The 1716 cm^{-1} (Benzene related) Raman peak seems to have disappeared for pTGO sample, indicating that the nucleates tend to break into smaller bonds in presence of N_2. The capacitance-voltage (C-V) measurements on both the samples were compared and pTGO proved to have a better device mobility in comparison to TGO implying fewer defects for passivated samples in full agreement with the other experiments and the MH-DFT simulations.

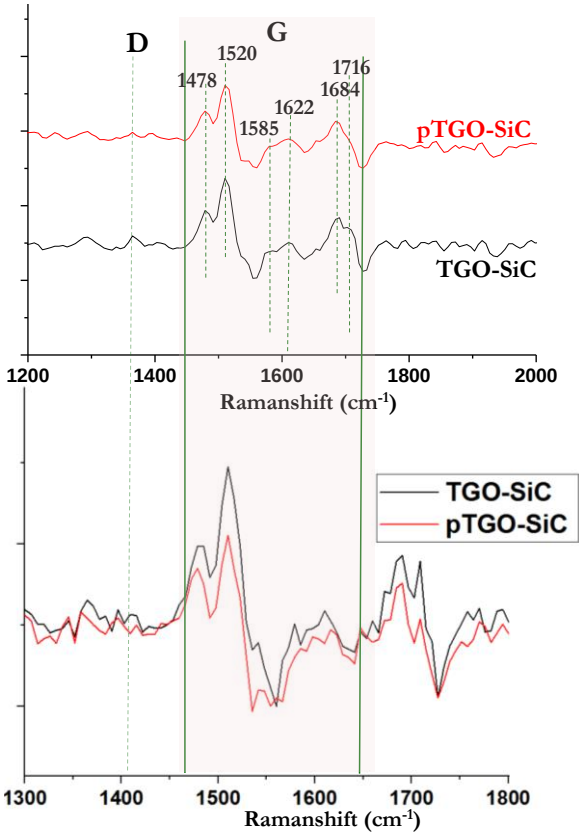

Figure V.3 Raman peak comparing TGO and pTGO sample. The peaks for defective C-bonds are marked in the upper panel and the evolution of the peaks for both the samples can be distinguished. The C-peaks for pTGO sample have reduced in intensity as can be clearly seen in the upper panel. The lower panel shows the difference in peak intensity for both samples after background correction using pure SiC signal.

In order to understand the physical mechanism of nitridation at the SiO_2/SiC interface theoretical simulations have been performed in Goedecker's group. To model the oxidation procedure in the NO and N_2O environment, an oxygen deficient reaction environment is created in order to mimic a two-step oxidation process. In the first step NO and N_2O are provided in the required amount to convert only the topmost layer into a stoichiometric SiO_2. In the second step the same amount of NO and N_2O is added

*Theoretical simulation performed by Prof. Goedecker et al. in Uni Basel.

again. In the initial oxide deficient step, the NO and N_2O oxidizes the surface of the SiC and forms the first SiO_2/SiC interface. The N_2O dissociates into NO and N on the SiC surface; the atomic N then migrates and reacts with another atomic N to forms N_2, whereas the NO oxidizes the surface. In this step the nitrogen does not seem to be incorporated within the SiC or SiO_2 matrix (Figure V.4).

As more N_2O is added, more of the SiC layer gets oxidized. Along with more N_2, also CO and CO_2 are formed. Few of the atomic nitrogen atoms while migrating, get trapped in the SiO_2 matrix and bind to the few Si dangling bonds at the interface. Since the environment is NO rich now, some nitrogen atoms not only get incorporated in the SiO_2 matrix but some also penetrate down into the SiC matrix (Figure V.4). Nitrogen atoms thus were found in not only Si but also in carbon sites. In the SiC and at the interface the atomic nitrogen mostly forms C≡N bonds, with an average bond length of 1.15 Å. As the oxidation proceeds some of the CN radical bind to either an oxygen or a silicon atom within the SiO2 matrix. Some of the nitrogen atoms saturate the Si dangling bonds by Si—N formation as was reported in earlier reports (see introduction).

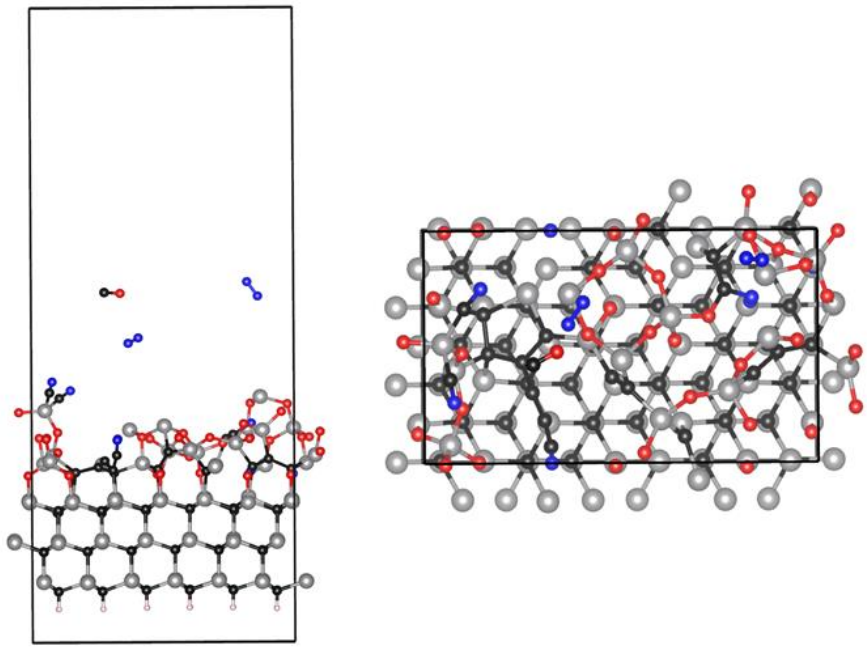

Figure V.4. Simulated oxidation of SiC in an N_2O environment (blue atoms being nitrogen). In the initial stage N_2 is formed and goes out of the matrix. As more N_2O is added, few of the N_2 gets trapped in the SiO_2 matrix near the interface. As oxidation progresses the nitrogen satisfies the dangling bonds by Si-N formation and less C-nucleates are detected at the interface due to the formation of C≡N bonds.

*Theoretical simulation performed by Prof. Goedecker et al. in Uni Basel.

Xu *et al*. concluded that most of the N atoms tend to bind with three Si atoms,[115] whereas, Umeda *et al*. reported that the N donors (tetra-coordinated N) also have a tendency to occupy substitutional C sites.[116] These nitrogen atoms are observed in the channel region after post-nitridation annealing. According to Mori *et al.* the simulated photoelectron intensity angular distribution (PIAD) pattern for the atomic arrangement around N atoms is qualitatively similar with their experimentally measured PIAD pattern.[117]

In our calculated structures it is observed that some of the nitrogen atoms partially replace the C atoms in the top SiC layer and directly bond to three Si atoms, while the Si atoms bond to the remaining C atom sites; this supports the previous experimental data discussed in chapter IV. The average bond length is around 1.75 Å, comparable with the Si –N bond length measured in the gas phase. The Si –N bond length has been determined in literature experimentally by photo-electron diffraction experiments to be 1.730 ± 0.08 Å, which agrees very well with our results.[118] The Si –N bond length is shorter than the Si – C bond length and because of this difference in their bond lengths, interfacial N causes interface strain within SiC at the SiO_2/SiC interface[119] as it has also been observed in our STEM/HR-TEM results (Figure IV.11).

The formation of CN molecules suggests that only few small carbon clusters are formed at the interface (Figure V.4) which agrees well with our Raman intensity profile (Figure V.3). However, it leads to the presence of carbon atoms in the SiO_2 matrix. Also it is observed that the formed CN molecules eventually react with oxygen and leave as the byproduct CO as a byproduct while the nitrogen atoms are left behind. This observation is again consistent with the experimental findings.[112]

The result of MH-prediction of CN and SiN formation matches perfectly with our Raman data for pTGO samples (Figure V.5). We found the peak for C≡N around 22600 cm^{-1} and Si-N at 2480 cm^{-1}.[120-122] There is also a peak at 2365 cm^{-1} which corresponds to the N_2 Raman peak. We associate the peak shift with the strain present in the system as is predicted due to nitrogen incorporation in a SiC matrix. The formation of CN molecules confirms that the concentration of C-defects in pTGO is lower. Since the mobility in pTGO samples is better it can be directly associated to the decrease in the

*Theoretical simulation performed by Prof. Goedecker et al. in Uni Basel.

number of C-nucleates which act as active defect sites. The oxidation rate for the pTGO process is also considerably slower. Compared to the TGO oxidation which takes 9 hours the pTGO oxidation takes place in 14 hours for the same oxide thickness. The slower oxidation rate gives enough time for carbon to get oxidized and to be removed to the reaction chamber via the SiO_2 matrix. The slower kinetics also helps the interface to attain a relaxed, less strained oxidation.

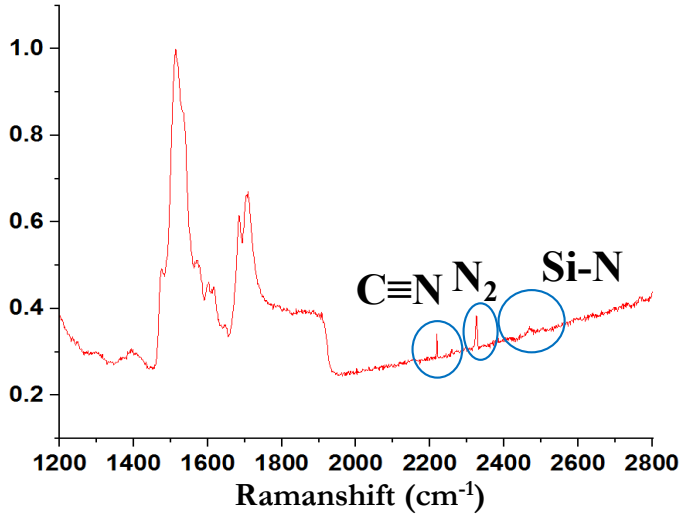

Figure V.5. Raman spectra of pTGO sample where both C≡N and Si-N bonds are confirmed as predicted from MH-DFT simulations.

The results in this study provide significant evidence that there is a trade-off relationship between interfacial N reducing the interface defects by capping the Si dangling bonds, reducing C-nucleates as well as the interfacial strain. Thus it is capable to reduce the three main causes degrading the inversion layer mobility.

V.4 Inference

The impact of nitrogen incorporation on the interface defects have been studied and understood in depth. By the growth of the oxide in a passivated Nitrogen atmosphere, the C-nucleates are reduced in their number density because of the C≡N formation.. Thus the presence of N is decisively improving the device channel mobility for pTGO samples. In test experiments on oxide stripped interface

*Theoretical simulation performed by Prof. Goedecker et al. in Uni Basel.

specimens, the interface treatment in ozone gas and HF baths for a prolonged time also reduce the number of C-nucleates as observed in AFM micrographs and in Raman spectroscopy.

*Theoretical simulation performed by Prof. Goedecker et al. in Uni Basel.

Chapter VI

Conclusion and Outlook (what's next?)

"I think and think for months and years. Ninety-nine times, the conclusion is false. The hundredth time I am right."

Albert Einstein

Summary

In this work we have focused on contributing to the extensive research effort going on towards realizing reliable SiC high power devices. Defects associated with oxide and specifically with interfaces and interface properties have been dealt with in great details. In some cases practical solutions to some of the issues were proposed. In this chapter all the main findings of my research have been assembled and conclusions have been deduced on the basis of my thesis work to date.

VI.1 Conclusions and Discussions

With the data and conclusions associated with my thesis we have tried to further enrich the understanding of the SiO_2/SiC interface.

Importance of sample preparation (Chapter II and chapter III)

- Sample preparation plays one of the most important roles in my thesis. The methods, the instruments used and the derivation of all the results are a consequence of how well the sample has been prepared. The results we obtain are thoroughly influenced by it. For STEM/ EELS/ LEAP specific sample geometries with a well-defined thickness lower than 30 nm are a must. Higher thickness will add to the background signal significantly which will interfere with the C-signal.

- We performed our experiments on MOS capacitor chip prototypes provided by Ascatron. The MOS capacitor has different layers of material on top of the oxide as would be for any fully functional capacitor chip. This made the sample preparation even trickier as the etching rates for each of this material are different. Unless proper measures are taken to safeguard homogeneous milling with the FIB, curtaining effects compromise HRTEM/ STEM experiments. Most importantly, a thick conducting protection layer (in our case Pt) is important.

- While preparing such thin lamella as they are needed for precise chemical analysis by HAADF-STEM, it is important to take adequate measures that no other defects are introduced into the sample. Reports on FIB prepared samples have to be critically reviewed for their sample preparation and preliminary characterization as they also impact the conclusiveness of STEM/ EELS/ LEAP results. This is because FIB uses Ga ions which are large in size and can create a lot of damage to the atomic lattice and leave amorphous layers behind. In the case of our 30 nm thin sample we observed a 20 nm amorphous layer surrounding it. For atomic resolution STEM imaging and for reliably obtaining data and drawing conclusions, nanomilling with a gentle ion

source is imperative. After each nanomill sesssion, samples were analyzed under TEM to check if the amorphous layer had been removed completely.

- Since we are looking for nm scale C-defects it is important that the analyzing window in STEM/HRTEM does not induce carbon into the sample regions to be analyzed. Thus, each sample before being introduced in the chamber should be plasma cleaned. After being introduced in the STEM/HRTEM system the sample should be allowed to stay in the vacuum chamber for an hour. These steps help in stabilizing the sample, reduce thermal drift and also reduce carbon formation induced by the high energy beam.

- Also the voltage applied for STEM/ HRTEM plays a vital role. Since C-nucleates are small in size and carbon is a very light element it can be easily removed if high energy beam currents are used. For most EELS experiments an acceleration voltage of 80 kV was used. If higher voltages were needed it was only for very short (~30 secs) time to avoid further damage to the sample.

The above mentioned conclusion regarding sample preparation was derived after many iterations and on the basis of the experiences gained during the experimental sessions.

Atomic scale investigation of SiC/SiO_2 interface (Chapter IV)

- We present conclusive evidence from AFM and Raman experiments that thermal oxidation of SiC leads to local, HF etch resistant carbon nucleates. The pearl necklace morphology indicates that certain interface features, e.g., step bunched areas may play a role towards the defect formation. Extensive atomistic simulations support this picture and further provide a detailed understanding on the origin of these nucleates and on how they form predominantly at the SiC step edges. DFTB proved their strong bond to the surrounding matrix via Si-C and O-C bonds, thus providing evidence for nucleates being highly resistant to HF etching. Our Raman results further provide conclusive affirmation of the presence of sp_2 carbon and semicircular rings as well as of amorphous carbon (sp_3 mixed in an sp_2 environment) which is different from the carbon contained in the SiC matrix. The DFT normal modes of vibration were compared with the experimentally

observed Raman data and surprisingly 6 out of the 10 defective C-bond peaks matched. Further, the DFT calculations also confirm the impact of the defective carbon accumulations on the electronic structure at the interface.

- Following up on the concerting evidence of the presence of C clusters chemically bonded with non-SiC bonds at the interface we wanted to understand the C-nucleates with regards to their exact position and composition inside the SiC/SiO_2 interface. LEAP is a unique instrument where the composition of the material can be determined with high spatial resolution (~nm). Since LEAP is being used for the first time to investigate SiC, several iterations were required to obtain the ideal threshold voltage of 6.7 kV for disassembling the needle shaped sample. After the 3D chemical pillar was reconstructed, the interface and the region of interface were established. The striking observation was that the interface was not atomically sharp and measured ≈ 1.8 nm across. C4 clusters were also present near and at the interface. For an optimized conclusion further measurements and statistical data analysis will be required. For this purpose new samples have to be prepared with a completely new geometry where the oxide will be vertically running parallel to the length of the pillar. This will help to yield the maximum data from the region of interest before the pillar is fractured by the high field.

- Chemical imaging by TEM has been used as a less destructive complimentary analytical technique compared to LEAP, where the atomic structure to be investigated was not disintegrated in the progress of the experiment. The HR-TEM data provides an accurate picture of how the oxidation proceeds at the interface i.e. in a layer by layer mode. Fast thermal oxidation produces stress and defects at the interface; this is more pronounced for TGO compared to pTGO. Also the exact steps towards the formation of Si dangling bonds were identified. EELS at the interface established the different oxidation states for Si atoms apart from Si^{+4} state. EELS results also confirmed the presence of C nucleates at 0.2 nm from the interface which is the bond length of Si-C. This result compliments our AFM and theory findings where we concluded that the C-

nucleates are not freely lying at the interface but rather attached to the interface via Si-bonds making them HF etch resistant .

- Further, periodic patterns within the SiO_2 in near interface regions have been thoroughly investigated using FFT/IFFT periodic filtering and analysis. Diffraction patterns appeared in certain regions within the amorphous SiO_2. This provides significant evidence that there are regularly appearing small crystallites embedded inside the amorphous SiO_2 layer. Although the diffraction signal is weak, it is distinct. Note that such crystalline structures cannot be detected for nucleates comprised by less than 8 to 10 atoms because FFT cannot be obtained from just a single unit cell but it requires repetition of the unit cell to identify the diffraction pattern. IFFT result showed graphitic sheets constituting a 5 and 6 membered C ring embedded inside the SiO_2 near the interface. DFTB simulations independently predicted the same result. The whole process of carbon accumulation is driven by the exceptional stability of the graphitic carbon-carbon bond which is a minority side reaction of the carbon oxidation to CO and eventually CO_2. Experimental and theoretical evidence support the conclusion that without further preventive measures graphitic carbon condensates provide a minority phase which coexists, in particular at specific interface locations, to the – intended -- thermal oxide. Theoretical simulation of the reaction has been recorded providing evidence towards the atomistic trajectory / chemical pathway of the formation of these 5 and 6 atom C-ring graphitic sheets inside the SiO_2 matrix.

Interface Treatment and Passivation (Chapter V)

- The difference between the passivated and non-passivated sample was prominent in the AFM micrographs. The interface for pTGO sample had less C-nucleates attached to the Si of SiC matrix compared to the TGO sample.
- The oxygen stripped TGO interface when treated with Ozone exhibited a significantly reduced number density of C-nucleates as evidenced by DFT, AFM and Raman. This is because ozone being a strong oxidizing agent attacks the C-defects to oxidize them as CO and CO_2. This further proves that the nucleates identified at the TGO sample interface are indeed carbon or carbon

compounds (SiO_xC_y). The TGO sample, when dipped in HF etch bath for a long time, surprisingly, showed a similar reduction in the number density of C-nucleates. This is because the dilute HF etch solution is a milder oxidizing agent compared to ozone and the oxygen from the water takes a longer time to oxidize the C-defects.

- The Raman spectra clearly indicate the reduced intensity for C- peaks for the passivated (and ozone etched) samples. Especially the decrease was prominent for the peaks at 1524 cm^{-1} and 1716 cm^{-1} which corresponds to 3 coordinated amorphous carbon and benzene like ring structures respectively. This proves that nitrogen incorporation not only terminates dangling bonds but due to the formation of CN radicals the C-nucleates fragment to either smaller defects or diminishes altogether. MH-DFT simulations in Goedecker's group proved that if N_2O is used for oxidation there is formation of SiN and also CN which hinders the formation of C-nucleates. This is because nitrogen terminates and pacifies the dangling bonds for Si and renders them electronically passive. Interestingly we found both CN and SiN peaks in our Raman spectra for pTGO samples providing evidence for the aforementioned hypotheses.

VI.2 Outlook

Using SiC, energy savings between 17 and 33% may be attained in railway propulsion systems[123] and in other genres of high power systems. Their realistic commercialization potential, however, still remains limited by the low channel mobility due to the high interface state density near the conduction band. Whether cleaning and treatment of the interface has reached its limits or not, remains to be discussed, also in view of the present results. The next step could be provided by optimizing the gate insulator fabrication (thermal, ALD, multilayer stacking) to overcome current limits in the channel mobility of SiC devices. Implementation of high-k gate dielectric insulators can potentially provide further advances: For obtaining the same gate capacitance a thicker gate insulator will be required as compared to SiO_2. High-k materials have generally relatively large band gaps, such as Al_2O_3, AlN, and AlON and are attractive for SiC-based MISFETs. Indeed, a high channel mobility of 100 – 200 $cm^2V^{-1}s^{-1}$ and a high breakdown electric field of 12–15 $MVcm^{-1}$ have been reported

utilizing Al_2O_3 and AlON gate layers on planar MIS structures .[124] The lower deposition temperatures will also favor high quality interfaces and diminish interlayer diffusion. Further, by implementing multilayer architectures for gate insulators, which is challenging, the reliability of the device may improve. Another very advantageous development would be the implementation of trench architectures aligned in different crystallographic directions to benefit from the anisotropy of the SiC wafer in the shaping of the trench and in the electronic characteristics.

The present study also motivates further research to investigate the carbon accumulation mechanisms contributing to the experimentally observed larger nucleates, and towards the role of passivating agents. This can be achieved by using unique techniques like LEAP but the sample preparation techniques and the operation conditions for highly insulating specimen like SiO_2 have to be improved. Also using XPS and SPM might throw new light onto the interface chemistry. Oxides can be grown in-situ inside the vacuum and the process can be simultaneously examined using XPS or even better Grand ARM Atomic Resolution Electron Microscope with unprecedented STEM image resolution of 55pm for atomic scale chemical imaging. Nitridation of the interface results in suppression of electron-induced states while there can be an increase in the density of hole traps because of the formation of SiON. Identifying the mechanisms of these two effects will be beneficial. Also by optimizing the NO annealing the nitrogen at the interface can be controlled so that both interface state densities and hole trap densities are curtailed. If excess nitrogen is avoided at the interface then along with passivation there will be enhancement in the reliability of SiC oxide-based devices. Nitrogen accumulation at the interface depends on the oxidation rate and the dosage of Nitrogen and NO annealing time. In the oxide of the silicon nitrogen can be incorporated as well to reduce gate leakage.[125-126] It will therefore be useful if the properties of NO-annealed SiO_2/SiC structures can be studied within the wider examined Si framework.

Studying different oxidation rate and oxidation pressure in order to understand the kinetics of the oxide growth might also be beneficial. With higher oxygen pressure the temperature and the time required for oxide growth can be lowered. This will lower the industrial oxide growth cost. The defect

formation mechanisms however has to be kept in mind as well and can be further investigated not only with respect to oxide pressure but also with varying oxide thicknesses. In the end a very critical and difficult to predict issue is whether deposited or native thermal oxidation will win the race for cost/ performance optimization as this will certainly affect the impact of SiC in different markets for power semiconductor and related devices.

Bibliography

1. Braun, F., Ueber die Stromleitung durch Schwefelmetalle. *Annalen der Physik* **1875,** *229* (12), 556-563.
2. Wilson, T. G., The evolution of power electronics. *IEEE transactions on power electronics* **2000,** *15* (3), 439-446.
3. Erickson, R. W.; Maksimovic, D., *Fundamentals of power electronics*. Springer Science & Business Media: **2007**.
4. Baliga, B. J., *Fundamentals of power semiconductor devices*. Springer Science & Business Media: **2010**.
5. Siddiqui, A.; Elgabra, H.; Singh, S., The Current Status and the Future Prospects of Surface Passivation in 4H-SiC Transistors. *IEEE Transactions on Device and Materials Reliability* **2016,** *16* (3), 419-428.
6. Kularatna, N., *Power electronics design handbook: low-power components and applications*. Elsevier: **1998**.
7. M. M. Atalla, E. T. a. E. J. S. Stabilization of silicon surfaces by thermally grown oxides. (accessed 3).
8. Östling, M.; Ghandi, R.; Zetterling, C.-M., *SiC power devices - Present status, applications and future perspective*. **2011**; p 10-15.
9. Šimonka, V.; Hössinger, A.; Weinbub, J.; Selberherr, S., Growth rates of dry thermal oxidation of 4H-silicon carbide. *Journal of Applied Physics* **2016,** *120* (13), 135705.
10. Kimoto, T.; Cooper, J. A., *Fundamentals of Silicon Carbide Technology: Growth, Characterization, Devices and Applications*. John Wiley & Sons: **2014**.
11. Wright, N. G.; Horsfall, A. B.; Vassilevski, K., Prospects for SiC electronics and sensors. *Materials today* **2008,** *11* (1-2), 16-21.
12. Brezeanu, G. In *Silicon carbide (SiC): a short history. an analytical approach for SiC power device design*, Semiconductor Conference, 2005. CAS 2005 Proceedings. 2005 International, IEEE: **2005**; pp 345-348.
13. Ortiz-Rodriguez, J.; Duong, T.; Rivera-Lopez, A.; Hefner, A. In *High-voltage, high-frequency SiC power MOSFETs model validation*, Power Electronics Specialists Conference, 2007. PESC 2007. IEEE, IEEE: **2007**; pp 1018-1022.
14. Cooper, J. A.; Melloch, M. R.; Singh, R.; Agarwal, A.; Palmour, J. W., Status and prospects for SiC power MOSFETs. *IEEE Transactions on Electron Devices* **2002,** *49* (4), 658-664.
15. Ueda, T.; Nishino, H.; Matsunami, H., Crystal growth of SiC by step-controlled epitaxy. *Journal of Crystal Growth* **1990,** *104* (3), 695-700.
16. SiC Technology Is Proving Its Value. *CS compound semiconductors* **2015**.

17. New York State Department of Environmental Conservation, Guidelines for conducting bird and bat studies at commercial wind energy projects. Division of Fish Wildlife and Marine Resources, Ed. Albany, NY, **2009**.

18. Kumar Gupta, S.; Akhtar, J., Thermal Oxidation of Silicon Carbide (SiC) ﷺ Experimentally Observed Facts. **2011**.

19. Jernigan, G. G.; Stahlbush, R. E.; Das, M. K.; Cooper, J. A.; Lipkin, L. A., Interfacial differences between SiO2 grown on 6H-SiC and on Si(100). *Applied Physics Letters* **1999,** *74* (10), 1448-1450.

20. Afanas'ev, V.; Ciobanu, F.; Pensl, G.; Stesmans, A., Contributions to the density of interface states in SiC MOS structures. In *Silicon Carbide*, Springer: **2004**, pp 343-371.

21. Afanasev, V.; Bassler, M.; Pensl, G.; Schulz, M., Intrinsic SiC/SiO2 interface states. *physica status solidi (a)* **1997,** *162* (1), 321-337.

22. Rozen, J. ELECTRONIC PROPERTIES AND RELIABILITY OF THE SiO2/SiC INTERFACE. Thesis, Vanderbilt University

Faculty of the Graduate School of Vanderbilt University, **2008**.

23. Plummer, J. D.; Michael, D., Deal, and Peter B. Griffin, Silicon VLSI Technology. Prentice Hall: **2000**.

24. Constant, A.; Camara, N.; Godignon, P.; Camassel, J., Benefit of H 2 surface pretreatment for 4 H-SiC oxynitridation using N 2 O and rapid thermal processing steps. *Applied Physics Letters* **2009,** *94* (6), 063508.

25. Pippel, E.; Woltersdorf, J.; Ólafsson, H. Ö.; Sveinbjörnsson, E. Ö., Interfaces between 4H-SiC and Si O 2: Microstructure, nanochemistry, and near-interface traps. *Journal of applied physics* **2005,** *97* (3), 034302.

26. Campi, J.; Shi, Y.; Luo, Y.; Yan, F.; Zhao, J. H., Study of interface state density and effective oxide charge in post-metallization annealed SiO/sub 2/-SiC structures. *IEEE Transactions on Electron Devices* **1999,** *46* (3), 511-519.

27. Chang, K.; Nuhfer, N.; Porter, L.; Wahab, Q., High-carbon concentrations at the silicon dioxide–silicon carbide interface identified by electron energy loss spectroscopy. *Applied Physics Letters* **2000,** *77* (14), 2186-2188.

28. Suzuki, S.; Harada, S.; Kosugi, R.; Senzaki, J.; Cho, W.-j.; Fukuda, K., Correlation between channel mobility and shallow interface traps in SiC metal–oxide–semiconductor field-effect transistors. *Journal of applied physics* **2002,** *92* (10), 6230-6234.

29. Shiraishi, K.; Chokawa, K.; Kamiya, K.; Kato, S.; Endo, K.; Araidai, M. In *The First Principles Investigation of SiC/SiO2 Interfaces Obtained by Thermal Oxidation*, Meeting Abstracts, The Electrochemical Society: **2014**; pp 2086-2086.

30. Park, C.; Cheong, B.-H.; Lee, K.-H.; Chang, K., Structural and electronic properties of cubic, 2H, 4H, and 6H SiC. *Physical Review B* **1994,** *49* (7), 4485.

31. Lohrmann, A.; Castelletto, S.; Klein, J.; Ohshima, T.; Bosi, M.; Negri, M.; Lau, D.; Gibson, B.; Prawer, S.; McCallum, J., Activation and control of visible single defects in 4H-, 6H-, and 3C-SiC by oxidation. *Applied Physics Letters* **2016,** *108* (2), 021107.

32. Moghadam, H. A.; Dimitrijev, S.; Han, J.; Haasmann, D., Active defects in MOS devices on 4H-SiC: A critical review. *Microelectronics Reliability* **2016,** *60*, 1-9.

33. Wang, S.; Dhar, S.; Wang, S.-r.; Ahyi, A.; Franceschetti, A.; Williams, J.; Feldman, L. C.; Pantelides, S. T., Bonding at the SiC− SiO 2 Interface and the effects of nitrogen and hydrogen. *Physical review letters* **2007,** *98* (2), 026101.

34. Senzaki, J.; Kojima, K.; Harada, S.; Kosugi, R.; Suzuki, S.; Suzuki, T.; Fukuda, K., Excellent effects of hydrogen postoxidation annealing on inversion channel mobility of 4H-SiC MOSFET fabricated on (11 2 0) face. *IEEE Electron Device Letters* **2002,** *23* (1), 13-15.

35. I. A. Khan, J. A. C., T. Isaacs-Smith, J. R. Williams, and L. C. Feldman, *Technical Program of 2002 Electronic Materials Conference* **2002**.

36. Tan, J.; Cooper, J. A.; Melloch, M. R., High-voltage accumulation-layer UMOSFET's in 4H-SiC. *IEEE Electron Device Letters* **1998,** *19* (12), 487-489.

37. Szilágyi, E.; Petrik, P.; Lohner, T.; Koós, A. A.; Fried, M.; Battistig, G., Oxidation of SiC investigated by ellipsometry and Rutherford backscattering spectrometry. *Journal of Applied Physics* **2008,** *104* (1), 014903.

38. M. Mooney, P.; Jiang, Z.; Basile, A.; Zheng, Y.; Dhar, S., *Effects of antimony (Sb) on electron trapping near SiO2/4H-SiC interfaces*. **2016**; Vol. 120, p 034503.

39. Yano, H.; Nakao, H.; Mikami, H.; Hatayama, T.; Uraoka, Y.; Fuyuki, T., Anomalously anisotropic channel mobility on trench sidewalls in 4H-SiC trench-gate metal-oxide-semiconductor field-effect transistors fabricated on 8° off substrates. *Applied Physics Letters* **2007,** *90* (4), 042102.

40. Afanas' ev, V.; Stesmans, A.; Harris, C. I. In *Observation of carbon clusters at the 4H-SiC/SiO2 interface*, Materials Science Forum, Trans Tech Publications: **1998**; pp 857-860.

41. Virojanadara, C. J., L. I., Oxidation studies of 4H-SiC(0 0 0 1) and (0 0 0 1¯) *Surface Science* **2002,** *505* (1-2,), 358-366.

42. Morales-García, Á.; Valero, R.; Illas, F., An Empirical, yet Practical Way To Predict the Band Gap in Solids by Using Density Functional Band Structure Calculations. *The Journal of Physical Chemistry C* **2017,** *121* (34), 18862-18866.

43. Wartewig, P. D. S., *IR and Raman Spectroscopy: Fundamental Processing*. Wiley Online Library: **2005**.

44. Rimini, E., *Ion implantation: basics to device fabrication*. Springer Science & Business Media: **1994**; Vol. 293.

45. Williams D.B., C. C. B., The Transmission Electron Microscope. In: Transmission Electron Microscopy. *Springer, Boston, MA* **1996**.

46. Goldstein, J., ed. , *Practical scanning electron microscopy: electron and ion microprobe analysis.* Springer Science & Business Media: **2012.**

47. Thust, A.; Barthel, J.; Tillmann, K., FEI Titan 80-300 TEM. *Journal of large-scale research facilities JLSRF* **2016,** *2*, 41.

48. Gault, B., et al., *Atom probe microscopy*. Springer Science & Business Media: **2012**; Vol. 160.

49. Larson, D. J.; Prosa, T.; Ulfig, R. M.; Geiser, B. P.; Kelly, T. F., Local electrode atom probe tomography. *New York, US: Springer Science* **2013**.

50. Knaup, J. M.; Deák, P.; Frauenheim, T.; Gali, A.; Hajnal, Z.; Choyke, W., Defects in SiO 2 as the possible origin of near interface traps in the SiC/ SiO 2 system: A systematic theoretical study. *Physical Review B* **2005,** *72* (11), 115323.

51. Perdew, J. P.; Burke, K.; Ernzerhof, M., Generalized gradient approximation made simple. *Physical review letters* **1996,** *77* (18), 3865.

52. Lely., J. A., Darstellung von Einkristallen von Silicium Carbid und Beherrschung

von Art und Menge der eingebauten Verunreinigungen. *Deutschen Keramischen Gesellschaft,* **1955,** *32*, 229–236.

53. Tairov, Y. M.; Tsvetkov, V. F., Investigation of growth processes of ingots of silicon carbide single crystals. *Journal of Crystal Growth* **1978,** *43* (2), 209-212.

54. Munding, A., *Interconnect technology for three-dimensional chip integration.* Cuvillier Verlag,: **2007**.

55. Hong, M. H.; Samant, A. V.; Pirouz, P., Stacking fault energy of 6H-SiC and 4H-SiC single crystals. *Philosophical Magazine A* **2000,** *80* (4), 919-935.

56. Mikhaylov, A. I.; Afanasyev, A. V.; Luchinin, V. V.; Reshanov, S. A.; Schöner, A.; Knoll, L.; Minamisawa, R. A.; Alfieri, G.; Bartolf, H., Tailoring the 4H-SiC/SiO2 MOS-interface for SiC-based power switches. *Japanese Journal of Applied Physics* **2016,** *55* (8S2), 08PC04.

57. Furukawa, Y.; Nakajima, K., *Advances in crystal growth research*. Elsevier: **2001**.

58. Borowicz, P.; Gutt, T.; Małachowski, T.; Latek, M., Carbonic inclusions on SiC/SiO2 interface investigated with Raman Scattering. *Diamond and Related Materials* **2011,** *20* (5-6), 665-674.

59. Makowska-Janusik, M.; Kassiba, A.; Bouclé, J.; Bardeau, J.; Kodjikian, S.; Désert, A., Vibrational density of states in silicon carbide nanoparticles: experiments and numerical simulations. *Journal of Physics: Condensed Matter* **2005,** *17* (33), 5101.

60. Saxey, D. W.; Cairney, J. M.; McGrouther, D.; Honma, T.; Ringer, S. P., Atom probe specimen fabrication methods using a dual FIB/SEM. *Ultramicroscopy* **2007,** *107* (9), 756-760.

61. Goedecker, S.; Hellmann, W.; Lenosky, T., Global minimum determination of the Born-Oppenheimer surface within density functional theory. *Physical review letters* **2005,** *95* (5), 055501.

62. Goedecker, S.; Deutsch, T.; Billard, L., A Fourfold Coordinated Point Defect in Silicon. *Physical Review Letters* **2002,** *88* (23), 235501.

63. Krukau, A. V.; Vydrov, O. A.; Izmaylov, A. F.; Scuseria, G. E., Influence of the exchange screening parameter on the performance of screened hybrid functionals. *The Journal of Chemical Physics* **2006,** *125* (22), 224106.

64. Goedecker, S., Minima hopping: An efficient search method for the global minimum of the potential energy surface of complex molecular systems. *The Journal of chemical physics* **2004,** *120* (21), 9911-9917.

65. Schaefer, B.; Alireza Ghasemi, S.; Roy, S.; Goedecker, S., Stabilized quasi-Newton optimization of noisy potential energy surfaces. *The Journal of chemical physics* **2015,** *142* (3), 034112.

66. Aradi, B.; Hourahine, B.; Frauenheim, T., DFTB+, a sparse matrix-based implementation of the DFTB method. *The Journal of Physical Chemistry A* **2007,** *111* (26), 5678-5684.

67. Rauls, E.; Elsner, J.; Gutierrez, R.; Frauenheim, T., Stoichiometric and non-stoichiometric (1010) and (1120) surfaces in 2H–SiC: a theoretical study. *Solid state communications* **1999,** *111* (8), 459-464.

68. Köhler, C.; Hajnal, Z.; Deák, P.; Frauenheim, T.; Suhai, S., Theoretical investigation of carbon defects and diffusion in α-quartz. *Physical Review B* **2001,** *64* (8), 085333.

69. Kodigala, S. R.; Chattopadhyay, S.; Overton, C.; Ardoin, I.; Gordon, B.; Johnstone, D.; Roy, D.; Barone, D., Growth and surface analysis of SiO2 on 4H-SiC for MOS devices. *Applied Surface Science* **2015,** *330*, 465-475.

70. S. Dimitrijev, H. B. H., P. Tanner, K. Y. Cheong, and J. Han, Silicon

Carbide: Recent Major Advances. *Springer, Boston, MA* **2004**, 373–386.

71. Dimitrijev, S.; Jamet, P., Advances in SiC power MOSFET technology. *Microelectronics Reliability* **2003,** *43* (2), 225-233.

72. Sun, J.; Hannon, J. B.; Tromp, R. M.; Pohl, K., Highly uniform step and terrace structures on SiC (0001) surfaces. *IBM Journal of Research and Development* **2011,** *55* (4), 7: 1-7: 6.

73. Starke, U.; Bernhardt, J.; Schardt, J.; Heinz, K., SiC surface reconstruction: Relevancy of atomic structure for growth technology. *Surface Review and Letters* **1999,** *6* (06), 1129-1141.

74. Kimoto, T.; Itoh, A.; Matsunami, H., Step-controlled epitaxial growth of high-quality SiC layers. *physica status solidi (b)* **1997,** *202* (1), 247-262.

75. Epler, J.; Jung, T.; Schweizer, H., Evolution of monolayer terrace topography on (100) GaAs annealed under an arsine/hydrogen ambient. *Applied physics letters* **1993,** *62* (2), 143-145.

76. Bokor, J., Ultrafast Dynamics at Semiconductor and Metal Surfaces. *Science* **1989,** *246* (4934), 1130-1134.

77. Liu, P.; Li, G.; Duscher, G.; Sharma, Y. K.; Ahyi, A. C.; Isaacs-Smith, T.; Williams, J. R.; Dhar, S., Roughness of the SiC/SiO2 vicinal interface and atomic structure of the transition layers. *Journal of Vacuum Science & Technology A* **2014,** *32* (6), 060603.

78. Phelps, G.; Wright, N.; Chester, E.; Johnson, C.; O'Neill, A., Step bunching fabrication constraints in silicon carbide. *Semiconductor science and technology* **2002,** *17* (5), L17.

79. Sakai, T.; Hemmi, M.; Murata, Y.; Yamakami, T.; Hayashibe, R.; Onuma, Y.; Kamimura, K. In *Effect of Direct Nitridation of 4H-SiC Surface on MOS Interface States*, Materials Science Forum, Trans Tech Publ: **2012**; pp 725-728.

80. Harris, C.; Afanas' ev, V., SiO2 as an insulator for SiC devices. *Microelectronic engineering* **1997,** *36* (1-4), 167-174.

81. Raj, R.; Terauds, K., Bubble nucleation during oxidation of SiC. *Journal of the American Ceramic Society* **2015,** *98* (8), 2579-2586.

82. Radić, N.; Pivac, B.; Meinardi, F.; Koch, T., Raman study of carbon clusters in W–C thin films. *Materials Science and Engineering: A* **2005,** *396* (1-2), 290-295.

83. Schwan, J.; Ulrich, S.; Batori, V.; Ehrhardt, H.; Silva, S., Raman spectroscopy on amorphous carbon films. *Journal of Applied Physics* **1996,** *80* (1), 440-447.

84. Chen, Z.; Zhao, J.; Yano, T.; Ooie, T.; Yoneda, M.; Sakakibara, J., Observation of sp 3 bonding in tetrahedral amorphous carbon using visible Raman spectroscopy. *Journal of Applied Physics* **2000,** *88* (5), 2305-2308.

85. Ferrari, A. C.; Robertson, J., Interpretation of Raman spectra of disordered and amorphous carbon. *Physical Review B* **2000,** *61* (20), 14095-14107.

86. Das, A.; Chakraborty, B.; Sood, A., Raman spectroscopy of graphene on different substrates and influence of defects. *Bulletin of Materials Science* **2008,** *31* (3), 579-584.

87. Ferrari, A. C.; Robertson, J., Raman spectroscopy of amorphous, nanostructured, diamond–like carbon, and nanodiamond. *Philosophical Transactions of the Royal Society of London A: Mathematical, Physical and Engineering Sciences* **2004,** *362* (1824), 2477-2512.

88. Shi, J.; Shi, X.; Sun, Z.; Liu, E.; Tay, B.; Lau, S., Ultraviolet and visible Raman studies of nitrogenated tetrahedral amorphous carbon films. *Thin solid films* **2000,** *366* (1-2), 169-174.

89. Maintz, S.; Deringer, V. L.; Tchougréeff, A. L.; Dronskowski, R., Analytic projection from plane-wave and PAW wavefunctions and application to chemical-bonding analysis in solids. *Journal of computational chemistry* **2013,** *34* (29), 2557-2567.

90. Maintz, S.; Deringer, V. L.; Tchougréeff, A. L.; Dronskowski, R., LOBSTER: A tool to extract chemical bonding from plane-wave based DFT. *Journal of computational chemistry* **2016,** *37* (11), 1030-1035.

91. Deringer, V. L.; Tchougréeff, A. L.; Dronskowski, R., Crystal orbital Hamilton population (COHP) analysis as projected from plane-wave basis sets. *The Journal of Physical Chemistry A* **2011,** *115* (21), 5461-5466.

92. Dronskowski, R.; Bloechl, P. E., Crystal orbital Hamilton populations (COHP): energy-resolved visualization of chemical bonding in solids based on density-functional calculations. *The Journal of Physical Chemistry* **1993,** *97* (33), 8617-8624.

93. Gavrikov, A.; Knizhnik, A.; Safonov, A.; Scherbinin, A.; Bagatur'yants, A.; Potapkin, B.; Chatterjee, A.; Matocha, K., First-principles-based investigation of kinetic mechanism of SiC (0001) dry oxidation including defect generation and passivation. *Journal of Applied Physics* **2008,** *104* (9), 093508.

94. Devynck, F.; Alkauskas, A.; Broqvist, P.; Pasquarello, A., Defect levels of carbon-related defects at the SiC/SiO 2 interface from hybrid functionals. *Physical Review B* **2011,** *83* (19), 195319.

95. Salemi, S.; Goldsman, N.; Ettisserry, D.; Akturk, A.; Lelis, A., The effect of defects and their passivation on the density of states of the 4H-silicon-carbide/silicon-dioxide interface. *Journal of Applied Physics* **2013,** *113* (5), 053703.

96. Devynck, F.; Giustino, F.; Broqvist, P.; Pasquarello, A., Structural and electronic properties of an abrupt 4 H− SiC (0001)⁄ SiO 2 interface model: Classical molecular dynamics simulations and density functional calculations. *Physical Review B* **2007,** *76* (7), 075351.

97. Bassler, M.; Pensl, G.; Afanas' ev, V., "Carbon cluster model" for electronic states at SiCSiO2 interfaces. *Diamond and Related Materials* **1997,** *6* (10), 1472-1475.

98. Beltrán, A. M.; Duguay, S.; Strenger, C.; Bauer, A. J.; Cristiano, F.; Schamm-Chardon, S., Atomic scale characterization of SiO2/4H-SiC interfaces in MOSFETs devices. *Solid State Communications* **2015,** *221*, 28-32.

99. Liu, G.; Tuttle, B. R.; Dhar, S., Silicon carbide: A unique platform for metal-oxide-semiconductor physics. *Applied Physics Reviews* **2015,** *2* (2), 021307.

100. Zheleva, T.; Lelis, A.; Duscher, G.; Liu, F.; Levin, I.; Das, M., Transition layers at the SiO2⁄SiC interface. *Applied Physics Letters* **2008,** *93* (2), 022108.

101. Hui-Feng, L.; Dimitrijev, S.; Harrison, H. B., Improved reliability of NO-nitrided SiO2 grown on p-type 4H-SiC. *IEEE Electron Device Letters* **1998,** *19* (8), 279-281.

102. Li, H.-F.; Dimitrijev, S.; Sweatman, D.; Harrison, H. B., Analysis of Fowler–Nordheim injection in NO nitrided gate oxide grown on n-type 4H–SiC. *Microelectronics Reliability* **2000,** *40* (2), 283-286.

103. Li, H.-f.; Dimitrijev, S.; Sweatman, D.; Harrison, H. B.; Tanner, P.; Feil, B., Investigation of nitric oxide and Ar annealed SiO2/SiC interfaces by x-ray photoelectron spectroscopy. *Journal of Applied Physics* **1999,** *86* (8), 4316-4321.

104. Johnson, C.; Wright, N.; Uren, M.; Hilton, K.; Rahimo, M.; Hinchley, D.; Knights, A.; Morrison, D.; Horsfall, A.; Ortolland, S., Recent progress and current issues in SiC semiconductor devices for power applications. *IEE Proceedings-Circuits, Devices and Systems* **2001,** *148* (2), 101-108.

105. Phelps, G.; Wright, N.; Chester, E.; Johnson, C.; O'Neill, A.; Ortolland, S.; Horsfall, A.; Vassilevski, K.; Gwilliam, R.; Coleman, P., Enhanced nitrogen diffusion in 4H-SiC. *Applied physics letters* **2002,** *80* (2), 228-230.

106. Wright, N. G.; Morrison, D.; Johnson, C. M.; O'Neill, A. G. In *Electrothermal simulation of 4H-SiC power devices*, Materials Science Forum, Aedermannsdorf, Switzerland: Trans Tech Publications, 1984-: **1998**; pp 917-920.

107. Chung, G. Y.; Tin, C. C.; Williams, J. R.; McDonald, K.; Ventra, M. D.; Pantelides, S. T.; Feldman, L. C.; Weller, R. A., Effect of nitric oxide annealing on the interface trap densities near the band edges in the 4H polytype of silicon carbide. *Applied Physics Letters* **2000,** *76* (13), 1713-1715.

108. Jamet, P.; Dimitrijev, S.; Tanner, P., Effects of nitridation in gate oxides grown on 4H-SiC. *Journal of Applied Physics* **2001,** *90* (10), 5058-5063.

109. McDonald, K.; Weller, R. A.; Pantelides, S. T.; Feldman, L. C.; Chung, G. Y.; Tin, C. C.; Williams, J. R., Characterization and modeling of the nitrogen passivation of interface traps in SiO2/4H–SiC. *Journal of Applied Physics* **2003,** *93* (5), 2719-2722.

110. Deák, P.; Hornos, T.; Thill, C.; Knaup, J.; Gali, A.; Frauenheim, T., The Mechanism of Interface State Passivation by NO. *Materials Science Forum* **2007,** *556-557*, 541-544.

111. Amsler, M.; Goedecker, S., Crystal structure prediction using the minima hopping method. *The Journal of chemical physics* **2010,** *133* (22), 224104.

112. Afanas'ev, V. V.; Stesmans, A.; Ciobanu, F.; Pensl, G.; Cheong, K. Y.; Dimitrijev, S., Mechanisms responsible for improvement of 4H–SiC/SiO2 interface properties by nitridation. *Applied Physics Letters* **2003,** *82* (4), 568-570.

113. Schörner, R.; Friedrichs, P.; Peters, D.; Stephani, D.; Dimitrijev, S.; Jamet, P., Enhanced channel mobility of 4H–SiC metal–oxide–semiconductor transistors fabricated with standard polycrystalline silicon technology and gate-oxide nitridation. *Applied Physics Letters* **2002,** *80* (22), 4253-4255.

114. Williams, J.; Chung, G.; Tin, C.; McDonald, K.; Farmer, D.; Chanana, R.; Weller, R.; Pantelides, S.; Holland, O.; Das, M., Nitrogen passivation of the interface states near the conduction band edge in 4H-silicon carbide. *MRS Online Proceedings Library Archive* **2000,** *640*.

115. Xu, Y.; Zhu, X.; Lee, H.; Xu, C.; Shubeita, S.; Ahyi, A.; Sharma, Y.; Williams, J.; Lu, W.; Ceesay, S., Atomic state and characterization of nitrogen at the SiC/SiO2 interface. *Journal of Applied Physics* **2014,** *115* (3), 033502.

116. Umeda, T.; Esaki, K.; Kosugi, R.; Fukuda, K.; Ohshima, T.; Morishita, N.; Isoya, J., Behavior of nitrogen atoms in SiC-SiO2 interfaces studied by electrically detected magnetic resonance. *Applied physics letters* **2011,** *99* (14), 142105.

117. Mori, D.; Oyama, Y.; Hirose, T.; Muro, T.; Matsui, F., Local structural determination of N at SiO2/SiC (000 1¯) interfaces by photoelectron diffraction. *Applied Physics Letters* **2017,** *111* (20), 201603.

118. Franco, N.; Avila, J.; Davila, M.; Asensio, M.; Woodruff, D.; Schaff, O.; Fernandez, V.; Schindler, K.; Bradshaw, A., Structure determination of using scanned-energy mode photoelectron diffraction. *Journal of Physics: Condensed Matter* **1997,** *9* (40), 8419.

119. Houston Dycus, J.; Xu, W.; Lichtenwalner, D. J.; Hull, B.; Palmour, J. W.; LeBeau, J. M., Structure and chemistry of passivated SiC/SiO2 interfaces. *Applied Physics Letters* **2016,** *108* (20), 201607.

120. Grazia Giorgini, M.; Arcioni, A.; Polizzi, C.; Musso, M.; Ottaviani, P., *Relaxation processes of the liquid crystal ME6N in the isotropic phase studied by Raman scattering experiments*. **2004**; Vol. 120, p 4969-79.

121. Stair, P. C., The Application of UV Raman Spectroscopy for the Characterization of Catalysts and Catalytic Reactions. In *Advances in Catalysis*, Gates, B. C.; Knözinger, H., Eds. Academic Press: **2007**, pp 75-98.

122. Dhakal, A.; Wuytens, P.; Peyskens, F.; Subramanian, A. Z.; Thomas, N. L.; Baets, R., *Silicon-nitride waveguides for on-chip Raman spectroscopy*. SPIE: **2014**; Vol. 9141.

123. Shinbo, M.; Sonoda, H.; Ishida, T.; Abiko, H.; Shibanuma, K.; Chiba, Y. In *Research of Efficient main power equipment using SiC power device*, 2014 International Power Electronics Conference (IPEC-Hiroshima 2014 - ECCE ASIA), 18-21 May 2014; **2014**; pp 634-639.

124. Hino, S.; Hatayama, T.; Kato, J.; Miura, N.; Oomori, T.; Tokumitsu, E., Anomalously High Channel Mobility in SiC-MOSFETs with Al2O3/SiOx/SiC Gate Structure. *Materials Science Forum* **2009,** *600-603*, 683-686.

125. Sasaki, T.; Kuwazawa, K.; Tanaka, K.; Kato, J.; Dim-Lee, K., Engineering of nitrogen profile in an ultrathin gate insulator to improve transistor performance and NBTI. *IEEE Electron Device Letters* **2003,** *24* (3), 150-152.

126. Islam, A. E.; Gupta, G.; Mahapatra, S.; Krishnan, A. T.; Ahmed, K.; Nouri, F.; Oates, A.; Alam, M. A. In *Gate Leakage vs. NBTI in Plasma Nitrided Oxides: Characterization, Physical Principles, and Optimization*, 2006 International Electron Devices Meeting, 11-13 Dec. 2006; **2006**; pp 1-4.

Curriculum Vitae

Dipanwita Dutta

Thalwil, Switzerland

+41 765073037

dipanwita.dutta@psi.ch

www.linkedin.com/in/dipanwita-dutta-71254864/

Education

- **PhD in Experimental Physics**
  University of Basel, Switzerland
  From June 2015 to June 2019
  Project in collaboration with ABB Switzerland

- **Master in Material Science**
  Jawaharlal Nehru Centre for Advanced Scientific Research, India
  From 2011 to 2014

- **Bachelor of Science (Physics Major)**
  St. Xaviers College, India
  From 2008 to 2011

Work experience

PhD Thesis (2015-2019) – Research on SiC high power devices

Advisor: Prof. T. A. Jung (PSI, Uni. Basel); Main Collaborators: Dr. J. Lehmann (ABB Baden-Dättwil), Dr. G. Alfieri (ABB Lenzburg), Prof. S. Goedecker (Uni. Basel)

Atomic scale analysis of SiC/Oxide interface towards improving channel mobility of Metal Oxide Semiconductor Field Effect Transistor MOSFET and MOS capacitors

- Reviewing existing procedures for implementing cost, quality, current-handling capability & reliability improvements for low-voltage MOSFET & high- voltage IGBT-based power devices.
- Electrical Characterization: SiC MOS capacitors/FETs (Ascatron): **Keithley sourcemeter 2400, HP LCR-meter**.
- Defect analysis using Scanning Electron Microscopy (**SEM**), Atomic Force Microscopy (**AFM**), **Raman Spectroscopy** & Local Electrode Atom Probe (**LEAP**) a unique technique for 3D chemical imaging.
- Fabricating 30 nm thin lamellae using Focused Ion Beam (**FIB**) & **Nanomill** leading to unambiguous detection of Near Interface Defects (NITs) using Scanning Transmission Electron Microscopy (**STEM**) & High Resolution TEM (**HRTEM**) towards strategic improvement of SiC MOSFET channel mobility.
- Led to multi-institution collaboration: **ETHZ** (Switzerland), **Ernst Ruska Center** (Germany), **CNR-IMM** (Italy). Collaboration with **Uni. Basel** for latest, advanced simulation tools to study industrially relevant properties in SiC based electronic devices to calibrate simulation tools, for a tailored process control for low-defect interfaces.
- Fabrication of MOS capacitor test structure: thermal oxidation at 1000 ^{o}C & Atomic layer deposition (**ALD**) for different oxides, processing surface/ interface of SiC in **acid (HF) etch bath** & **Ozone cleaner** in clean room and thorough knowledge on dopant profiling.
- Teaching and supervision of master and summer students.

Skills

- **Fluent:** English, Hindi, Bengali, Urdu**; Beginner:** German.
- **Microscopes & related:** STEM, HR-TEM, SEM, AFM, FIB, LEAP.
- **Electrical Measurements:** Keithley 2400, 236, HP-LCR, Four Probe, Hall, IR-photoresponse.
- **Metal Deposition techniques:** PVD, CVD, PLD.
- **Spectroscopy related:** UV-IR, XRD, Raman.
- Thorough knowledge in Density function theory, minima hopping simulation.
- Wet bench use in clean room.

Additional qualification

- **Organizing Staff for the International Conference QMol (**Operating quantum states in atoms and molecules at surfaces**), 2017, Ascona, Switzerland**
- **DST (**Department of Science & Technology**) Fellowship, 2012-2015, India**
- **Inspire Scholarship from 2008-2011** for top 5% score in state in higher secondary.
- **Rank holder in WBJEE (**West Bengal Joint (Engineering) Entrance Examination**), AIEEE (**All India Engineering Entrance Examination**)**

Hobbies

- Skiing, Jiu Jitsu, Badminton.
- Worked with NGOs; Member of Asha Zurich.
- Trained in contemporary dance, Jive & Rabindra Sangeet (music).

R&D (2014-2015) – Development of Transparent Solar cell/ Heaters

Jawaharlal Nehru Center for Advanced Scientific Research: Prof. G. U. Kulkarni

Ag wire network transparent conducting electrodes (TCEs) were produced with transmittance up to 86%, sheet resistance below 11 Ω/□ for transparent solar cell and heaters.

- Processing & manufacturing of (TCEs) on flat or flexible surfaces, using unique spray coating precursor (developed in lab) to form a crack template.
- Conducting highly interconnected metal (Ag) nanometer scale networks produced on desired surface using physical/chemical vapor deposition (**PVD/CVD**) on the crack template towards transparent, flexible electronics.
- Teaching assistant for master students.

Research Assistant (2013-2014) – Fabrication of FETs & pressure sensors

Jawaharlal Nehru Center for Advanced Scientific Research: Prof. G. U. Kulkarni

Fabrication of graphene based FETs, RC low pass filters & developing pressure sensors using Au Nanoparticle- PDMS Nanocomposite capacitors (Master Thesis)

- Passive devices like resistor-capacitor filters produced employing graphene as a resistor and ion gel as dielectric.
- FETs fabricated out of pencil traces on papers with aid of ion gel having high specific capacitance.
- Touch sensors, stress and strain gauges as well as flexible biocompatible devices developed using Au-PDMS nanocomposite as a gel capacitor.

Project Assistant (May 2012- Oct 2012) – Graphene on Si for detectors

Jawaharlal Nehru Center for Advanced Scientific Research: Prof. G. U. Kulkarni, Dr. Narendra Kurra

Electrical Characterization & Potential Applications of Graphene-like Nanocarbon on Si surface (Summer Intern)

- Development and characterization of large area graphene on Si toward IR detector.
- Analytical methods: Xray diffraction (XRD), SEM, AFM, Raman, Kiethley 236, UV-IR spectroscopy, Hall measurement, Four probe, Pulsed Laser Deposition, Optical Stylus and profiler, IR photoresponse.

Project Assistant (Oct 2011- Feb 2012) – Simulation and theoretical studies

Jawaharlal Nehru Center for Advanced Scientific Research: Prof. U. Waghmare

Theoretical studies on 2-D materials (metals and crystals) like graphene WS2 (Winter Internship)

- Theoretical studies on low dimensional materials.
- Writing code for numerical solution of problems: Root Finding, Interpolation, ODEs, PDEs, Monte Carlo

Conferences

- **D. Dutta**, D. Jarzabek, H. Schift, Z. Rymuza, T.A. Jung, Atomic Structure and Nano-Fracture Mechanics of Semiconductor-Oxide Interfaces Investigated by Transmission Electron Microscopy and Scanning Force Microscopy, **American Physical Society (APS)**, Boston, USA, 2019.
- **D. Dutta**, D. De, G. Alfieri, J. Lehmann, T. Jung et al., Atomistic investigations of carbon-related defects and their passivation in SiC/SiO_2 Interfaces, **European Conference on SiC and Related Materials (ECSCRM)**, Birmingham, UK, 2018.
- D. Jarzabek, H. Schift, **D. Dutta**, Z. Rymuza, T.A. Jung, Nano Fracture Mechanics with Scanning Force Microscope: Applications in Material Science, **Material Research Society (MRS)**, Phoenix, USA, 2018.
- **D. Dutta**, D. De, E. Müller, T. Jung et al., Atomic Scale Investigation of Near Interface Defects at the SiC/SiO2-Interface: Microscopy, Atom Probe Tomography and Theory, **German Physical Society DPG Physik**, Berlin, Germany, 2018.
- **D. Dutta**, S. Gödecker, H. Bartolf, J. Lehmann, G. Alfieri, M. Camarda et al., Defects at SiC/SiO_2 interface, **International Symposium on Surface Science (ISSS-8)**, Tsukuba, Japan, 2017.
- **D. Dutta**, S. Gödecker, S. Gerstl, E. Mueller, T. Jung, J. Lehmann, H. Bartolf, G. Alfieri et al., Defect Analysis at the SiC/SiO_2 Interface to Improve MOS-FET Performance in High Power Devices, **Swiss Nanoscience Institute (SNI) annual meeting**, Lenzerheide, Switzerland, 2017
- **D. Dutta**, D. De, E. Müller, S. S. A. Gerstl et al., Atomic scale investigation of near interface defects at the SiC/SiO_2 Interface, **International Conference on Functional Nanomaterials and Nanotechnology (ICFNN)**, Nepal, 2017.
- **D. Dutta**, A. Sologubenko, S. Goedecker, J. Lehmann, G. Alfieri et al., Atomistic insight into carbon defects at thermally grown SiC / SiO_2 interfaces. **International Conference on SiC and Related Materials (ICSCRM)**, Washington DC, USA, 2017.
- H. Rossmann, U. Gysin, **D. Dutta**, H. Bartolf, E. Meyer et al., Space charge mapping of semiconductor device cross-sections. **ECSCRM**, Greece, 2016.
- **D. Dutta**, H. Rossmann, S. Goedecker, J. Lehmann, T. Jung, et al., Defects-A Challenge towards Realizing SiC HighPower MOSFET Devices. **SNI meeting**, Lenzerheide, Switzerland, 2016.
- **D. Dutta**, L. Zhu, S. Roy, S. Gerstel, E. Müller, J. Lehmann, T. Jung, J. Gobrecht, A. Schöner, H. Bartolf et.al., Direct Atomistic Inspection of the MOS-Interface for SiC-Based Power Switches by Local Electrode Atomic Probe, **International Symposium on Power Semiconductor Devices and ICs (ISPSD)**, Switzerland, 2015.
- **D. Dutta,** N. Kurra, G. U. Kulkarni Carbon nano-materials & graphene, **Annual meeting JNCASR**, Bangalore, India, 2013

Publications

- “Field Effect Transistor and RC Filters from Pencil Trace on Paper”, Phys. Chem. Chem. Phys., April 25, 2013, 15, 8367-8372. N. Kurra, **D. Dutta**, G. U. Kulkarni
- "Evidence for carbon nucleates present nearthermal gate oxides affecting the electronic band structure in SiC-MOSFET” **D. Dutta**, D. Shankar De, D. Fan, A. Schöner, L. Zhu, S. Roy, G. Alfieri, H. Bartolf, M. Camarda, S. Goedecker, J. Lehmann, T. Jung (Manuscript submitted to APL)
- "The SiO_2/4H-SiC Interface on Stepped Surfaces" J. Woerle, B. C. Johnson, **D. Dutta**, C.Bongiorno, G. Ferro, T. A. Jung, H. Sigg, U. Grossner, M. Camarda (Manuscripts submitted to ACS Applied Materials and Interfaces)